UNIVERSITÀ DEGLI STUDI FIRENZE

UNIVERSITÁ DEGLI STUDI DI FIRENZE

SCUOLA DI INGEGNERIA

Dottorato di Ricerca in

Ingegneria Industriale

COORDINATORE: Prof. Maurizio De Lucia

CICLO XXXI

Design and testing of innovative thrusters and their integration in the design of a reconfigurable underwater vehicle

Dottorando

Dott. Ing. Marco Pagliai

Tutor

Prof. Benedetto Allotta

Coordinatore

Prof. Maurizio De Lucia

Anni 2015/2018

Summary

Abstract

Nowadays, Unmanned Underwater Vehicles (UUVs) are increasingly used in underwater operations (e.g. exploration, monitoring, maintenance), because they make safe working under the water. Since their use is growing, it is extremely important to ensure better maneuverability and lower power consumption to improve the performances of this kind of vehicles. The work carried out in the last three years at the Mechatronics and Dynamic Modelling Laboratory (MDM Lab) of the Department of Industrial Engineering of University of Florence (UNIFI DIEF), focused exactly on these problematics. More in details, the study presented below concerned both an in-depth analysis of current commercial and research UUVs, with the aim to define the specifications and the design of a new type of underwater vehicle, and the study of commercial low cost motors, with the purpose of improving their performance thus the one of the mobile robots they are mounted on.

In the introduction a short summary of the UUVs history is reported and all the vehicle of UNIFI DIEF are presented. In the first chapter, instead, a deep analysis of the state of art of underwater vehicles is reported. This study has been divided into AUVs (Autonomous Underwater Vehicles), ROVs (Remotely Operated Vehicle) and Gliders features, taking into account especially their propulsion systems. In addition, based on also the study of the state of art, the conceptual design of an innovative vehicle capable of changing its shape and its thrusters layout is synthetized. In the following chapter (chapter 2), the design of the innovative vehicle is described, in order to verify the feasibility of the vehicle itself exploiting current technology and to estimate its performances and the budget required for its realization. In chapter 3, a low cost commercial thruster is presented. With these thrusters all the vehicles of UNIFI DIEF have been equipped; for this reason, the third chapter reports a deep experimental study to define the relation between thruster parameters and the input command. This study has been very important because it allows improving the thruster parameters estimation and consequently the control performances. In addition, in this third chapter the new vehicle designed by UNIFI DIEF with the collaboration of MDM Team s.r.l. (an University of Florence Spin Off) and named ZENO is presented. In chapter 4, it is shown how the thruster studied in the previous chapter has been upgraded and hardware modifications have been made. More in details, in this chapter it is explained how a Hall effect sensor has been integrated in the thruster in order to measure the rotor speed. In addition, it is shown how a low cost closed loop control system has been implemented for the thruster previously described and the results obtained on dedicated test rig are given. Finally, in the conclusion the results obtained are summarized, highlighting how the designed innovative vehicle is feasible and has the performances required by its hypothetical application. In addition, it is summarized how the studied thrusters have improved the UNIFI DIEF vehicles performances.

Introduction

Introduction

I.1 Unmanned Underwater Vehicles.

UUVs are vehicles able to operate underwater without a human occupant. Over the years, the evolution of underwater vehicles has led to the realization of several kind of drones, with particular characteristics tailored for the specific tasks or environments. For this reason, the world of UUVs is extremely wide, but it is possible to identify two main classes (Figure I.1):

- **AUV**: this kind of UUVs are completely autonomous. For this reason, they do not require any type of connection cable and operator to carry out their tasks. An AUV can perform a mission on long distance, with the only limit of power consumption.
- **ROV**: a human operator drives this kind of vehicles by means of a control station, usually located on a support ship. The UUV is linked to the ship by an umbilical cable, which ensures the power supply and the communication with the vehicle.

These two classes have particular differences, due to their specific use. Indeed, most of ROVs have a cubic shape, with a strong motion symmetry, because the main application is the underwater inspection and manipulation. Otherwise, most of AUVs have a torpedo shape and are equipped with one or two thrusters on the stern and some rudders to dive for long distance. Only in the last few years, with the improving of control algorithms their shape and thrusters layouts, some AUVs have become more similar to standard ROVs, allowing to improve the maneuverability of autonomous vehicles.

Figure I.1: UUVs examples.

I.2 UUVs applications.

In early 50s, research centers started to study and develop vehicles for underwater exploration. The first UUV ever built was the ROV named POODLE [1] [2] (Figure I.2). This vehicle was built by

Dimitri Rebikoff a French engineer with the desire to take a look at some Mediterranean wrecks, that were too deep for divers. The vehicle was very simple. He installed a camera in a pressure-resistant housing, added a water-corrected lens, and mounted it on a tether-controlled vehicle, equipped with a stern thruster and two bow rudders.

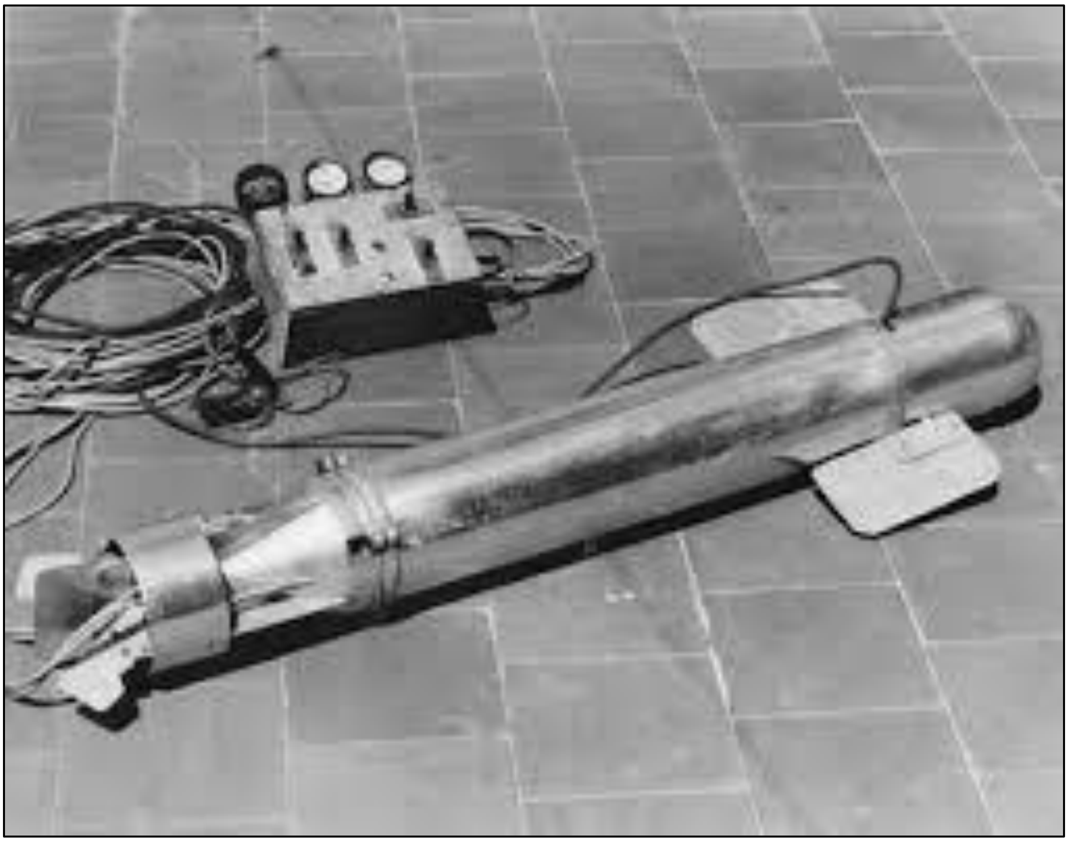

Figure I.2: POODLE ROV.

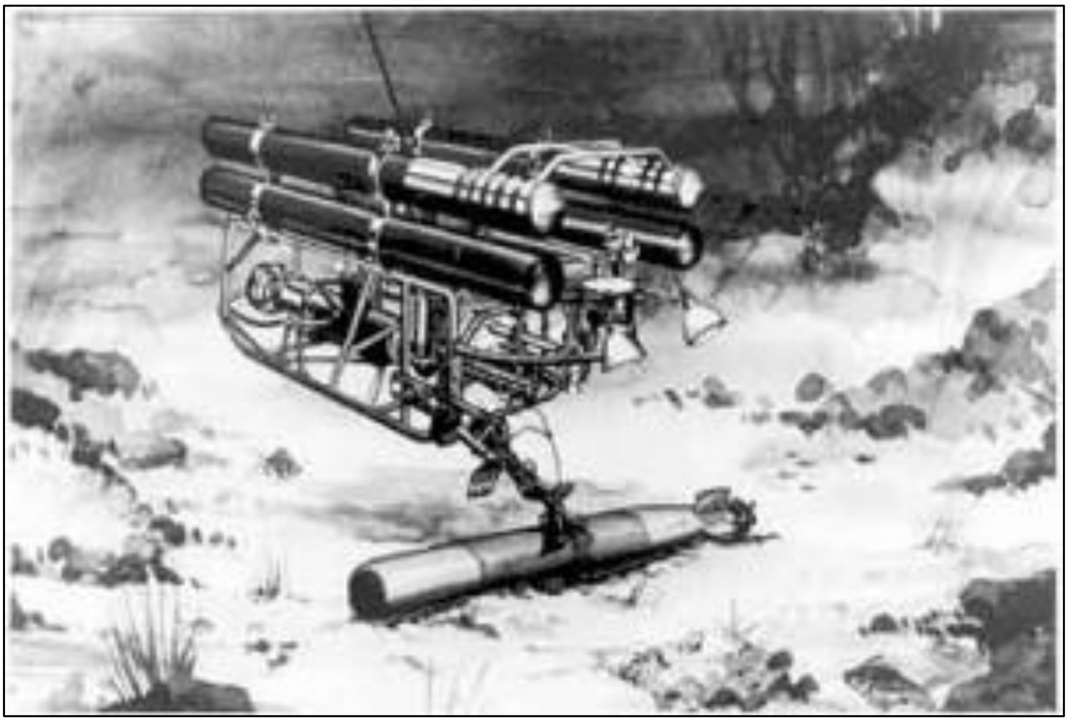

Figure I.3: Drawing of CURV-I.

Suddenly, in the early of the 60s, the U.S. Navy presented to the world the first "modern" ROV named CURV [1] [2] (Cable-controlled Undersea Recovery Vehicle), visible in Figure I.3. This UUV had simply defined the concept of ROV: a metal frame/truss that supports all the watertight casings and motors. However, this was not the only revolutionary intuition of the designers, because it was the first armed ROV in the history. Indeed, this vehicle was thought to bring back torpedoes that failed to rise to the surface after test shots up to 3000 m.

Figure I.4: SPURV by University of Washington's Applied Physics Laboratory.

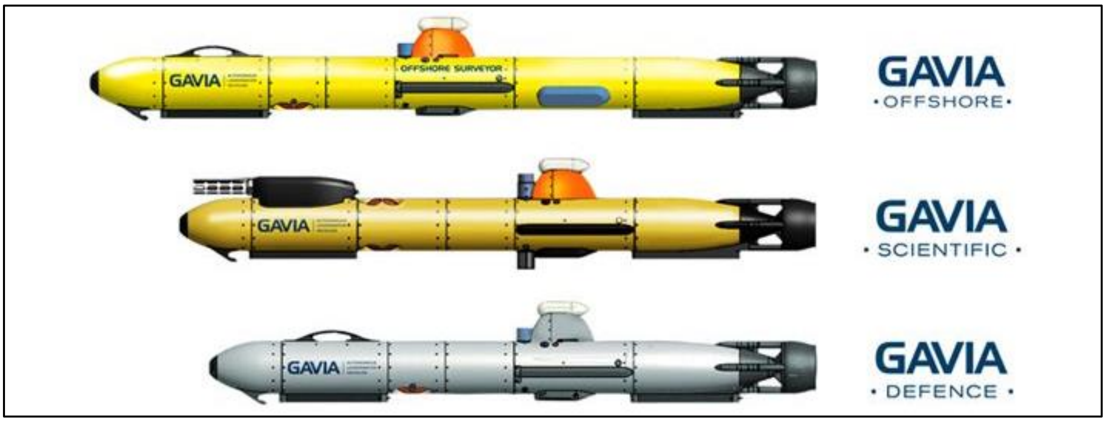

Figure I.5: GAVIA by TELEDYNE GAVIA ehf.

Surprisingly, only few years after the first ROV the research about AUV started. Indeed, at the end of the 50s the first autonomous vehicles appeared. One of the first AUV built was the SPURV (Special Purpose Underwater Research Vehicle) [3] in 1957 by the University of Washington's Applied Physics Laboratory and it is visible in Figure I.4. The Office of Naval Research funded this vehicle, which could dive up to 3000 meters and operate for four hours. In the following years, the research on underwater vehicles significantly grew, because UUVs remained an extremely attractive option for deep-sea researchers. Later, it became evident that underwater vehicles can make easier work on the seabed: for this reason, the ROVs use grew and different commercial vehicles were available for different applications such as mine countermeasures [4], maintenance of oil and gas plants, shipwrecks exploration, etc. In the meanwhile, the development of automation led to creation of autonomous vehicle increasingly reliable; over the years, many AUVs were thus presented, as e.g. GAVIA [5] (Figure I.5), especially thought for underwater archaeology and sea monitoring. In addition, a new subgroup of AUVs, named gliders, was born. Gliders are simply UUVs that mainly use small changes in their buoyancy and rudders, in order to move up and down in the ocean with very low power consumption. This solution allows the vehicles to stay in water for long period and to dive for very long-distances, making them perfect to monitor the marine environment.

I.3 UNIFI DIEF vehicles.

Underwater robotics activities at the Department of Industrial Engineering of the University of Florence started in the 2010, and in the last eight years, different AUVs and control and localization algorithms were developed and tested. One result of this work has been the construction of four different vehicles:

- Typhoon [6] [7] [8],
- MARTA (MArine Robotic Tool for Archaeology) [9],
- FeelHippo [10],
- ZENO (ZENO Environment Nautical Operator) [11].

All these vehicles were developed principally for archeological applications, although with different performance, as explained below. It is worth noting that these tools can be exploited for different purpose and in other applications just changing their payload.

I.3.1 Typhoon AUV [6] [7] [8].

THESAURUS (TecnicHe per l'Esplorazione Sottomarina Archeologica mediante l'Utilizzo di Robot aUtonomi in Sciami) was the first project concerning underwater robotics faced by our research group (2011-2013). More in details, the project, funded by the Tuscany Region, had among its goals the development of technologies and methodologies for archaeological search with autonomous underwater vehicles working as a team in exploration mission. For this reason, one of the principal goals of THESAURUS was the development of a swarm of AUVs, equipped with optical and acoustic payloads, capable of cooperating, through acoustic modem, to identify areas of archeological interest on the seabed. The team of AUVs was made up of three Typhoon-class vehicles. More in details, the MDM Lab had the task to design and build Typhoon AUVs (Figure I.6). These vehicles are a middle-sized class AUVs and present some innovative features, which greatly contribute to reduce production and maintenance costs. The particular features can be easily summarized:

- extended use of fiberglass: composite materials are cheap and offers great corrosion resistance, so the production cost of the hull is quite low;
- modular mechanical design with commercial components: lots of components are standardized and interchangeable, for this reason the vehicle is easy to maintain;
- extended use of fast prototyping techniques: the vehicle is easy customizable since many components and accessories are built using ABS plastic material, shaped using 3D printers.

The thruster layout chosen for these vehicles is based on 6 different thrusters and allow controlling 5 DOFs (Degree Of Freedoms). More in details, Typhoons have two thrusters with ducted propeller placed on the stern. These two motors provide the thrust needed to perform longitudinal translation, and also yaw turns at high speed. The other 4 motors are tunneled and pass through the hull. Two of them (one placed near the bow, the other one placed near the stern) allow the vehicle to move itself in lateral direction and to turn itself around the vertical axis (for yaw at low speed). The last two allow the Typhoons to perform translation along the vertical direction and rotation around the transversal axis of the vehicle. The choice to control only 5 DOFs is related to the shape of these AUVs. Indeed, the torpedo shaped does not require a precise control of the rotation around longitudinal direction (roll), because external disturbances do not produce wide rotations. For this reason, roll movements are limited just putting the AUV center of gravity below its center of buoyancy (hydrostatic stability).

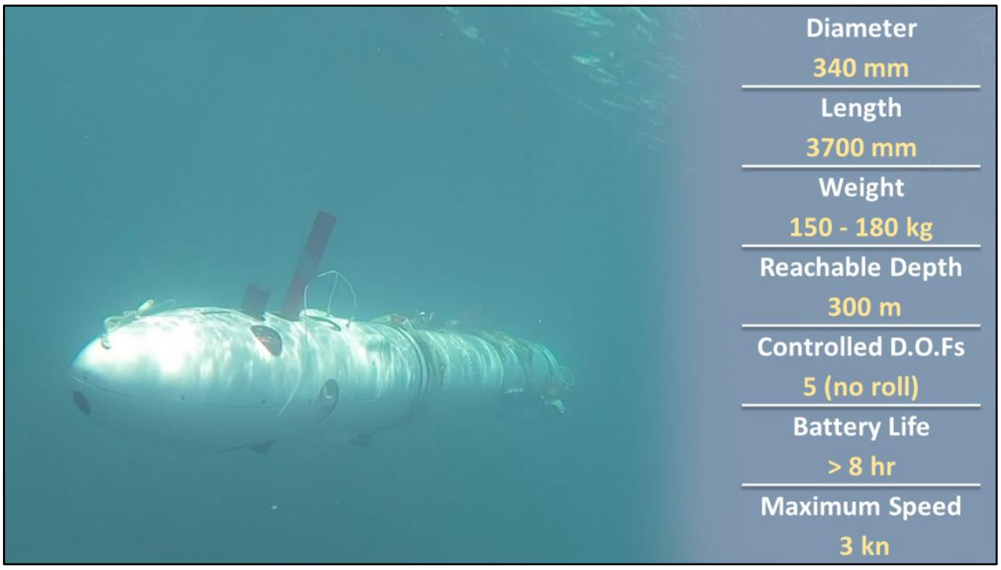

Figure I.6: Typhoon AUV main specifications.

I.3.2 MARTA AUV [9].

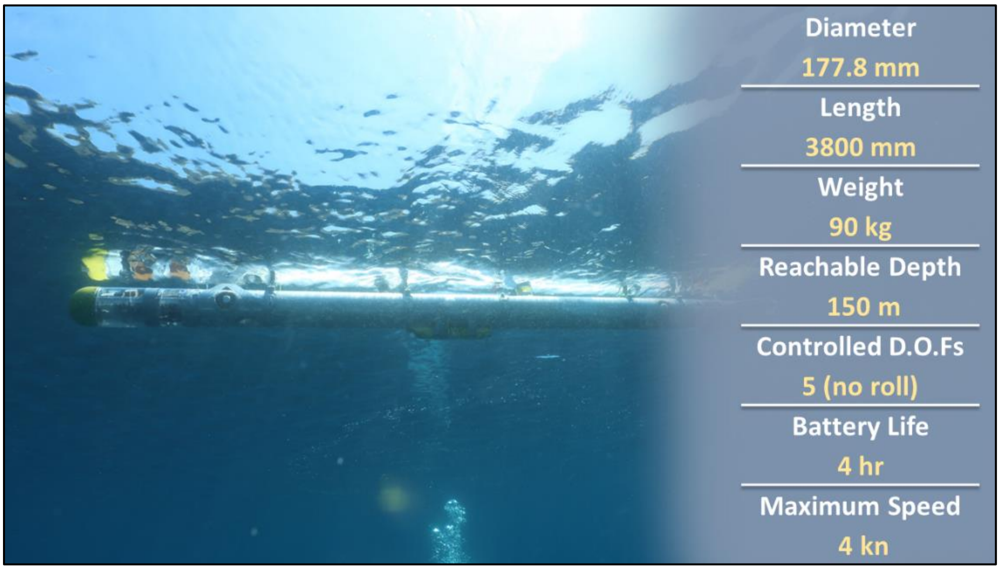

Figure I.7: MARTA AUV main specifications.

The ARROWS [12] (ARchaeological RObot systems for the World's Seas) project was funded by the European Commission in the framework of the FP7 call ENV-2012, challenge 6.2-6, devoted to development of advanced technologies and tools for mapping, diagnosing, excavating, and securing underwater and coastal archaeological sites (2012-2015). The project proposed to adapt and develop low cost autonomous underwater vehicle technologies to reduce the cost of archaeological operations. The main aim of ARROWS was to identify the archaeologist's requirements in all phases of the campaign, identify problems and propose technological solutions suitable for archaeologist's needs. During this project, the task of MDM Lab was the design and construction of a small-sized AUV, named MARTA (Figure I.7), acronym for MArine Robotic Tool for Archaeology. MARTA is light enough in order to be deployable by three people from a small boat or pier. The most interesting feature of this vehicle is its modularity. This solution allows to easily adapt the vehicle to exploration needs. Unlike Typhoon, the hull was made in anodize aluminum: the choice of Al Anticorodal type 6082 T6 is a good trade-off among workability, lightness and mechanical strength. The modules are connected together with suitable plastic wires to make fast and easy the assembling and disassembling phases. MARTA AUV becomes watertight only after the modules have been connected together, (the only wet sections are the bow and the stern): two radial O-rings are placed at the end of each module and assure a watertight connection. After the whole vehicle assembly, it is necessary to create a depressurization of 0.3 bar inside by means of a vacuum pump to ensure a better alignment between the modules and to provide an adequate stiffness. Regarding the thrusters layout, MARTA has the same layout of Typhoons-class AUVs.

I.3.3 FeelHippo AUV [10].

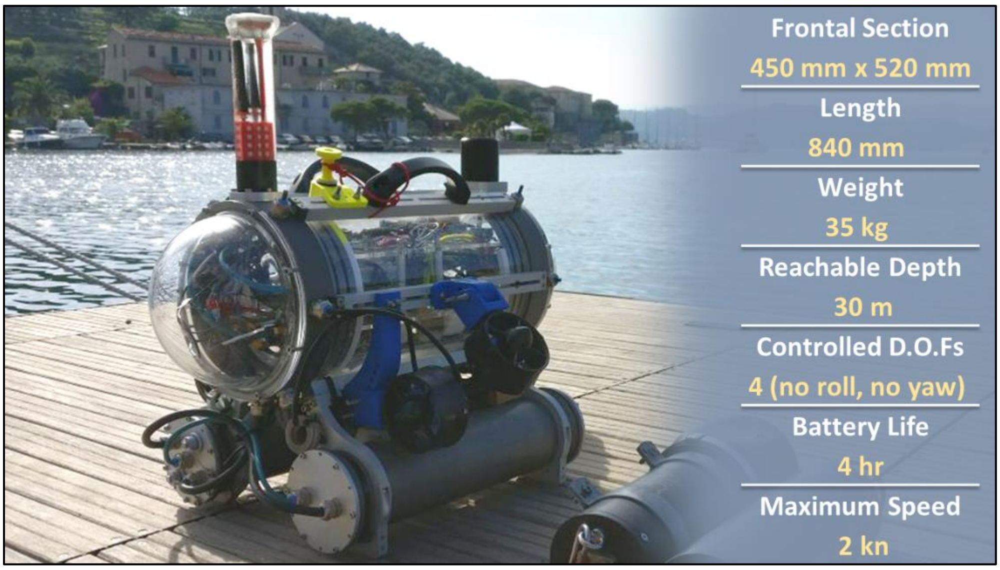

Figure I.8: FeelHippo AUV main specifications.

Unlike the other vehicles of the MDM Lab, FeelHippo (Figure I.8) is not the result of a founded project. This vehicle has been specially designed to be a development platform to test new payloads and new control algorithms for both the MDM Lab researchers and for the students of the University of Florence. Proof of this, the vehicle took part to several monitoring tasks and international student competitions:

- SAUC-E (Student Autonomous Underwater Challenge - Europe) in 2013 [13];
- euRathlon in 2015 [14];
- SAUC-E in 2016 [13];
- ERL Emergency Robots in 2017 [15];
- SAUC-E in 2018 [13].

In these events, it has always achieved good results, until reaching the first price in the last competition (SAUC-E 2018). The vehicle is light, cheap, small and with an operating depth of a few meters (up to 30 m). The result of these choices is a vehicle with a main structure made of Aluminum alloy Anticorodal type 6082-T6 and PMMA, commercially known as Plexiglas®. More in details, the vehicle central body is a Plexiglas® tube containing the instrumental hardware, while the structural connections and the two tubes under the main body, in which are located the batteries, are in Anticorodal type 6082-T6. Other external elements have been printed in ABS (Acrylonitrile Butadiene Styrene) with a 3D printer of the MDM Lab (Stratasys Dimension Elite). In addition, to reduce the number of motors of the vehicle, FeelHippo AUV has only 4 thrusters. According to this choice, FeelHippo AUV is an under-actuated mobile motion; indeed only 4 DOFs are controlled. Therefore, the vehicle design is thought to have limited roll and pitch angles during the vehicle navigation. This feature is commonly adopted in AUV design and is obtained, as mentioned also before, by putting its center of gravity below its center of buoyancy.

I.3.4 ZENO AUV [11].

The ARCHEOSUb (Autonomous underwater Robotic and sensing systems for Cultural HEritage discovery cOnservation and in SitU valorization) [16] EASME EU project aims to develop products and services in support of the discovery of new Underwater Cultural Heritage (UCH) sites and of the surveying, conservation, protection, and valorization of new and existing ones (2017-2019). In particular, the project will try to realize an in-situ underwater sensor network for real-time monitoring and surveillance. The network will be a complex system composed by mobile nodes and static nodes, which allow to a real time communication of multimedia and accurately locate underwater vehicle and divers. In ARCHEOSUb the mobiles nodes are AUVs. For this reason, ZENO (ZENO Environment Nautical Operator), visible in Figure I.9, is a compact AUV designed and developed by the Department of Industrial Engineering of the University of Florence in collaboration with MDM Team S.r.l., an official spin-off company of the University of Florence. More in details, it has been designed as a low cost, light, compact and high-performance AUV to provide support during all the steps of a typical archaeological campaign; the AUV is indeed configurable and customizable with different sensors and payloads. For these features, it can be easily deployed from a pier or a small boat and it is transportable by two people. The basic platform is fully controlled in each DOF, ensuring accurate positioning and hovering capability, by means of 8 marine propellers, i.e. 4 vertical thrusters and 4 horizontal thrusters in vectored configuration. More details are given in §3.3.

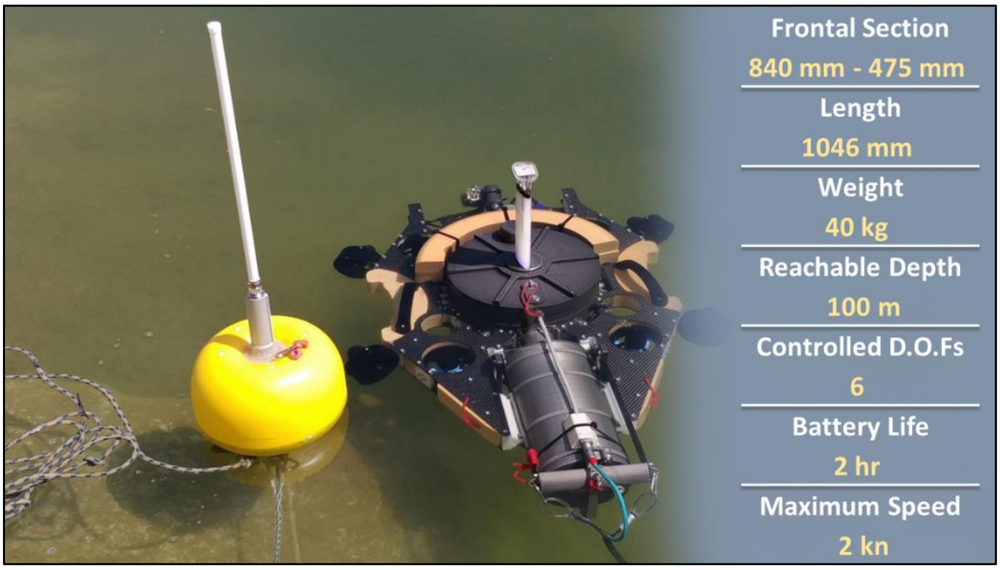

Figure I.9: ZENO AUV main specifications.

Chapter 1

A new kind of vehicle

1.1 A meeting point.

Nowadays, the use of UUVs can be divided into two big classes that can be named survey and servicing, for reasons of simplicity. The survey category includes all the applications of surveillance and monitoring, while servicing includes applications that require interactions with structure, plants and wrecks (e.g. underwater intervention/manipulation). It is worth noting that the vehicles design is strongly affected by survey and servicing features. Indeed, we can observe that in the sector of surveillance all kinds of UUVs are employed. Otherwise, in the sector of servicing the types of vehicles normally used are ROVs. This important difference is related to the necessity of having human supervision to control the underwater operations, during the interaction with the environment. Obviously, this need is due to the risk of damages working structures and priceless shipwrecks, because, currently, artificial intelligence is not yet completely reliable and studied, even if this situation will likely change in the near future.

Otherwise, concerning the use of UUVs for monitoring mission, this is related to the capability to bring onboard payloads. For this reason, both AUVs and ROVs can be employed. Obviously, AUVs are used mainly for long-distance exploring and monitoring, while ROVs are employed only for short-distance monitoring especially for shipwrecks and underwater structures, due to the umbilical cable constrain. Within this context, it is extremely important to observe that needs of long-distance and short-distance dives are antithetical. In the first case, the main needs are a low power consumption navigation and high fluid dynamics efficiency to travel the longest possible distances, taking into account of course the limited amount of power stored in the batteries. In the second case, as for serving operations, the most important things are stability, the capability to face water streams, high maneuverability and high power (this is usually not a problem, considering the physical link with a support ship), especially in case of underwater manipulation.

Figure 1.1: SMART-E AUV [17].

As argued above, these two categories are mainly characterized each by a particular shape: torpedo and cubic. Obviously, a torpedo shaped is more suitable for long-distance dives due to the good fluid-dynamics features in the longitudinal direction, while a cubic shape is more suitable for short-distance navigation due to the possibility of having symmetric thrusters layout leading to high maneuverability.

However, in the last years, new demands are born and a new kind of vehicles have been studied and developed for particular applications. For example, the SMART-E AUV [17] has been developed especially for exploration tasks that require a high maneuverability and agility in order to provide access in hard-to-reach areas. This vehicle, visible in Figure 1.1, is a fully holonomic AUV inspired by the ODIN project [18]. Its shape is very peculiar; indeed an elliptical hull encloses the electronic hardware, while three podded thrusters, arranged at 120° angles to each other, ensure a 3D propulsion to the vehicle. This solution, allows using the minimal number of thrusters to perform a 3D navigation. Performances of the vehicle are very limited due to its extreme lightweight; indeed, despite its high maneuverability, the power stored is very low and only optical are on board.

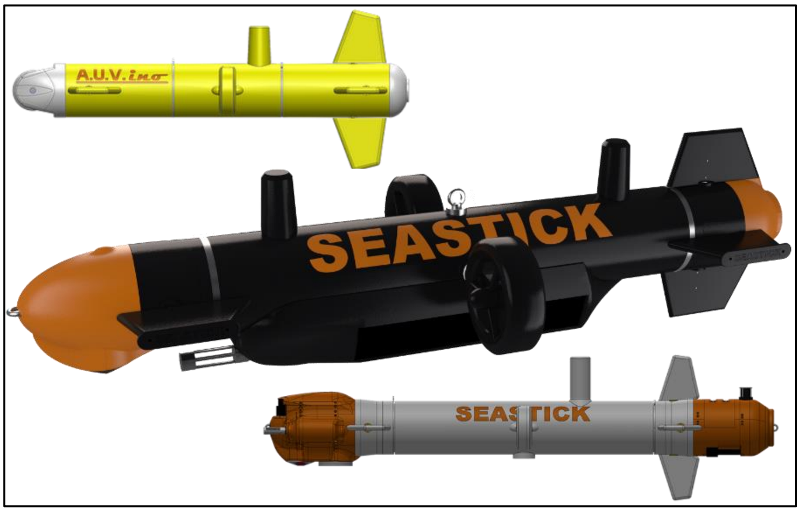

Figure 1.2: Seastick family. A.U.V. ino on top, Seastick 300 in the middle and Seastick 1000 on below.

Another interesting group of vehicles is the Seastick family [19], visible in Figure 1.2. The difference between these three AUVs is simply in their dimensions: A.U.V. ino is the smallest and lightest, Seastick 300 is the intermediate AUV, while Seastick 1000 is the biggest one with highest performances. All these vehicles were developed as payloads platforms, for this reason, the battery can be easily replaced and the structure is made of three main sections: bow, stern and main body. The main innovation of this kind of vehicle is the employment of two lateral rotating podded thrusters that confer to common torpedo shaped AUVs a considerable capability of maneuver.

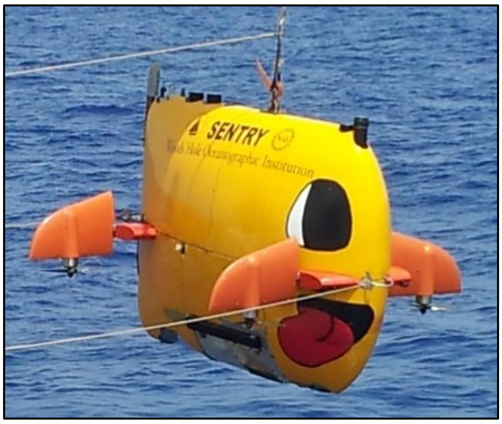

Figure 1.3: Sentry AUV.

In addition to the vehicles described above, there is an AUV with a similar propulsion system named Sentry [20], visible in Figure 1.3. This vehicle has been designed and built in 2010 by Woods Hole Oceanographic Institution (WHOI), USA, thanks to the experience in developing a previous vehicle called ABE (Autonomous Benthic Explorer) [21]. The aim of this vehicle was preserving the thrusters configuration of its predecessor able to provide hovering abilities and having a large distance between the center of buoyancy and the center of mass to minimize vehicle pitch and roll, with the addition of the hydrodynamic efficiency of a torpedo shaped AUV. The adopted solution is an elongated body in vertical direction with the goal of maximizing the distance between the center of buoyancy and the center of mass. In addition, the vehicle is equipped with four thrusters mounted on articulated wings, so the podded thrusters act as rudder.

Figure 1.4: EELUME AUV.

Currently, one of the most innovative vehicles is made by EELUME [22] (Figure 1.4); this biomimetic vehicle is the result of the work of the last 10 years of research on snake robotics at NTNU and SINTEF in Trondheim (Norway). This AUV was thought as a synthesis of a torpedo AUV, a small inspection UUVs and an intervention ROV, with the main aim of residing on the sea bottom to provide immediate response to unpredicted inspection, maintenance and repair requirements. More in detail, it is a modular, flexible robot capable of swimming like a snake, or being propelled by conventional thrusters. The vehicle can be assembled with an arbitrary number of elements linked each other with a flexible joint. Currently, only five or six different modules are available. In the last few years, the vehicle from EELUME has been tested as inspection ROV, but tests as an AUV are scheduled during this year to explore its manipulation capability. The main features of the vehicle are high flexibility, that allow changing its shape, and the capability to move itself in narrow structures. In this way, it can dive as a torpedo shaped vehicle on long distance, but it is also able to manipulate objects with appropriate terminal elements, as visible in Figure 1.4.

In light of this, it is quite clear that UUVs are evolving to improve their maneuverability and diving capability. In addition, the new frontier of underwater vehicles could be combining the diving capability of AUVs with the intervention and inspection capability of ROVs. The goal is making the management of underwater structures autonomous, e.g. maintenance of underwater power plants or surveillance of some underwater sites, located in the same area but not too close to each other. Such an innovation will be relevant for offshore marine operation, because it will allow the reduction of the employment of support ships, reducing one of the most important cost items for the service marine companies. An UUV capable of this has to combine the capability to dive for long distance in a very efficient way with the capability to maneuver and accurately intervene near and on underwater structure and shipwrecks, of course even in presence of underwater streams, usually present in real scenarios. The easiest solution is to develop a vehicle able to change its hydrodynamic shape. The basic idea is a vehicle with a high hydrodynamic efficiency during longitudinal navigation to minimize power consumption and a high hydrodynamic symmetry during inspection tasks to make UUV behavior more predictable and more controllable. Houston Mechatronics presented a concept of a similar vehicle in spring 2018. Houston Mechatronics is a subsea service company with deep expertise in robotics and intelligent automation, founded by former NASA roboticists responsible for designing and developing some of the most advanced robots in the world. The conceptual vehicle, named Aquanaut [23], employs a patented shape-shifting transformation from a hydrodynamic UUV to a UUV with two arms able to manipulate object on the seabed (Figure 1.5). More in details, in the closed version the vehicle appears as a classical UUV with a torpedo shape. In this configuration, it can move itself with only three motor for long distance, controlling only three D.O.Fs. In the open version, the upper part of the hull moves away from the main body, exposing other four motors and two arms. In addition, the rear motors change their position and give to the vehicle a vectored motors configuration. In this way, Aquanaut becomes a full 6 DOFs controllable UUV with the capability of stably manipulating.

Figure 1.5: Transformation of Aquanaut AUV by Houston Mechatronics.

The main goal of this thesis work is overcome the simple hydrodynamics shape change, adding to an innovative vehicle the capability of changing its structure and its motor configuration in a more substantial manner.

The change of the structure geometry has three main advantages:

1. Redistribution of the vehicle mass.
2. Reconfiguration of thrusters.
3. Changing hydrodynamics behavior.

The first point allows optimizing the mechanical stability of the vehicle. Indeed, during the long-distance navigation all the mass of the vehicle is very close to the longitudinal axis of the vehicle improving high-speed forward navigation. Otherwise, an enlargement of the vehicle structure allows to increase the momentum of inertia of the vehicle in all the directions. It is this condition that gives more mechanical stability to the UUV, during manipulation tasks.

The second point, allows optimizing the thrusts of the propellers, maximizing their effects and reducing the power consumption. Indeed, during long-distance navigation it is possible to focus the overall available thrust to push forward the vehicle. Otherwise, a more symmetrical thrusters layout during intervention or manipulation tasks allows to rapidly response to water streams change or to other unexpected external disturbances.

The third point, as mentioned above, not only allow reducing the power consumption during long-distance navigation, but also gives hydrodynamics stability during inspection or manipulation.

The conceptual idea is based on an articulated quadrilateral with equal rods. This kind of solution allows switching between a stocky and symmetrical shape and an elongated one (Figure 1.6). In the first case, the vehicle has symmetrical fluid-dynamic behavior and it is able to withstand tilting load with its shape stability. In the close configuration, instead the vehicle has a shape very similar to a torpedo maximizing the longitudinal fluid-dynamic efficiency and its capability to dive a navigate on long-distances.

The conceptual idea shares some elements compared to EELUME vehicle. Indeed in this work, a synthesis between a standard AUV and an intervention/inspection ROV is investigated giving to the vehicle the capability to change its motors positions and its shape. However, the approach to obtain this result is antithetical. Actually, here the study starts from a closed loop kinematics concept instead of an open loop kinematics, as did by EELUME. This choice is related to the intention of maximizing the shape stability and of giving to the vehicle the capability to store different instruments inside even of a considerable size.

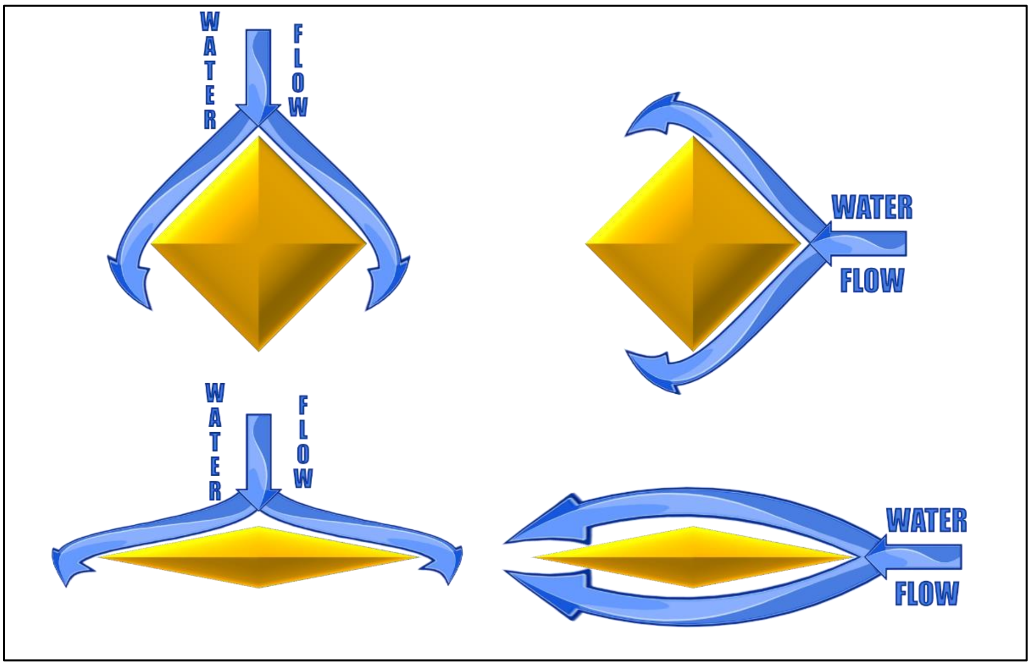

Figure 1.6: Water flow around concept shapes.

1.2 Common AUVs features.

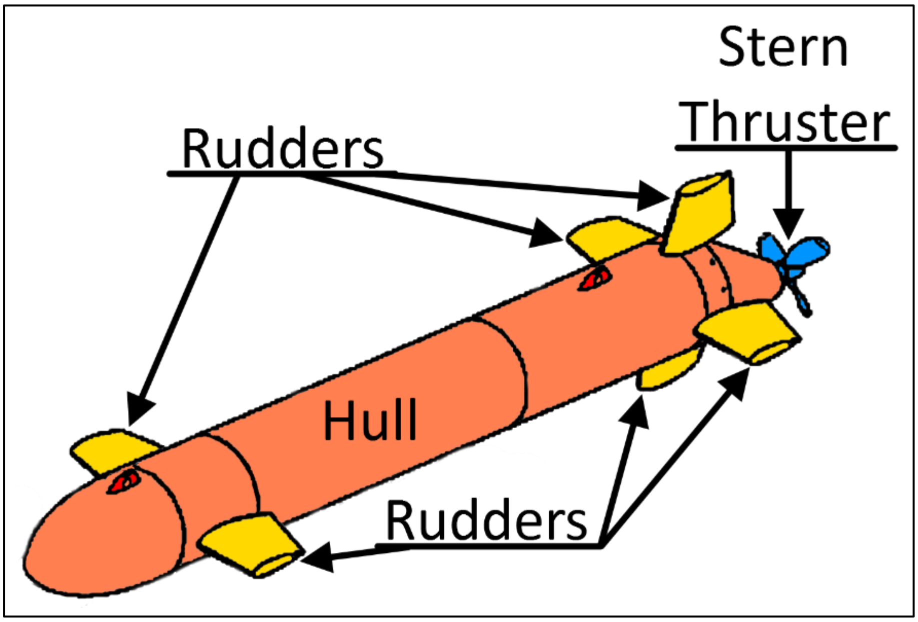

Figure 1.7: Generic AUV mechanical scheme.

Company	Name	Category	N. Motors	Vectored	Gimbaled thruster	N. Fins	Roll	Pitch	Yaw	Surge	Sway	Heave
Bluefin Robotics (General Dynamics Mission Systems)	Bluefin-21	Heavy	1	✗	✓	0	✗	✓	✓	✓	✗	✗
Bluefin Robotics (General Dynamics Mission Systems)	Bluefin SandShark	Ultra-Light	1	✗	✗	3	✓	✓	✓	✓	✗	✗
Bluefin Robotics (General Dynamics Mission Systems)	Bluefin HAUV	Light	5	✗	✗	0	✗	✓	✓	✓	✓	✓
Gabri s.r.l	Seastick 300 AUV	Light	2	✗	✗	6	✓	✓	✓	✓	✓	✓
Girona Underwater Vision and Robotics	SPARUS II AUV	Light	3	✗	✗	2	✓	✓	✓	✓	✗	✓
Hydroid (Kongsberg)	Remus 100	Light	1	✗	✗	4	✓	✓	✓	✓	✗	✗
Hydroid (Kongsberg)	Remus 600	Middle	1	✗	✗	3	✓	✓	✓	✓	✗	✗
Hydroid (Kongsberg)	Remus 6000	Heavy	1	✗	✗	4	✓	✓	✓	✓	✗	✗
Kongsberg	HUGIN	Heavy	1	✗	✗	4	✓	✓	✓	✓	✗	✗
Kongsberg	MUNIN	Middle	1	✗	✗	3	✓	✓	✓	✓	✗	✗
Oceanscan	LAUV	Ultra-Light	1	✗	✗	4	✓	✓	✓	✓	✗	✗
Ocean Server Technology	Iver3	Light	1	✗	✗	4	✓	✓	✓	✓	✗	✗
Saab	Sabertooth	Heavy	5	✗	✗	0	✓	✓	✓	✓	✗	✗
SRS	Fusion	Ultra-Light	6	✓	✗	0	✓	✗	✓	✓	✓	✓
Subsea7	AIV	Middle	6	✓	✗	0	✓	✗	✓	✓	✓	✓
TELEDYNE	Gavia	Middle	1	✗	✗	4 (in duct)	✓	✓	✓	✓	✗	✗

Table 1.1: AUVs comparison.

In Table 1.1 some AUVs both from companies and research groups, and their main features are reported. For each vehicle, some details are underlined: the dimension (category), the number of thrusters, if thrusters are vectored or gimbaled, the number of fins and what kind of motions could the vehicle directly perform with its thrusters layout. Motions are only pure rotations and pure translations with respect to axes of the vehicle reference system. In particular, surge, sway and heave are respectively the longitudinal, the lateral and the vertical translation.

As noted above, the mechanical design of a common AUV is usually very simple: it consists of a watertight hull with a torpedo shape, a stern thruster and some mobile (rudders) or fixed flaps, as visible in Figure 1.7. In this configuration, the stern thruster provides all the propulsion power while rudders steer the vehicle in the desired direction and fixed fins increase the overall stability. In Table 1.1 the 56% of the presented vehicles adopts this simple design. They have one motor and 3 or 4 flaps. In this way, it is possible to combine a good maneuverability with a simple design. Indeed, this kind of AUVs can perform almost all the basic motions, except sway and heave. For this reason, they can turn and change their depth only with a combination of other basic movements. For example, to change their depth, the vehicles need to modify their pitch orientation and then push themselves forward. A possible variant to this layout is the use of a gimbaled stern thruster. With this solution, only one orientable thruster replaces rudders, fins and stern thruster. The vehicle (i.g. Bluefin-21) can perform its movements simply steering the thruster in the desired direction. The drawback of this solution is that the roll movement is not controllable. Obviously, this problem can be resolved adding two lateral rudders or using counter-rotating propellers. In addition, it is possible to add other rudders or fins to increase the stability and maneuverability of the vehicle. However, for a torpedo shaped AUV, such as SPARUS II [24] [25] or MARTA, it is possible to use other propulsion schemes simply combining rudders, fins and thrusters. SPARUS II adopts a particular propulsion system based on 3 thrusters and 2 rudders. One vertical thruster is located on the center of mass of the vehicle, while other two thrusters are located on the side of stern in front of the two rudders. In this way, the vehicle is able to perform all basic movements except for lateral translation. On the other hand, MARTA uses 6 thrusters to control all the DOFs except roll, as mentioned in the previous chapter. Finally, in Table 1.1 all vehicles with 5 or 6 thrusters not have a torpedo shape and are very similar to ROVs: these vehicles are thought especially for inspection tasks. As can be seen, the number of this kind of vehicles is scarce. Indeed, in the table, only the 27% of the AUVs reported have stocky shape, but considering other real vehicles, not reported for reason of brevity, the percentage is even lower.

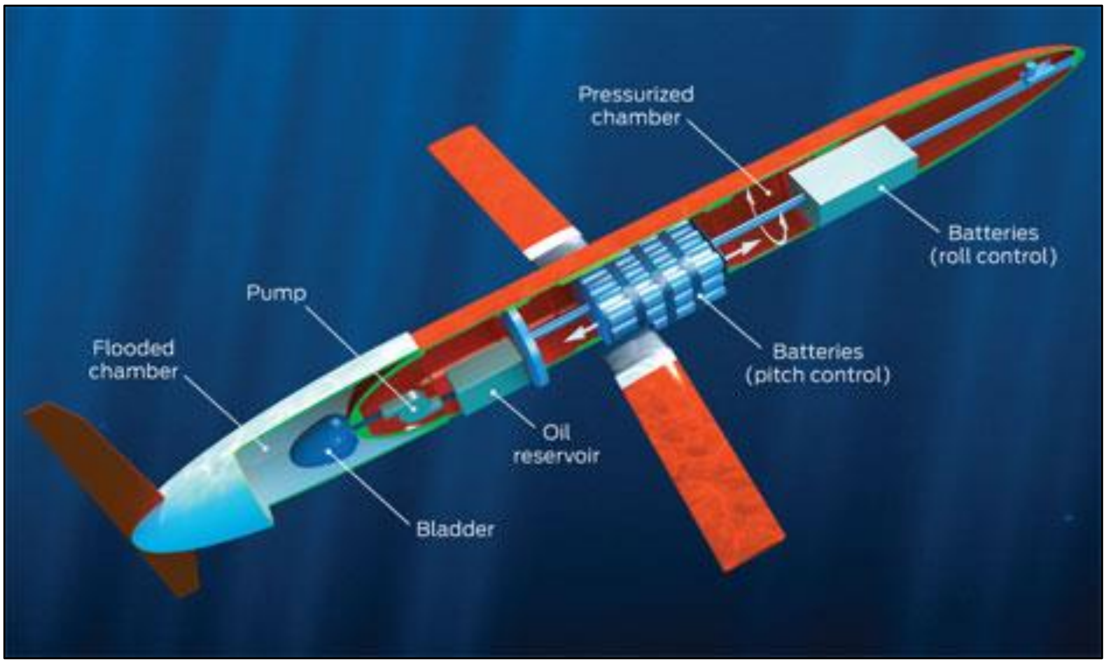

Figure 1.8: Generic glider mechanical scheme (Bluefin SPRAY).

Company	Name	N. Motors	N. Fins (no motion)	N. Fins	Roll	Pitch	Yaw	Surge	Sway	Heave
Alseamar	SEAEXPLORER	0	4	0	✓	✓	✗	✓	✗	✗
Bluefin	Spray	0	4	0	✓	✓	✗	✓	✗	✗
Kongsberg	Seaglider AUV	0	4	0	✓	✓	✗	✓	✗	✗
TELEDYNE	Slocum G3 Glider	0	3	0	✓	✓	✗	✓	✗	✗

Table 1.2: Gliders comparison.

Gliders belong to a special category of AUVs. More in details, these vehicles are especially thought to dive at low speed for long-distances and for long period of time with the least power consumption possible. These goals are cleverly obtained combining bladders, fins and electro-mechanics systems able to change the vehicle weight and buoyancy balancing. As visible in Figure 1.8, a glider does not have any kind of propulsion systems, because it exploits the underwater streams to glide over the seabed. Unlike air gliders, underwater gliders do not use rudders to sail water streams, but they simply change their attitude moving their center of mass and center of buoyancy. In Figure 1.8, it is clearly visible that it is possible to tune the center of mass position of the vehicle, moving the batteries pack. In Table 1.2 some gliders are reported. Differently from other AUVs, all of these AUVs have the same propulsion layout.

1.3 Common ROVs features.

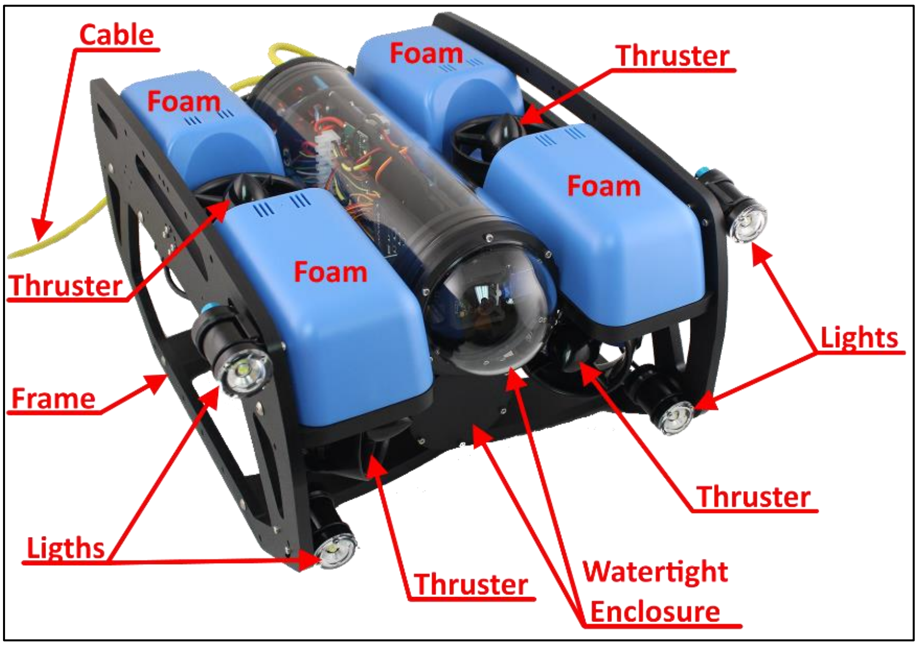

Figure 1.9: Generic ROV mechanical scheme (BlueRobotics BlueROV2).

In Table 1.3 some AUVs both from companies and research groups, and their main features are reported. As noticed above, ROVs are used mainly for inspection and intervention tasks. In these tasks, their operative speeds are usually very low and thus their hydrodynamics performance are not very important. Otherwise, ROVs need to have a high capability of maneuvering in narrow spaces, near expensive or important submerged object and structures without hitting anything and sometimes they are used for objects manipulation. For this reason, most of ROVs have a stocky and symmetrical shape and are built with a rigid frame supporting all other components without any fins, gimbaled or podded thrusters. More in details, a typical ROV has some buoyancy foam blocks on top, has many thrusters in a vectored configuration and some watertight casings for electronics. The most common thrusters layout entails the use of 4 vectored thrusters placed in the horizontal plane and at least one vertical thruster. This configuration gives to the vehicle a good maneuverability on the horizontal plane, but with only one vertical thruster controlling pitch and roll movements is not allowed. Obviously, by adding other vertical thrusters these rotations can be controlled. In addition, it is possible to use a thrusters layout that could be named “double vectored”, such as Saab Seaeye Jaguar and Ocean Modules V8 SII HD. These two vehicles have 4 vectored thrusters in the horizontal plane and other 4 vectored thrusters with an additional vertical angle. The first group of thrusters gives to the vehicles the capability of moving in the horizontal plane, while the second group adds a vertical thrust to control heave, roll and pitch, but also gives in this case additional thrust for longitudinal and lateral motion. This configuration allows the capability of stably maneuvering at any attitude and diving with high precision movements.

As regards small ROVs, the thrusters layout configurations are quite various. Another important feature of ROVs is the presence of a cable. The umbilical cable is the main difference between AUVs and ROVs and provides commands and power to the vehicle. Only in small vehicles, the cable provides only commands while the on-board batteries provide the required power (e.g. BlueROV2); when there is a considerable length, of the cable this imposes the necessity to use high voltage supply system and this is an uncomfortable solution for very small ROVs.

Company	Name	Category	N. Motors	Vectored	Gimbaled thruster	N. Fins	Roll	Pitch	Yaw	Surge	Sway	Heave
BlueRobotics	BlueROV2	Ultra-Light	6	✓	✗	0	✓	✗	✓	✓	✓	✓
DEEPOCEAN	WR-1	Heavy	7	✓	✗	0	✓	✓	✓	✓	✓	✓
Idrobotica	MULTIPLUTO	Light	4	✗	✗	0	✗	✗	✓	✓	✓	✓
Idrobotica	PLUTOPALLA	Light	4	✗	✗	0	✗	✗	✓	✓	✓	✓
Idrobotica	Pluto Plus ROV	Middle	4	✗	✗	0	✓	✓	✓	✓	✗	✗
Idrobotica	Pluto Gigas ROV	Heavy	8	✗	✗	0	✓	✓	✓	✓	✓	✗
Kystdesign	Constructor	Heavy	7	✓	✗	0	✓	✓	✓	✓	✓	✓
Kystdesign	Survey ROV	Heavy	11	✓	✗	2	✓	✓	✓	✓	✓	✓
NovaRay	NovRay 305/550	Ultra-Light	2	✗	✗	3	✓	✓	✓	✓	✗	✗
Ocean Modules	V8 SII HD	Light	8	✓	✗	0	✓	✓	✓	✓	✓	✓
Ocean Modules	V4 S300 OBSERVATION	Ultra-Light	3	✓	✗	0	✗	✗	✓	✓	✗	✓
SAAB	Seaeye Falcon	Light	5	✓	✗	0	✗	✗	✓	✓	✓	✓
SAAB	Seaeye Tiger	Middle	5	✓	✗	0	✗	✗	✓	✓	✓	✓
SAAB	Seaeye Lynx	Middle	6	✓	✗	0	✓	✗	✓	✓	✓	✓
SAAB	Seaeye Cougar-XT Compact	Middle	6	✓	✗	0	✓	✗	✓	✓	✓	✓
SAAB	Seaeye Panther	Middle	6	✓	✗	0	✗	✓	✓	✓	✓	✓
SAAB	Seaeye Panther-XT Plus	Heavy	10	✓	✗	0	✓	✗	✓	✓	✓	✓
SAAB	Seaeye Leopard	Heavy	11	✓	✗	0	✓	✓	✓	✓	✓	✓
SAAB	Seaeye Jaguar	Heavy	8	✓	✗	0	✓	✓	✓	✓	✓	✓
SAAB	Saab DOUBLE EAGLE	Heavy	8	✓	✗	0	✓	✓	✓	✓	✓	✓
SAAB	Saab DOUBLE EAGLE SAROV	Heavy	6	✓	✗	0	✓	✓	✓	✓	✓	✓
Sub-Atlantic	Mojave	Light	5	✓	✗	0	✗	✗	✓	✓	✓	✓
Sub-Atlantic	Mohawk	Middle	5	✓	✗	0	✗	✗	✓	✓	✓	✓
Sub-Atlantic	Mohican	Middle	6	✓	✗	0	✓	✗	✓	✓	✓	✓
Sub-Atlantic	Super Mohawk	Middle	6	✓	✗	0	✓	✗	✓	✓	✓	✓
Sub-Atlantic	Comanche	Heavy	7	✓	✗	0	✓	✓	✓	✓	✓	✓
Sub-Atlantic	XLX 200HP	Heavy	8	✓	✗	0	✓	✓	✓	✓	✓	✓
TELEDYNE	SeaBotix LBV200-4	Ultra-Light	4	✗	✗	0	✗	✗	✓	✓	✓	✓
TELEDYNE	SeaBotix LBV300-5	Ultra-Light	5	✗	✗	0	✓	✗	✓	✓	✓	✓
TELEDYNE	SeaBotix vLBV950	Ultra-Light	6	✓	✗	0	✓	✗	✓	✓	✓	✓
TELEDYNE	SeaBotix vLBV-10 SeaLift	Light	8	✓	✗	0	✓	✓	✓	✓	✓	✓
VideoRay	VideoRay PRO 4	Ultra-Light	3	✗	✗	0	✗	✗	✓	✓	✗	✓
VideoRay	VideoRay Mission Specialist	Ultra-Light	7	✓	✗	0	✓	✓	✓	✓	✓	✓

Table 1.3: ROVs comparison.

1.4 Design philosophy.

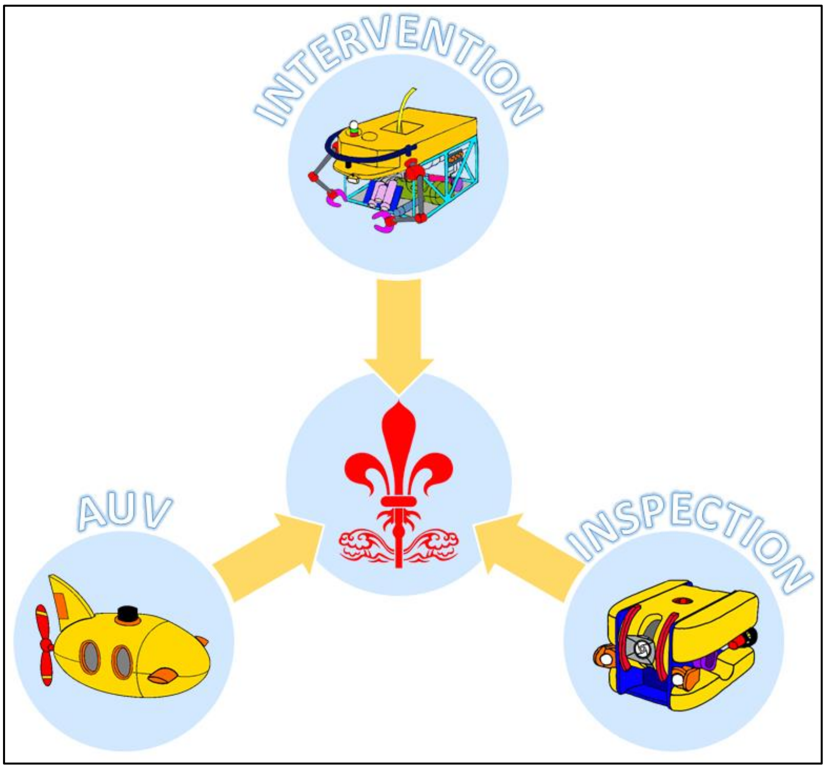

Figure 1.10: Vehicle concept.

As mentioned in the first paragraph of this chapter, the conceptual idea presented in this work concerns the definition of a multiclass reconfigurable vehicle. In other words, the study focused on the synthesis among an AUV, an inspection UUV and an intervention ROV, as shown in Figure 1.10. As noticed above, the starting point of the mechanical design was related to the vehicle shape and fluid dynamics considerations (Figure 1.6). The basic idea concerns an AUV with two main configurations (closed and open) and the ability autonomously to switch between them. The vehicle uses the closed configuration, to dive with the best fluid dynamic efficiency for long distance with minimum power consumption, while it uses the open configuration when it reaches a point of interest. In this way, exploiting the open configuration, it can maximize its own stability and its fluid dynamics symmetry to maneuver with precision and in safety condition around underwater objects. This ability is extremely important not only for stably inspecting underwater structures without hitting them, but it is also extremely important to safely manipulate objects. Obviously, being focused only on the shape would be very restrictive, so in this work the capability of reconfiguring the AUV thrusters layout, to maximize performances and exploit the whole potential of changing shape, has been deepened too.

To find the best thrusters layout, it is necessary a deep analysis of the possible thrusters configurations of UUVs. As mentioned above, the best motor configuration to maximize the vehicle controllability consists of using a vectored thrusters layout similar to common professional ROVs. With this consideration, it is possible to reduce the number of possible layouts to five configurations. In Table 1.4, an overview of the controllable DOFs with these five layouts is given. The table highlights that the 7 thrusters and the 8 thrusters are the most interesting configurations, because only these two configurations allow controlling all the mobile robot DOFs. More in details, as summarized in Table 1.5, the 5 thrusters layout has too many drawbacks. Indeed, a vehicle with 5 motors dives in a stable way only if the central thruster is perfectly in correspondence with the centers of mass and buoyancy of the vehicle. This condition makes impossible to safety control the vehicle near underwater objects.

Likewise, the 6 thrusters layouts give more controllability to the vehicle and a better components distribution, but they do not solve all the control problems. With the 7 thrusters layout there is only one problem, but sometimes non-negligible: the disposition of the three vertical thrusters leads to structural constraints making complicate closing the vehicle and locating the other components. Differently, the 8 thrusters layout satisfies all the motion and the mechanical needs. Indeed, with 8 thrusters it is possible to control all the DOFs, leaving free the central part of the vehicle.

Scheme	Name	Roll	Pitch	Yaw	Surge	Sway	Heave
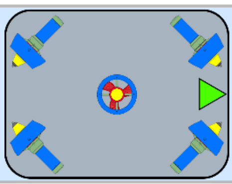	5 thrusters	✗	✗	✓	✓	✓	✓
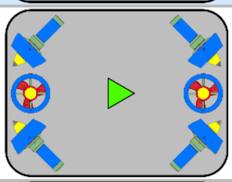	6 thrusters pitch	✗	✓	✓	✓	✓	✓
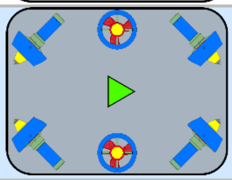	6 thrusters roll	✓	✗	✓	✓	✓	✓
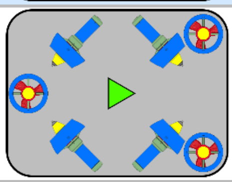	7 thrusters	✓	✓	✓	✓	✓	✓
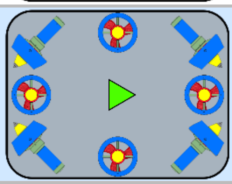	8 thrusters	✓	✓	✓	✓	✓	✓

Table 1.4: Thrusters layouts comparison.

Judgment	Scheme	Advantages	Disadvantages
✗	5 thrusters	– Minimum number of thrusters	– Underactuated – Low maneuver capability – Balancing problems – Only one motor to vertical thrust – Central motor reduce space of payloads
✗	6 thrusters pitch	– Limited number of thrusters – Good components disposition	– Underactuated – Critical balancing of roll DOF especially in open configuration
✗	6 thrusters roll	– Limited number of thrusters – Good components disposition	– Underactuated – Critical balancing of pitch DOF
✗	7 thrusters	– Minimum number of thrusters to control 6 DOFs	– Asymmetrical configuration (not suitable for torpedo shaped)
✓	8 thrusters	– Completely symmetrical – 6 DOFs completely controlled	– More thrusters than necessary

Table 1.5: Thrusters layouts advantages/disadvantages comparison.

The choice of 8 thrusters in a vectored configuration on horizontal plane allows easily changing thrusters configuration of the vehicle. Indeed, if the thrusters are connected to each side of the conceptual quadrilateral of Figure 1.11, in the open configuration the thrusters have a perfect vectored layout, while in the closed configuration the thrusters result aligned maximizing the thrust in the longitudinal direction.

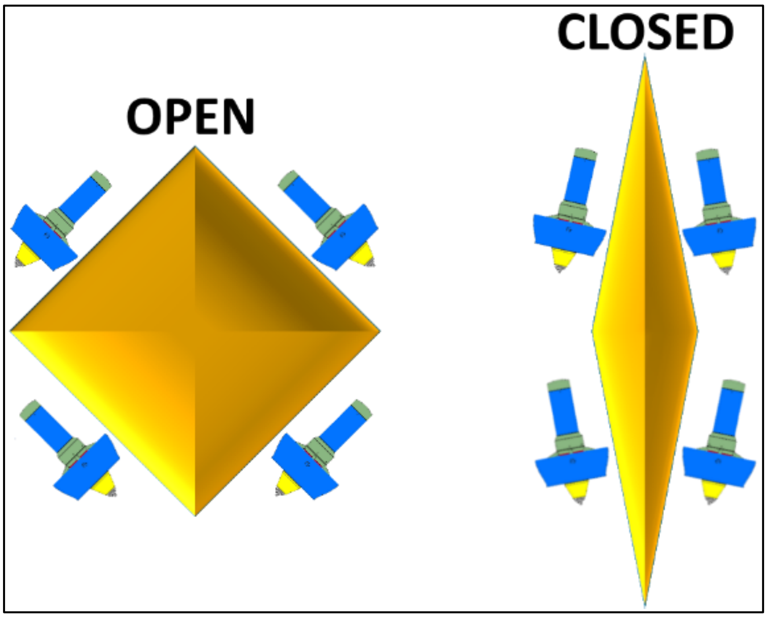

Figure 1.11: Vectored thrusters reconfiguration examples.

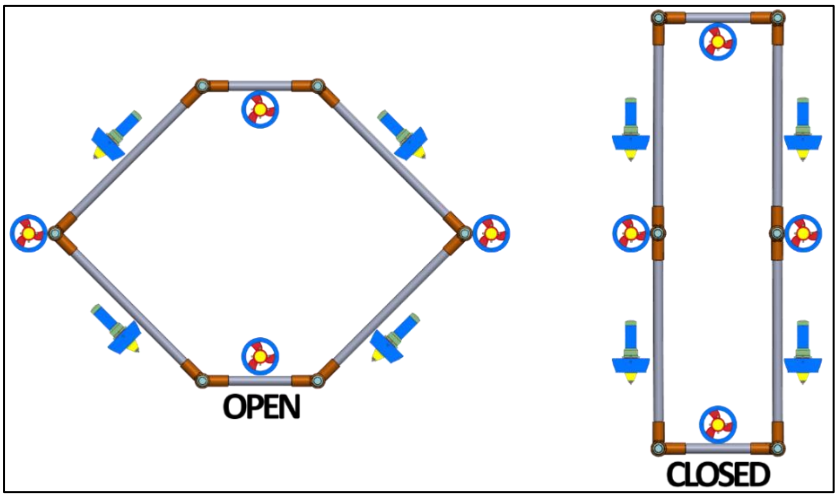

Figure 1.12: Thrusters layouts of the vehicle.

The transformation entails a big challenge: the vehicle has to maintain its balance in both the configurations, because compensating balancing errors with the thrusters would lead to an unnecessary waste of energy. The easiest solution is to design a vehicle with a modular structure and a symmetric thruster layout. In this way, it is possible to individually manage the balance of each elements. All these elements can be divided into three main groups: the frame, the hull and the electronics casings. The main frame, visible in Figure 1.12, is composed of six joints and six structural rods/links. These joints and structural elements allow the transformation and a better distribution of the components and payloads. On the contrary, the use of the simplest frame configuration, with only four joints and four rods, does not allow to easily place payloads in front of the vehicle. In addition, the frame is symmetrical and this condition allows maintaining the balance of the frame in both the configurations. Obviously, the frame also supports all the other elements of the robot. In addition, the hull provides buoyancy to the whole vehicle, provides protection to electronics casings and payloads and gives a hydrodynamic shape to the vehicle itself. Finally, the electronics casings are watertight and give protection to the electronics components. In addition, these housings have another important feature: each electronic casing has to have the same density of water, i.e. their motion can not unbalance the vehicle.

It is worth noting that the modularity of the vehicle gives to the project a big advantage: the scalability. Indeed, starting from the conceptual design it is possible to change the dimension and performances simply changing a few elements to adapt the vehicle to different classes of customers. For instance, to change the vehicle dimensions it is enough to just change the frame.

As noticed in the first part of this paragraph, it is clear that the vehicle proposed in this work can not be too small and light. Indeed, its closed loop structure requires to pay attention to collisions between internal parts when the vehicle is closed. Fortunately, this constraint is not a real problem for the vehicle. Indeed, the vehicle is thought for long distance navigation and for manipulation; for these reasons it is necessary to leave enough space to place both the batteries and robotic arms.

According to the vehicle modularity, it is useful to split all the vehicle elements into distinct modules. The best solution is to split them in functional groups with the aim to reduce as much as possible the internal electromagnetic noise:

- Core Module;
- Antenna Module;
- Power Module;
- Driver Module;
- Battery Module;
- Connection Module (additional element).

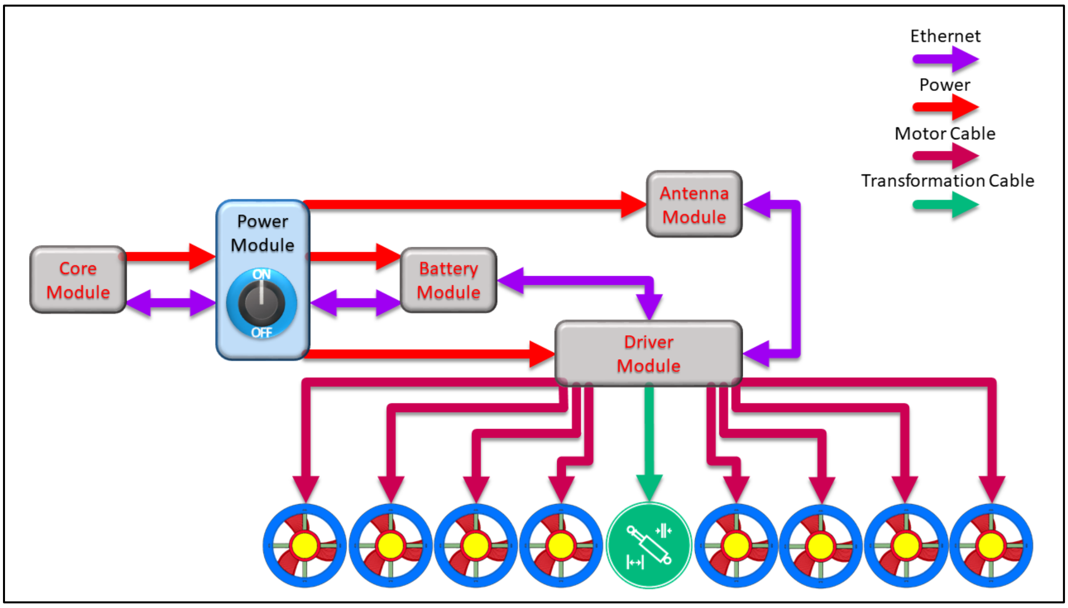

Figure 1.13: Conceptual AUV scheme.

The Core Module contains the main pc and the main navigation sensors. This is the most sensitive element of the whole vehicle, because every kind of noise can disturb the navigation. For this reason, it is important to keep this module far away from each kind of motor, driver and power DC/DC.

The Antenna Module contains a secondary pc and all the wireless connections (radio, Wi-Fi and GPS) and it is directly connected to the antenna and allows the communication between the vehicle and the ground station, when the AUV is on surface. The Driver Module and Power Module are the main source of noise, that is why the separation of the modules allows reducing these problems on the AUV. More in details, the Power Module contains the elements necessary to provide voltages required by vehicle devices and to switch on or off the vehicle itself. On the other hand, the Driver Module contains all the drivers to pilot the motors. The Battery Module contains the batteries and the vehicle can even have more than one of them. Obviously, the vehicle can also have additional modules, e.g. a Connection Module that allows connecting external payloads to local networks.

Secondly, it is necessary to define how all the modules communicate each other. The selected solution exploits an Ethernet communication between the modules, because the Ethernet connection allows transferring a great amount of data without picking up external noise and using only one cable. In other words, all the modules are connected through a local network. In this way, is possible to reduce to minimum the number of connections between the modules and it is possible to reconfigure or add other connections, according to the design or tasks needs. Indeed, all module are connected each other with an Ethernet connection and with the Power Module by means of a power cable. Figure 1.13 summarizes all these considerations and shows how simple the conceptual structure of the vehicle is.

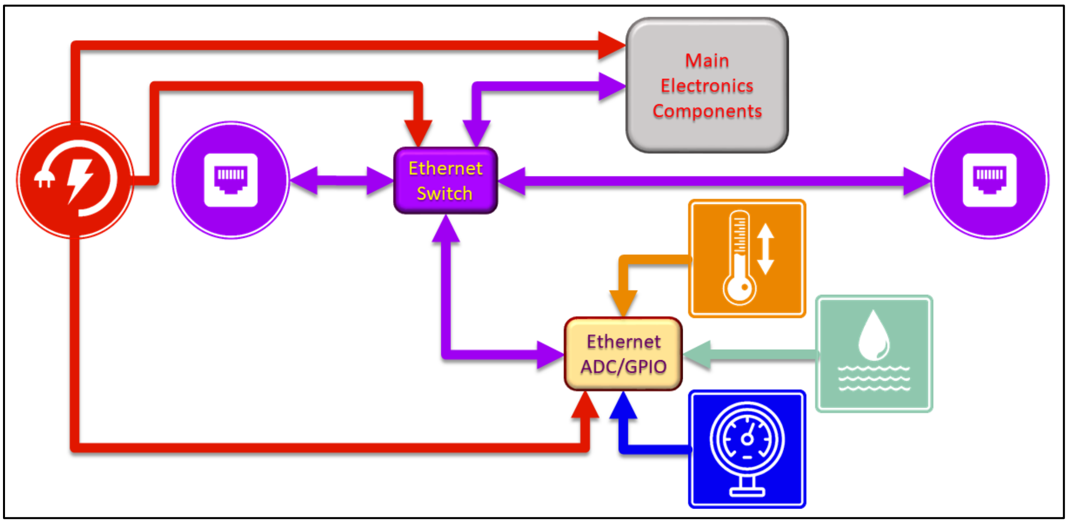

Figure 1.14: Conceptual module scheme.

A standardized scheme for all the modules has been defined. In each module, it is possible to identify four basic groups of elements (Figure 1.14):

- Main electronics components;
- Power connection;
- Ethernet switch with external connections;
- Ethernet ADC/GPIO with module status sensors;

Obviously, the main electronics components provide the basic functionality of the module, while the power connection provides the power to all the components. The Ethernet switch with two ports provides the connection between this module, other modules and optional external devices. The choice of using two Ethernet ports allows the connection of all the modules as an array of elements. being possible to easily change the connections and dispositions. Ethernet ADC/GPIO with module status sensor is the most important element of the module. Indeed, this element can provide the connection at the local network of the vehicle to every kind of additional sensor or analogical devices and allows the use of three essential status sensors: temperature sensor, pressure sensor and water sensor. In other words, these three sensors can alert if there are some kinds of failure in each module. More in details, the temperature sensor allows monitoring the internal temperature of electronics components to identify overheating problems. The water sensor allows identifying any water leakage in each module to allow a safety return of the vehicle on surface. In addition, the pressure sensor is a redundant status sensor, because not only allows identifying exploding failure of electronics components but also allows predicting leakage problems. Finally, it is a good practice to put underwater casings under vacuum, if they are not full of oil. The vacuum not only allows verifying impermeability of the module but also any change of the internal pressure may be an indicator of some leakage problems even if the water does not change the status of the water sensor.

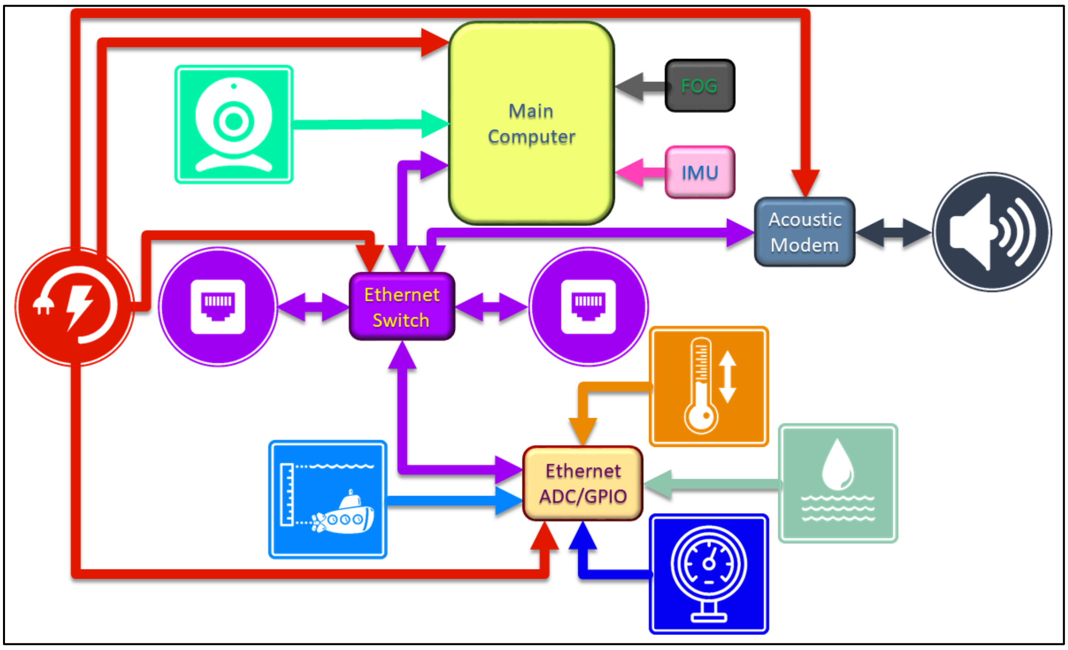

Figure 1.15: Conceptual scheme of the Core Module.

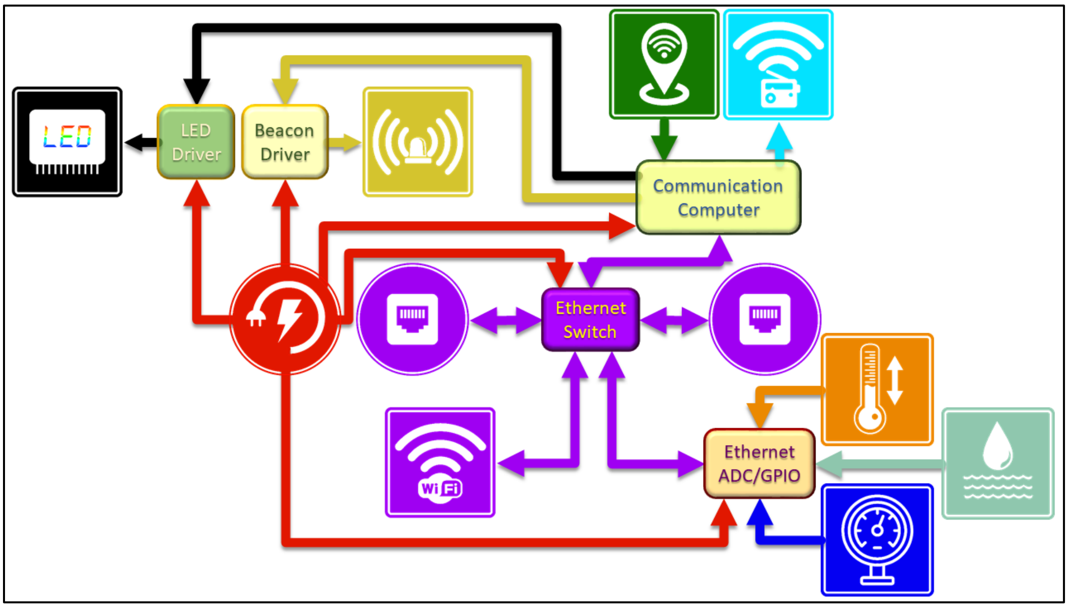

Figure 1.16: Conceptual scheme of the Antenna Module.

Figure 1.15 shows the conceptual scheme of the Core Module. In addition to the basic component previously described, there are the main pc, the acoustic modem, FOG (Fiber Optical Gyroscope), IMU (Inertial Measurement Unit), the camera and the external pressure sensor. More in details, the main pc takes data from the FOG, the IMU and camera, the acoustic modem allows underwater communication while the external pressure sensor provides the depth value during the navigation.

Figure 1.16 shows the conceptual scheme of the Antenna Module. Here, there are the communication computer, radio, GPS, Wi-Fi, beacon flash driver and LED driver. More in details, the communication computer is a secondary computer that manages the external communications by means of radio and GPS and with operators by means of light communications. The Wi-Fi device directly connects the vehicle local network to an external network.

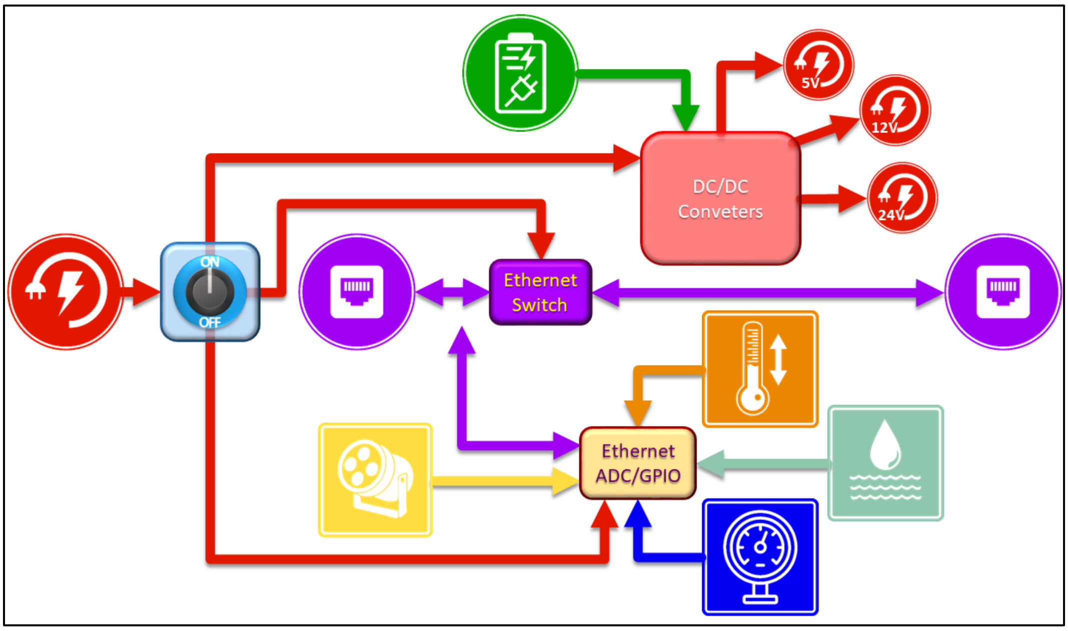

Figure 1.17: Conceptual scheme of the the Power Module.

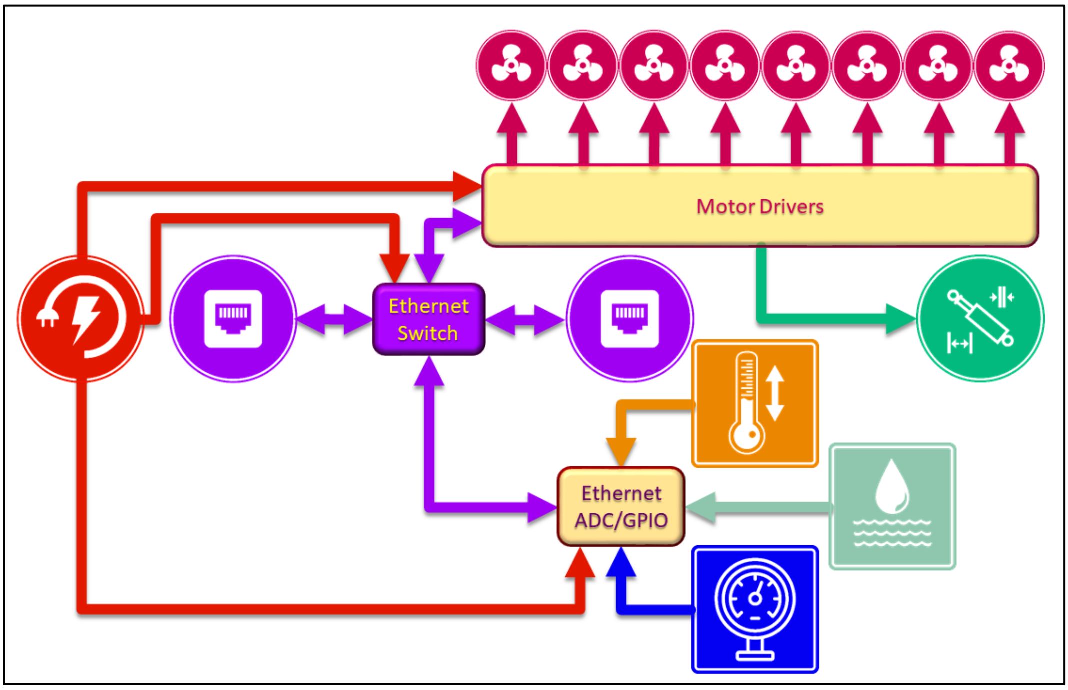

Figure 1.18: Conceptual scheme of the Drive Module.

Figure 1.17 shows the conceptual scheme of the Power Module. In addition to the basic components previously described, there are here all the DC/DC converters to provide all the voltage levels required by the internal devices. In addition, Ethernet ADC/GPIO controls the frontal LEDs.

Figure 1.18 shows the conceptual scheme of the Driver Module. There are only drivers for thrusters and actuators, required to perform the robot "transformation".

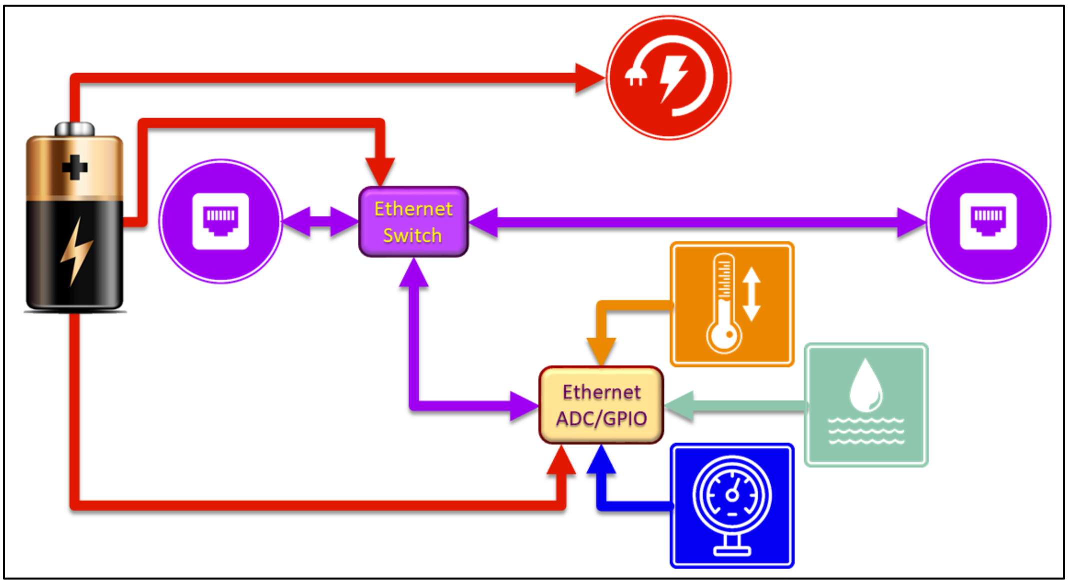

Figure 1.19: Conceptual scheme of the Battery Module.

Figure 1.19 shows the conceptual scheme of the Antenna Module. In addition to the basic components previously described, only battery packages are located in this module.

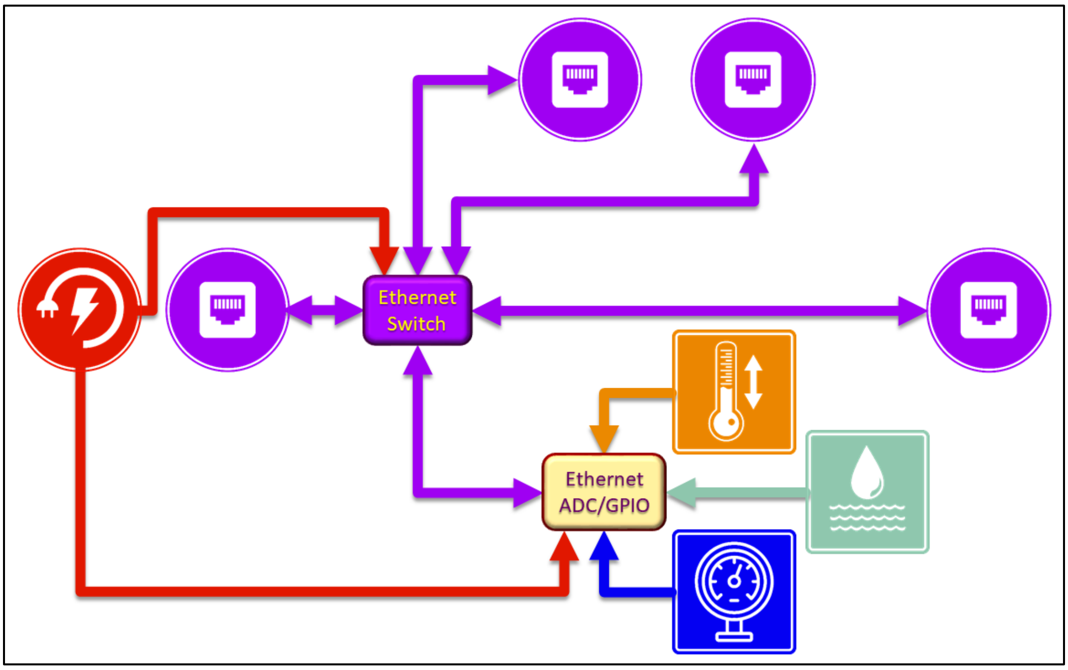

Figure 1.20: Conceptual scheme of the Connection Module.

Figure 1.20 shows the conceptual scheme of the Connection Module. This additional module is the simplest one, because the main electronics components is the Ethernet switch. This module provides only additional Ethernet connections for external devices, such as DVLs (Doppler Velocity Logs) or FLS (Forward Locking Sonar). For this reason, it is equipped with many Ethernet ports.

Chapter 2

Vehicle design

2.1 A low cost implementation.

2.1.1 A real vehicle.

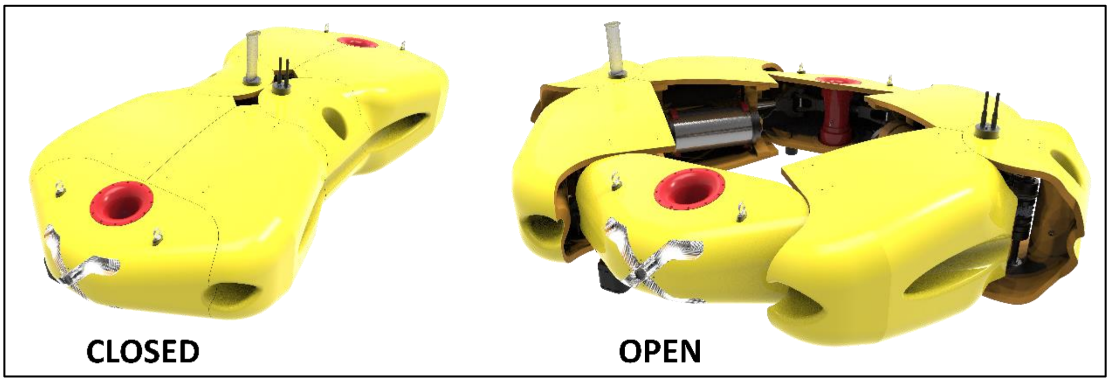

Figure 2.1: Renderings of the vehicle: Closed configuration on the left and Open configuration on the right.

In the previous chapter; the conceptual design of the reconfigurable vehicle has been defined. Obviously, only conceptual considerations are not enough to establish the quality of an idea. Therefore, it is important to study a real implementation of the vehicle to assess its feasibility. A low cost implementation is the first attempt design chosen, in order to test the first prototype in the real scenario and verify its performances. Indeed, an innovative project, such as the one described in this thesis, presents many small problems that will have to be considered and solved to define the final design of the vehicle. In addition, the choice of a low cost implementation and a high scalability, have to be faced. For this reason, the motor chosen for the implementation is a low cost one produced by BlueRobotics and named M200 (shown in §3.1). It is a small and powerful three-phase brushless motor designed to be directly used into the water, i.e. without any watertight casing. In addition, as will be argued in chapter 4, a method to add a speed sensor to this kind of motors has been studied. For this reason, the final designed thruster (the same presented in §3.2.1) has the performances required by this kind of vehicle, despite its low cost. As regard other design decisions, the vehicle does not have small dimensions due to the capability of changing its shape and because of the necessity to avoid the interpenetration of internal components in the closed configuration. But big dimensions imply high weight, for this reason, it has been chosen to use the buoyancy foam directly as a real building material. In this way, it is possible to minimize the dimensions and the weight of the vehicle reducing the number of components, and therefore it is necessary to use syntactic foam with good performances. The foam taken into account is a syntactic foam of BMTI® by ALSEAMAR® with density of 400 kg/m^3 and maximum depth rating of 2000 m. For this reason, a maximum operating depth of 1500 m for the vehicle has been chosen. This choice does not limit the performances of the vehicle, because it is suitable for different applications (i.e. inspection of power plants or shipwrecks). In addition, the hull has to provide the buoyancy for the whole main structure, while each housing has to have the same density of the water to maintain the balance of the whole vehicle in both configurations.

The design of the vehicle has been quite complex, because the characteristics of each components depend to each other for weight savings and to ensure the vehicle functionality. In addition, to reduce the vehicle cost commercial components have been chosen and their dimensions have been chosen in order to guarantee at least a safety factor of 2. Obviously, in most cases the safety factor is extremely greater than 2, due to the availability of commercial components and the maximization of the components standardization.

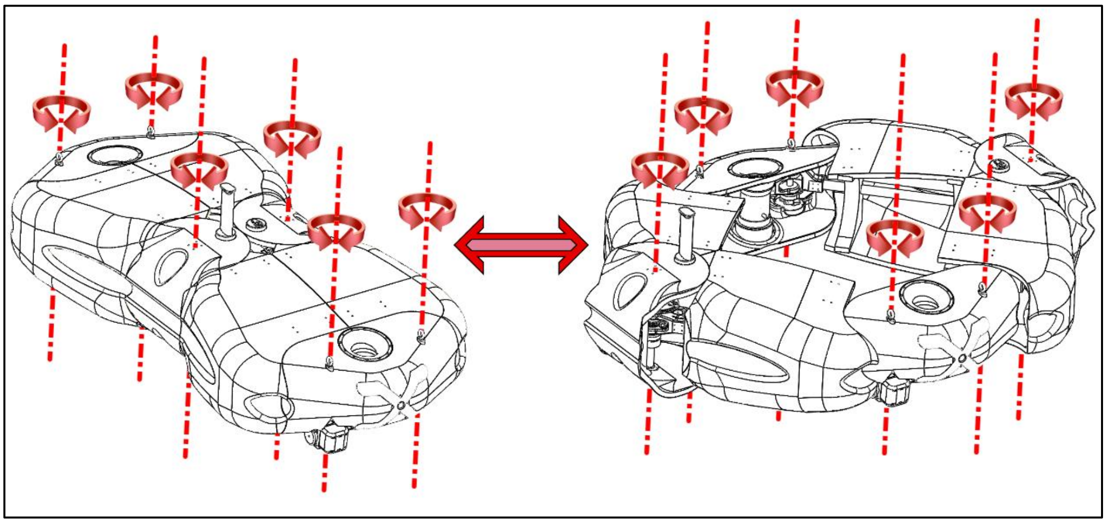

Figure 2.2: Scheme of the vehicle joints.

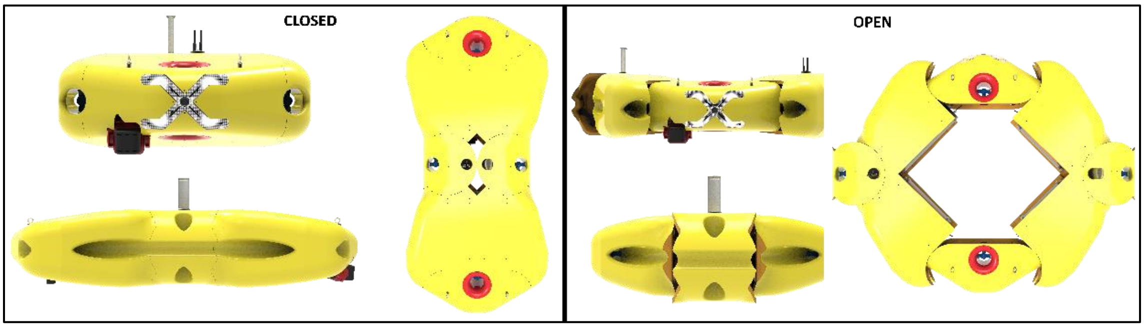

Figure 2.3: Main views of the vehicle: Closed configuration on the left and Open configuration on the right.

Regarding the speed performance, the maximum design speed is about 2 kn, because it is a quite good peak speed for an AUV and it can be obtained with a low cost approach. Considering all the constraints and requirements, the designed prototype, visible in Figure 2.1, is an eight thrusters AUV and has a weight of about 210 kg, with the capability of bringing about 40 kg of payloads. In the closed configuration it has a length of about 2.2 m, a width of about 1 m and a height of 0.45 m. Otherwise in the open configuration it has a length of about 1.7 m, a width of about 2.1 m and a height of 0.45 m.

As previously mentioned, the vehicle is designed around on a hexagonal frame with two actuated joints and four free joints. Figure 2.2 shows more in details the motions of the rotational joints, placed inside the hull. Finally, Figure 2.3 shows the principal views of the vehicle in the closed and open configurations.

2.1.2 Performances estimation.

The estimation of navigation performances is very important to verify the feasibility and the quality of the vehicle design, and, especially to verify if the stored power is sufficient. Indeed, the choice of use commercial component has brought to use two batteries with a capacity of 18 Ah. These batteries are the batteries with higher-capacity, small dimension, low weight and equipped whit a BMS, but 36 Ah of total capacity could be considered a small amount of energy for the vehicle under study. In this case, the preliminary estimation of the vehicle drag has been carried out on the whole CAD drawings by means of SOLIDWORKS Flow Simulation®, for the open and the closed configuration in all the main directions. These fluid dynamics simulations have been very basic (maximum mesh cell 25 mm, with default element of Flow Simulation®), because their aim is just the preliminary verification of the shape of the vehicle and especially its power consumption. In the near future, more advanced fluid dynamics simulations will be made, for sure, to analyze the fluid dynamics behavior of each elements of the vehicle and their interaction during the navigation, in order to forecast the real dynamic and fluid dynamic behavior.

Table 2.1 summarizes the used data during the CFD simulations to calculate the drag coefficients in all the main directions. The geometrical values have been derived from the CAD drawings. On the other hand, the estimation of vehicle thrusts has been made through dedicated experimental tests, as explained in §3.2.3 of this work. In these preliminary performances estimations, the same propellers of MARTA AUV tunneled thrusters have been used. It is possible to assume that each thruster could provide a thrust of about 18 N at maximum RPM (about 3100 RPM in bollard condition). At the moment, the multi-quadrant behavior of the thruster has been neglected, because it is not known the fluid dynamic interaction between the water flow around the propeller and the water flow around the vehicle. In the near future, this condition will be investigated, in order to improve these estimations and optimize the hull geometry of the vehicle.

	OPEN CONFIGURATION	CLOSED CONFIGURATION
Frontal Area [m²]	0.94	0.47
Lateral Area [m²]	0.75	0.8
Horizontal Area [m²]	1.81	1.81
Reference Speed [kn]	2	2
Total Longitudinal Thrust [N]	51	72
Total Lateral Thrust [N]	51	0
Total Vertical Thrust [N]	72	72
Battery Capacity [mAh]	36000	36000
Max Motor Current [A]	10	10

Table 2.1: Reference data for drag estimation.

	OPEN CONFIGURATION	CLOSED CONFIGURATION
Frontal Drag Coefficient [-]	0.25	0.23
Lateral Drag Coefficient [-]	0.34	0.32
Vertical Drag Coefficient [-]	0.24	0.43
Frontal Drag Force [N]	123.0	58.3
Lateral Drag Force [N]	134.1	151.2
Vertical Drag Force [N]	222.7	417.8

Table 2.2: Drag data estimated.

Obviously, future studies and experimental campaigns on propellers and motors will allow identifying an optimal matching between the propeller and the motor, to increase the thrust. In addition, the motor current has been limited to 10 A, even if the chosen thruster can tolerate a current up to 20 A (i.e. the vehicle performance could be easily increased, increasing the power consumption). The current limitation is related to the idea of preserving the batteries with the reduction of their workload. In particular, as said, the chosen thrusters are BlueRobotics M200 that offer high performances even if they are cheap and very compact, as it will be further discussed in Chapters 3 and 4 below. Finally, batteries capacity is related to the choice of using low cost commercial Li-Po battery to keep cost low. It is for instance possible to increase the vehicle autonomy designing a battery module based on small cylindrical Li-Ion cells.

The preliminary CFD simulations highlight a good hydrodynamics efficiency of the vehicle. In Table 2.2 the values of the estimated drag forces and drag coefficients in all the main directions are shown. The drag coefficients have been calculated with the relation below:

$$\boldsymbol{C_x} = \frac{\boldsymbol{2(Drag\ Force)}}{\boldsymbol{(Water\ Density)(Velocity)^2(Area)}} \tag{2.1}$$

Where the drag forces have been estimated by means of SOLIDWORKS Flow Simulation® and the areas have been calculated as the projection of the vehicle on the longitudinal, frontal and horizontal plane of the vehicle. These data allow estimating both max speeds and operating ranges of the vehicle. Obviously, it is necessary to add another hypothesis to calculate these important parameters. Indeed, during navigation the water flow around the vehicle influences the thrusters efficiency reducing thrusts when the speed increases. For this reason, all the data; presented below; have been calculated in ideal conditions and only a future experimental analysis will allow identifying the thrusts reduction due to speed. With drag coefficients and the total thrust it is possible to easily calculate the maximum speeds of the vehicle. On the other hand, assuming an ideal motion at maximum speed, using maximum motor current (limited to 10 A), battery capacity values it is possible to estimate the operative ranges of the robot. Conversely, the maximum accelerations have been calculated as the ratio between the thrust and the mass of the vehicle with the assumption to start from standstill and to apply instantly the maximum thrust. At the moment, added masses have been neglected, because of the complexity of the vehicle geometry. In the near future, with more accurate CFD simulations it will be possible to evaluate also these important parameters.

	OPEN CONFIGURATION	CLOSED CONFIGURATION
Longitudinal Max Speed [m/s]	0.66 (1.28 kn)	1.14 (2.22 kn)
Lateral Max Speed [m/s]	0.64 (1.24 kn)	- (- kn)
Vertical Max Speed [m/s]	0.59 (1.15 kn)	0.43 (0.83 kn)
Longitudinal Direction Range [km]	2.15	3.71
Lateral Direction Range [km]	2.06	-
Vertical Direction Range [km]	1.90	1.39
Longitudinal Max Acceleration [m/s²]	0.24	0.34
Lateral Max Acceleration [m/s²]	0.24	-
Vertical Max Acceleration [m/s²]	0.34	0.34

Table 2.3: Estimated motion performaces.

Table 2.3 summarizes the estimated vehicle performances. From these preliminary data, the behavior of the vehicle seems to be the desired one. Indeed, in the open configuration the AUV can more or less reach the same speed or can resist to the same sea flow in all the directions, while in the closed configuration the vehicle can reach the highest speed possible in forward direction. In addition, these motion performances allow supposing that the vehicle can operate at its maximum operating depth for about 10 minutes. Indeed, the vehicle can reach a depth of 1500 m in about 40 minutes assuming that it goes down with a pure vertical motion at top speed and in open configuration (more stable configuration). In this way, if the vehicle dives for 10 minutes at top speed it has a remaining stored energy of about 22 Wh, sufficient for a controlled re-emergence, since the AUV is slightly positive. With these considerations, it is possible to observe that the vehicle can operate to maximum operative depth, despite a limited capacity of the installed modules batteries. Indeed, with the Battery Module version presented in this work only 800 Wh are available, provided by two Li-Po batteries located in two different Battery Modules. The operative time seems enough only for short mission, but the best solution for this kind of vehicle could be its use in presence of underwater recharging station: the vehicle could thus reach different sites without limitations. Fortunately, this condition could be easily guaranteed in the supposed operative scenarios (i.e. off-shore power plants, submerged pipelines), because this kind of vehicles will dive within known sites.

2.1.3 Cost analysis.

Cost analysis can be divided into two main parts: electronics components and mechanical components. The most substantial cost of electronics components is due to four elements:

- FOG KVH® DSP-1760: about 7000 €;
- Nortek® DVL 1000: about 15000 €;
- Acoustic Modem EvoLogics® S2CR 18/34: about 8000 €;
- FLS (Forward Looking Sonar) Teledyne® BlueView M900: about 27000 €.

These components could be considered optional, but they are needed to give good performances to the vehicle. Indeed, FOG and DVL strongly affect navigation performances, because these components allow a satisfactory underwater navigation reducing dead-reckoning navigation error. A good acoustic modem is instead indispensable for underwater vehicle, because only this device allows underwater communication. The FLS is the real optional device, because without it the vehicle can navigate well. The only drawback due to lack of FLS is a reduction of vision capability of the AUV. Indeed, without the FLS, only the frontal camera can provide visual information and an obstacle avoidance system, but it is useless in poor visibility conditions. Conversely, the cost of remaining electronics components is quite low. Indeed, it has been possible to contain the cost to about 6000 €, looking at common industrial components and low cost prototype boards, such as Arduino® and UDOO®. Regarding the mechanical components, it has been possible, thanks to the know-how of the research group in underwater vehicles design, to estimate a cost about of 40000 € taking into account hull molds, carbon components and motors.

Fortunately, the modular approach gives to the prototype high versatility and a good scalability. Indeed, it is very easy to reconfigure the vehicle and add new features. For example, changing Arduino® board, with custom ADC/GPIO and potted cable glands with underwater connectors allow improving the usability and reliability of the vehicle. Obviously, these modifications increase not only the performance, but also the vehicle cost. Other easy improvements could be adding more Ethernet devices, fins and battery with extended capacity. In the first case, it is enough adding a connection module to add three more input/output connection, leading to AUV new functionalities. To improve long-distance navigation performances, it is possible to add external fins to the hull, while to extend battery capability Li-Ion cylindrical cells can be considered. Finally, with this estimated global cost it is possible to hypothesize that a product derived from the designed prototype could have a competitive market price with respect to AUV of its dimension category and this is an interesting additional reached goal.

2.2 Hardware and connection design.

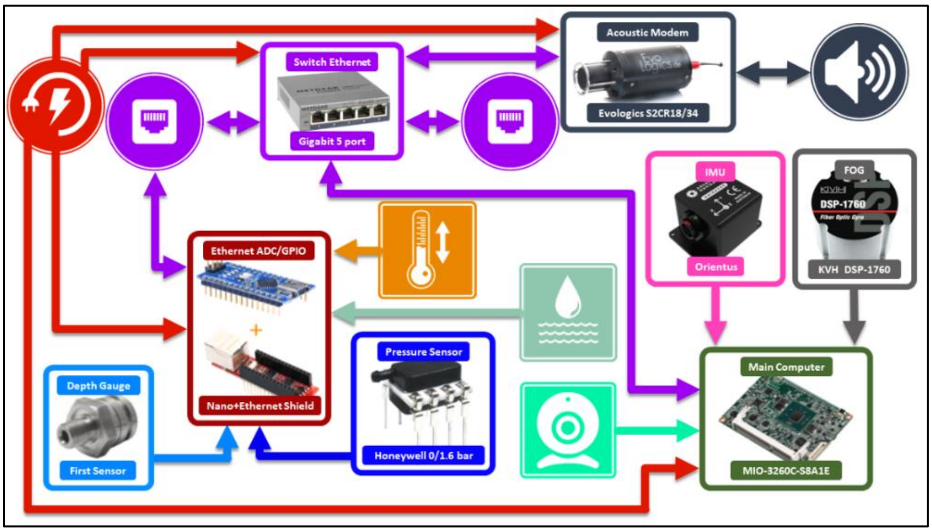

Figure 2.4: Scheme of the Core Module.

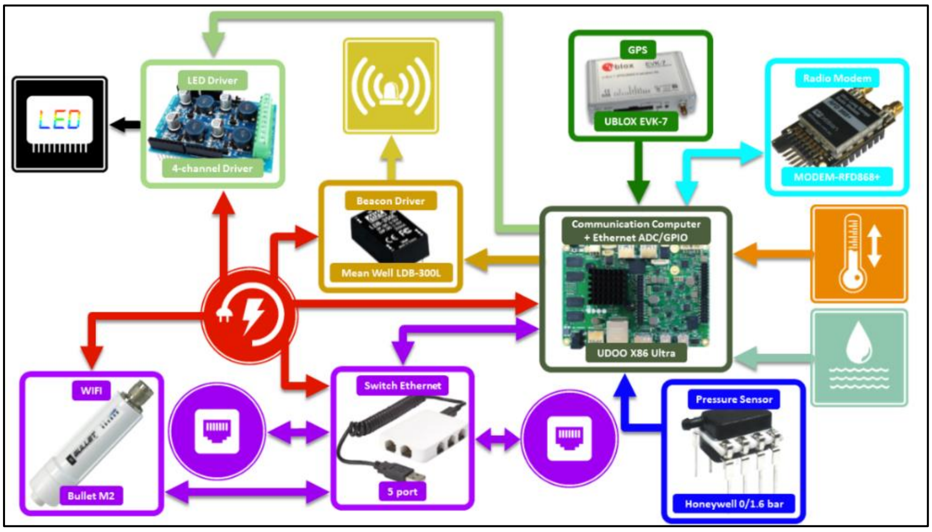

Figure 2.5: Scheme of the Antenna Module.

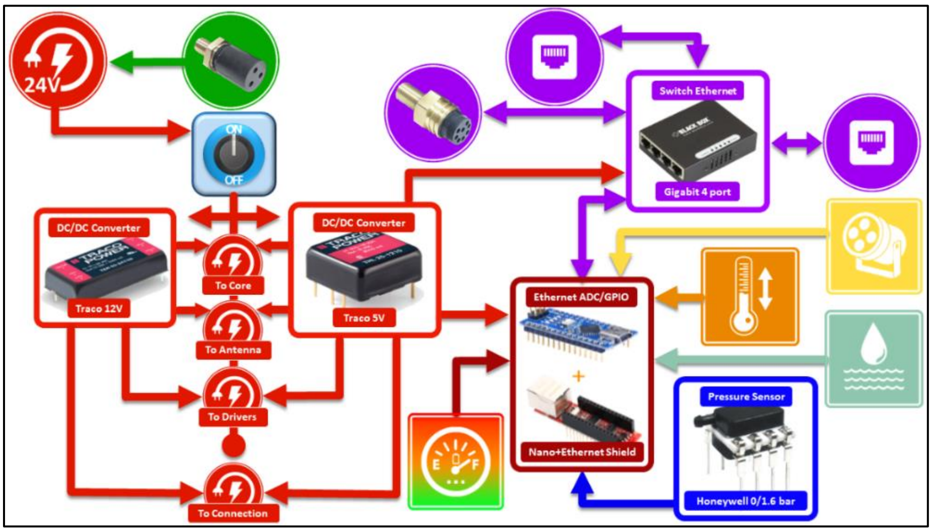

Figure 2.6: Scheme of the Power Module.

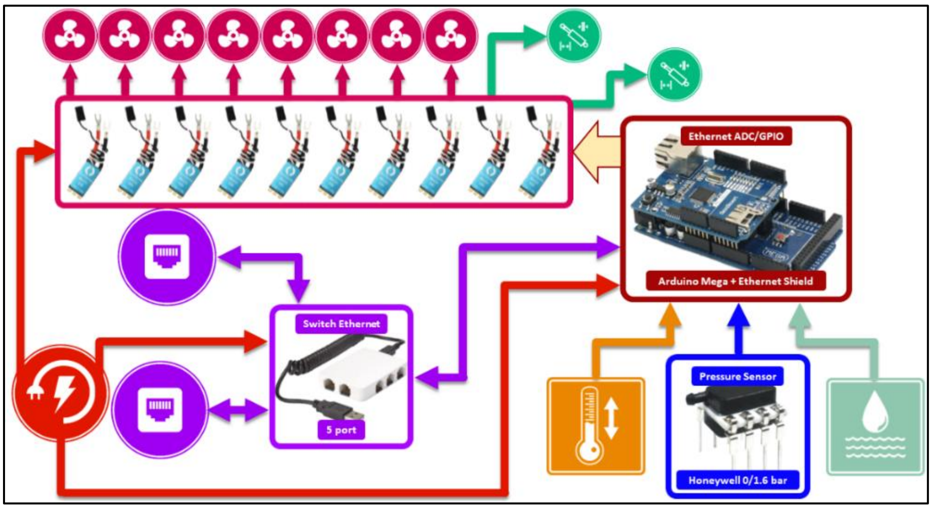

Figure 2.7: Scheme of the Driver Module.

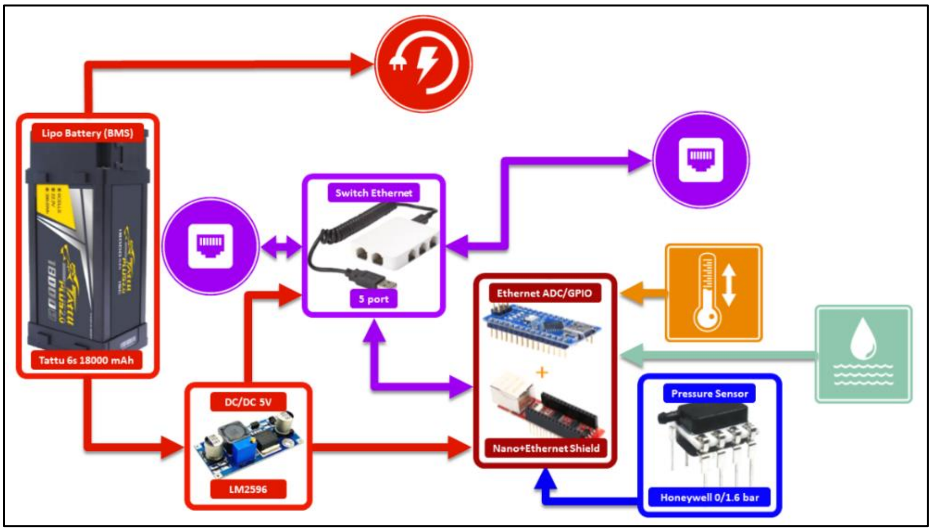

Figure 2.8: Scheme of the Battery Module.

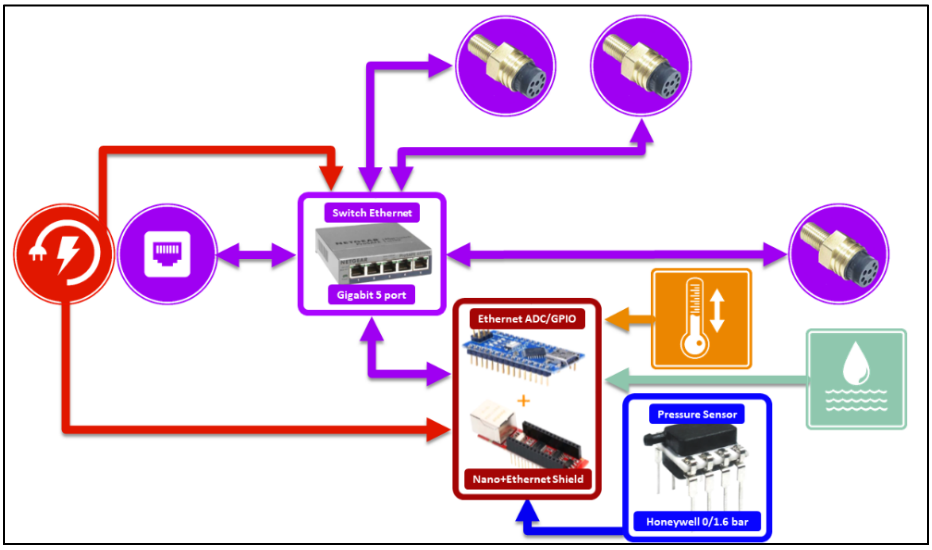

Figure 2.9: Scheme of the Connection Module.

As mentioned above, an important goal of the design of this first version of the vehicle is to minimize the cost of the vehicle. In addition, another important constraint is minimizing the weight of the AUV to obtain a vehicle easy to manage. For this reason, during the whole design process the reported below considerations have been taken into account:

- Components integration;
- Components standardization;
- Minimization of components number;
- Innovative light material;
- Modular approach.

The results of these constraints are specific design choices about the hull, the internal structure, modules allocation and modules connection. First, it has been chosen to use syntactic foam, necessary to vehicle buoyancy, as a structural material. This choice allows reducing the number of components and the weight of the vehicle, because the foam provides the connection between both the internal components and modules and the internal frame. Obviously, this kind of solution entails the use of syntactic foam with good performances. Secondly, the internal structure has been made by six standardized joints (described in §2.3.1) connected to each other with pultruded carbon bars. This solution not only allows reducing the variety of component employed on the vehicle but also gives to the AUV a light and resistant structure. Finally, the connection between the modules are realized with potted cable glands to reduce the employment of expensive underwater connectors, even if this solution makes the reconfiguration of the module more complex. Obviously, all these problems will be explained in detail in the following paragraphs.

Regarding low cost electronics components, the ones already used in other UNIFI DIEF vehicles have been considered to ensure the proper functioning of the vehicle. From Figure 2.4 to Figure 2.9 are shown the implementation of conceptual modules described in §1.4, are presented. In these schemes, the presence of the potted cable glands for connection is represented as generic power or Ethernet connection. In addition, it has been chosen that all the Ethernet ADC/GPIO prototypes are built with cheap Arduino boards.

2.3 Mechanical design.

2.3.1 Joints design.

The vehicle needs two different kinds of joint to work properly: two actuated joints and four free joints (Figure 2.10). As mentioned above, the fundamental design requirements are minimizing the number of components and maximizing the components standardization, so actuated joints and free joints differ from each other only for the actuation system and the presence of proper end-stops. For this reason, the joint has been designed around the actuation system. In addition, the actuation system should be:

- Light;
- Cheap;
- Reliable;
- Compact;
- Irreversible.

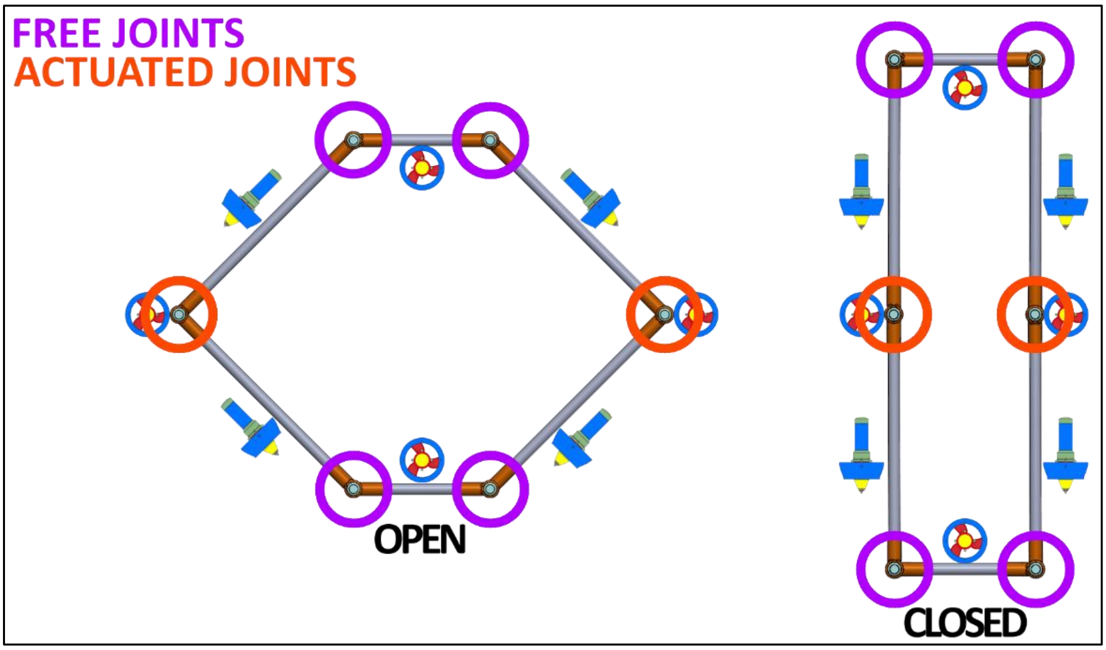

Figure 2.10: Position of the actuated joints and free joints.

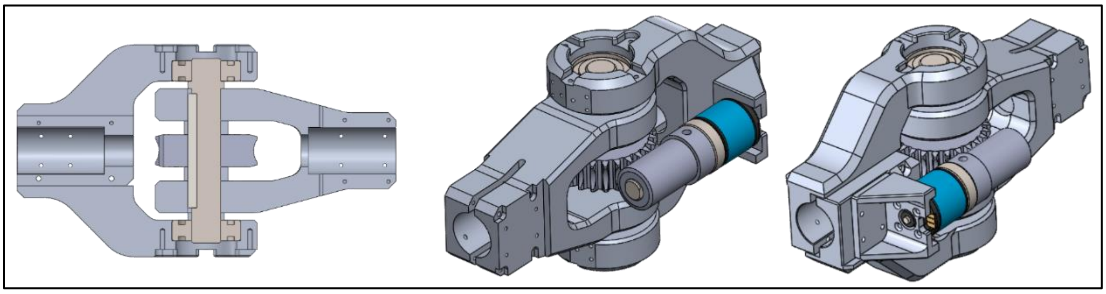

Figure 2.11: Three views of the actuated joint.

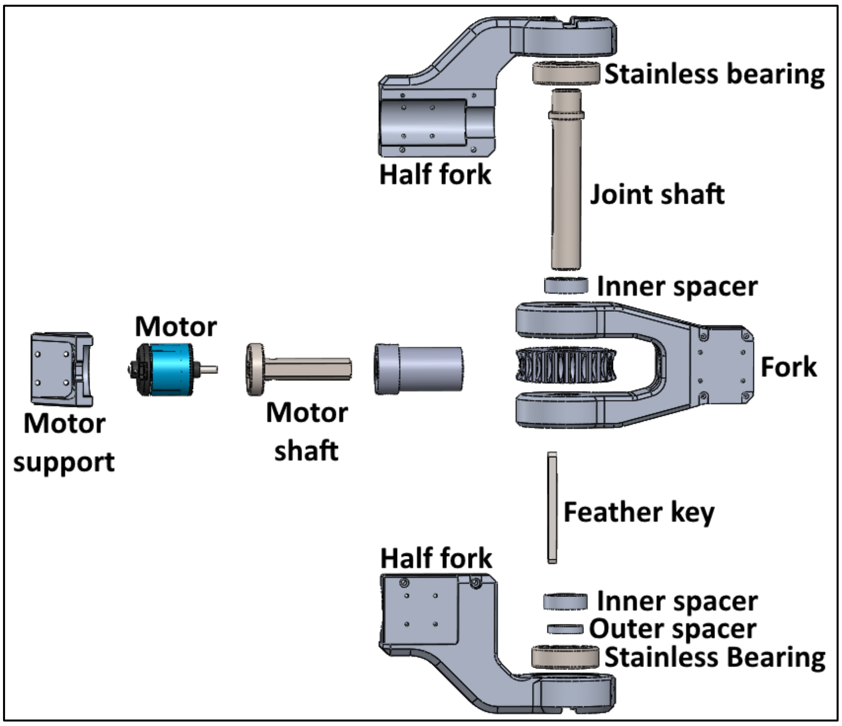

Figure 2.12: Exploded view drawing of actuated joint.

The best way to obtain a light, cheap, reliable and compact actuation is designing an actuation system that could work directly in water, because in this way it is possible to use the minimum number of components. For this reason, the motor M200 of BlueRobotics has been selected, i.e. the same motor used for the thrusters. In fact, other kinds of actuation, such as pneumatic or oleo dynamic one, need complex and heavy supply systems. Designing an irreversible actuation system is very important, because it is the best way to reduce power consumption especially with a brushless motor as the M200 is: when the joint reaches the desired position, the joint has to maintain its position even if the motor is switched off. The simplest transmission systems to obtain irreversibility are linear transmissions or worm drives. Obviously, actuating a rotational joint with a linear system does not bring to a compact solution. In addition, it is very hard to find linear transmission compatible with a permanent use in water, while it is easy to find Derlin® worm drive. For this reason, the adopted solution is a Derlin® worm drive, with transmission ratio of 25:1, a throat diameter of 67.5 mm and module of 2.5.

Other eight different components complete the actuated joint, as visible in Figure 2.11 and in Figure 2.12:

1. Fork (x1).
2. Half fork (x2).
3. Stainless bearing (x2).
4. Inner spacer (x2).
5. Joint shaft (x1).
6. Outer spacer (x1).
7. Motor support (x1).
8. Motor shaft (x1).
9. Feather key (x1)

More in details, 12 custom components and 3 commercial parts create the actuated joint. All custom components are made in anodized Aluminum 6082 T6 while the joint shaft and the motor shaft are made in Stainless Steel AISI36L. In this way, the actuated joint weighs 3.1 kg and occupies a 260x145x100 mm space.

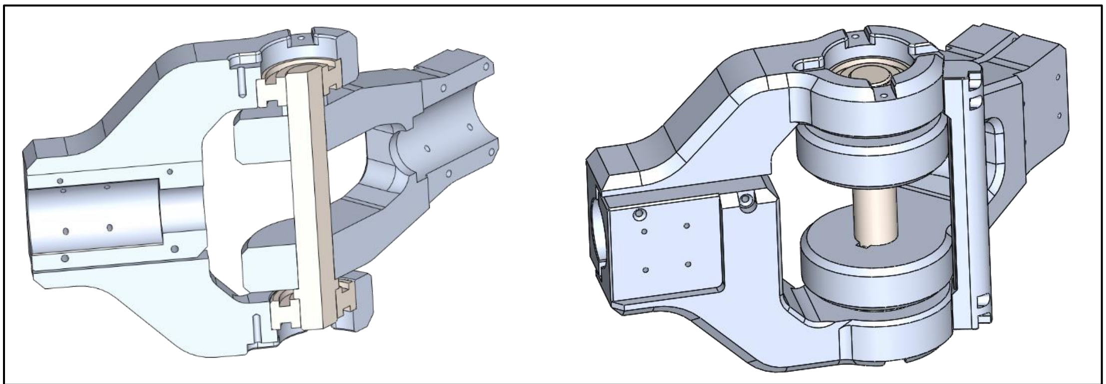

Figure 2.13: Two views of the free joint.

As mentioned above, the free joint is substantially similar to actuated one. The only three differences are the lack of transmission components, the presence of two feather keys instead of only a big one and the presence of the end-stop, as clearly visible in Figure 2.13. These differences allow reducing the weight and the dimension of the joint. Indeed, the weight decrease to 2.68 kg and the dimensions become 120x145x70 mm. The end-stop is an important mechanical element, because it prevents undesirable translation between the front and the back, when the vehicle is in the open configuration.

As visible in Figure 1.12, the position of the central vertical thrusters is near the actuated joints. This choice is very important to have a symmetrical thrusters layout, but it requires a positioning system to control the position of each central thrusters. Indeed, connecting the central thruster to its actuated joint entails that thrusters layout is not symmetrical in one of two possible configurations. Otherwise, leaving floating the central thruster position does not allow knowing the real thrusters layout. For these reasons, the central thrusters have to be connected to their actuated joint with a positioning system that constraints these thrusters to remain on the plane of transverse symmetry of the vehicle. The simplest positioning system is composed of a slider put on one of two principal elements of the joint and a conrod that connects the slider to the floating element that supports the thruster. In addition, the slider needs to be guided by means of a cam to ensure the correct motion of the thruster during the vehicle transformation. Figure 2.14 shows the scheme of this positioning system. Obviously, the cam can have only one profile that satisfies the required constraint.

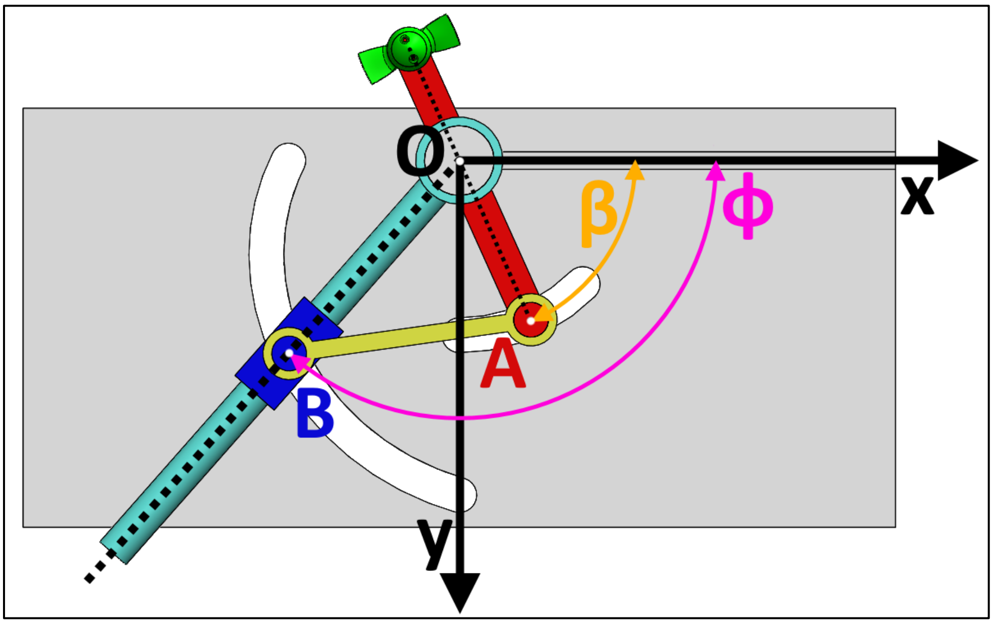

Figure 2.14: Central thruster positioning system scheme.

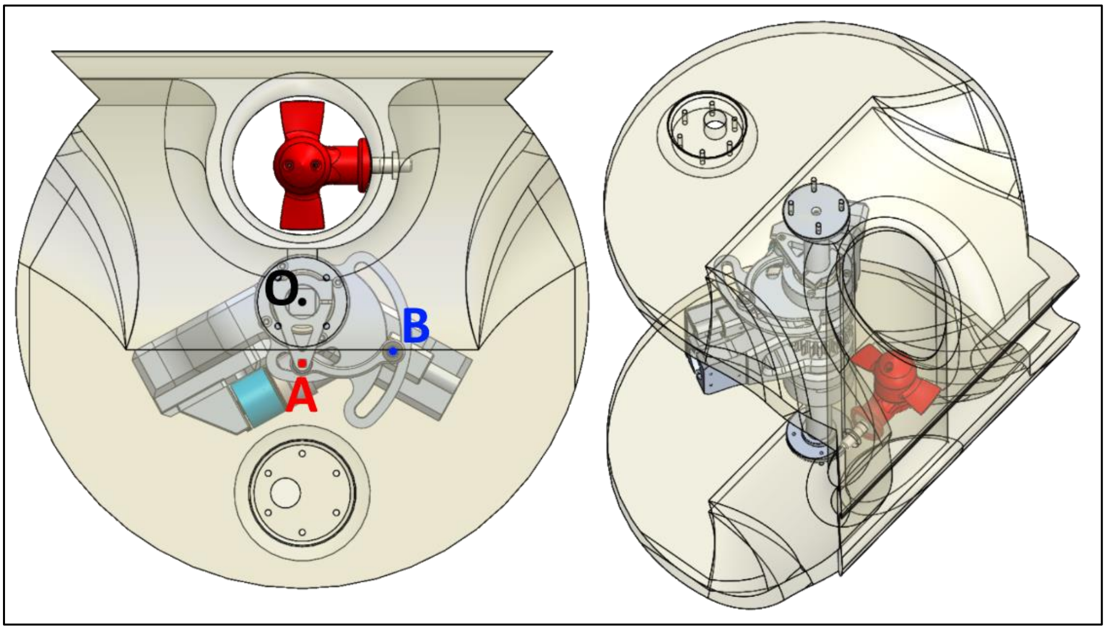

Figure 2.15: Two views of the central thruster positioning system.

The calculation of the profile could be obtained referring to Figure 2.14 under the following hypothesis:

$$\begin{gathered}\boldsymbol{\beta} = \frac{\boldsymbol{\varphi}}{\mathbf{2}} \\ |\overline{\boldsymbol{B}-\boldsymbol{A}}| = \boldsymbol{b} \\ |\overline{\boldsymbol{A}-\boldsymbol{O}}| = \boldsymbol{R_a} \\ |\overline{\boldsymbol{B}-\boldsymbol{O}}| = \boldsymbol{r}(\boldsymbol{\varphi})\end{gathered} \tag{2.2}$$

The relation between the slider position, the thruster angle β and joint angle φ could be found, applying the law of cosines to AOB triangle:

$$|\overline{\boldsymbol{B}-\boldsymbol{A}}|^2 = |\overline{\boldsymbol{B}-\mathbf{0}}|^2 + |\overline{\boldsymbol{A}-\mathbf{0}}|^2 - 2|\overline{\boldsymbol{B}-\mathbf{0}}||\overline{\boldsymbol{A}-\mathbf{0}}| \cos(\boldsymbol{\varphi}-\boldsymbol{\beta}) \tag{2.3}$$

$$\boldsymbol{b}^2 = \boldsymbol{r}(\boldsymbol{\varphi})^2 + \boldsymbol{R_a}^2 - 2\boldsymbol{r}(\boldsymbol{\varphi})\boldsymbol{R_a}\cos\left(\frac{\boldsymbol{\varphi}}{2}\right) \tag{2.4}$$

$$\boldsymbol{r}(\boldsymbol{\varphi})^2 - \left[2\boldsymbol{R_a}\cos\left(\frac{\boldsymbol{\varphi}}{2}\right)\right]\boldsymbol{r}(\boldsymbol{\varphi}) + (\boldsymbol{R_a}^2 - \boldsymbol{b}^2) = \mathbf{0} \tag{2.5}$$

At this point, it is possible to obtain the value of $r(\varphi)$, solving the quadratic equation derived by the law of cosines and considering only the positive solution:

$$\boldsymbol{r}(\boldsymbol{\varphi}) = \boldsymbol{R_a}\cos\frac{\boldsymbol{\varphi}}{2} + \sqrt{\boldsymbol{R_a}^2\left(\boldsymbol{cos}^2\left(\frac{\boldsymbol{\varphi}}{2}\right) - 1\right) + \boldsymbol{b}^2} \tag{2.6}$$

The knowledge of the module of vector $\overline{B-O}$ allows knowing the position of the slider needed to maintain the central thruster on the plane of transverse symmetry of the vehicle:

$$\begin{gathered}\boldsymbol{x_B} = \boldsymbol{r}(\boldsymbol{\varphi})\cos(\boldsymbol{\varphi}) \\ \boldsymbol{y_B} = \boldsymbol{r}(\boldsymbol{\varphi})\sin(\boldsymbol{\varphi})\end{gathered} \tag{2.7}$$

In Figure 2.15 it is possible to see the central thruster positioning systems with all its components and the central part of the hull.

2.3.2 Chassis design.

The design of the chassis has followed the same principle of lightness and cheapness. In addition, to connect the joints to each other it is necessary to use materials with a good resistance and stiffness. For these reasons, the material chosen has been pultruded carbon. Indeed, this material is cheap but ensures all mechanical needs even if it does not reach the performances of laminated carbon. More in details, the joints are connected each other by means of carbon pultruded rods with a diameter of 32 mm, as visible in Figure 2.16. The choice of rods instead of tubes is related to structural problems. Indeed, the use of pultruded carbon tubes would make choosing between filling them with external water or not. In the first case, some holes on the tubes should be made reducing their structural integrity. In the second case, a deep buckling study would be mandatory. In addition, the balancing of the vehicle could be compromised in presence of water leakage due to damages.

The verification of the chassis has been made by means of FEM analysis (SOLIDWORKS Simulation®). The most important case studied are the lifting of the vehicle, reported in Figure 2.18 and Figure 2.19, and the vehicle leaning on the central parts of the hull. In the lifting case, the vehicle is lifted from its four eyebolts, an example is shown in Figure 2.17, directly connected to the frontal and rear free joints. In both the analyzed cases, the loads applied to pultruded carbon rods are twice the estimated weight of hull parts and the heaviest module. In addition, on the frontal and rear rod 550 N has been added referring to a hypothetical couple of manipulation arms. More in details, the loads on each lateral rod are equal to 400 N and 750 N on frontal and rear rods.

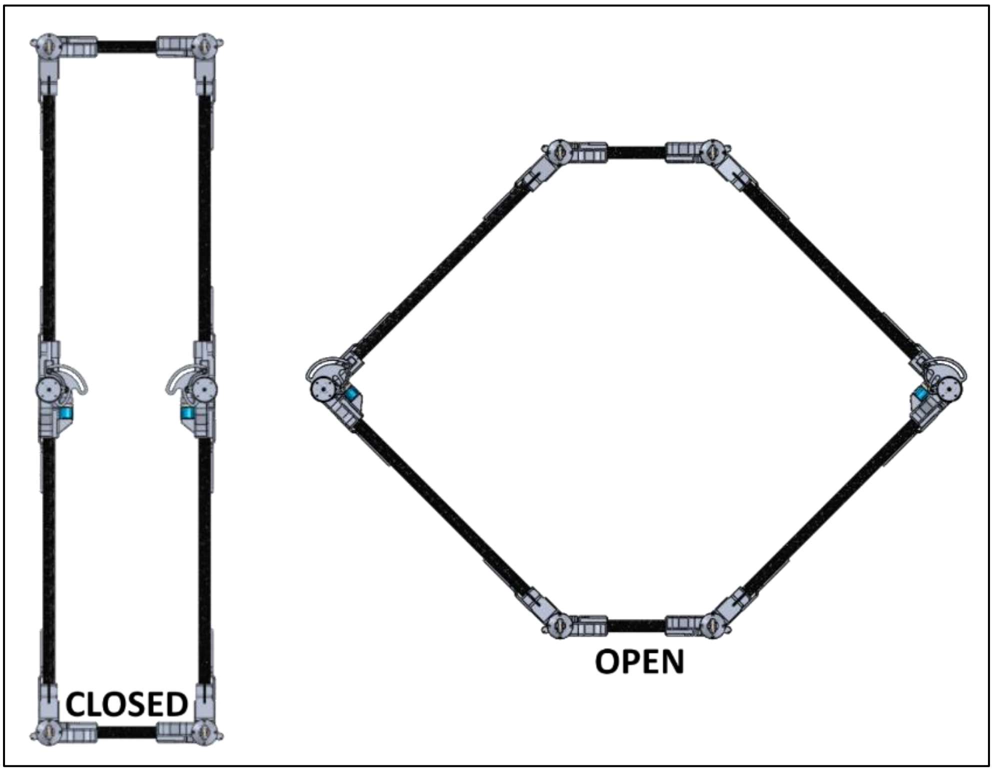

Figure 2.16: Designed chassis in closed configuration on the left and in open configuration on the right.

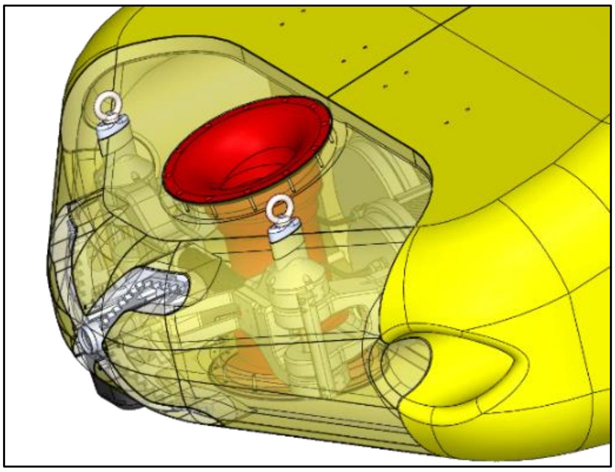

Figure 2.17: A particular of frontal lifting eyebolts.

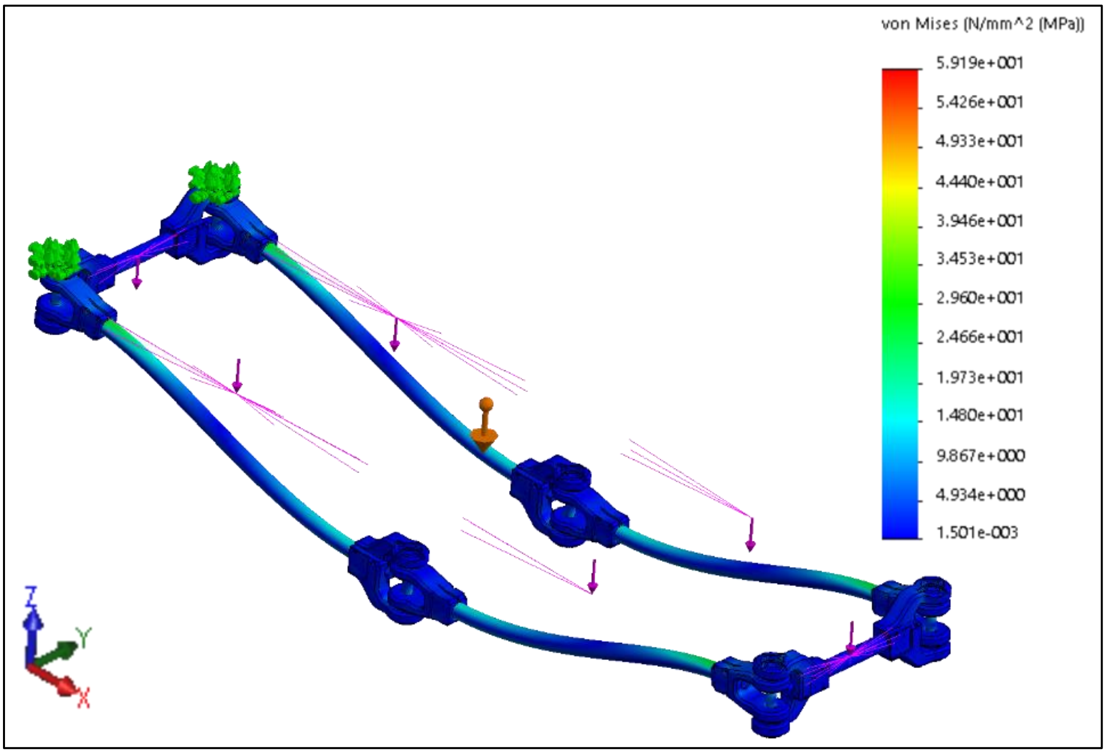

Figure 2.18: Stress on chassis during vehicle lifting.

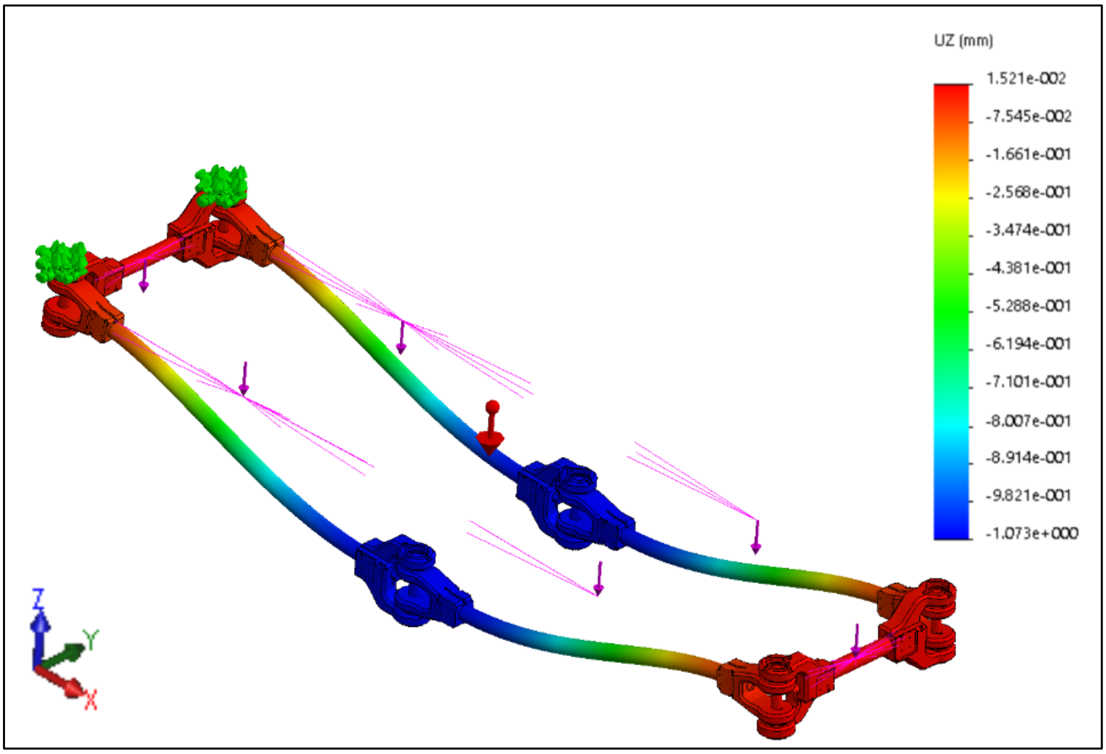

Figure 2.19: Displacements on chassis during vehicle lifting.

The result of the stress simulation for the lifting case is reported in Figure 2.18 and it is clear that the maximum stress (about 59 MPa) value is less than the Aluminum yield stress. In addition, it is worth noticing that also the displacements are limited (minus than 2 mm), as visible in the reported displacement analysis, in Figure 2.19.

2.3.3 Hulls design.

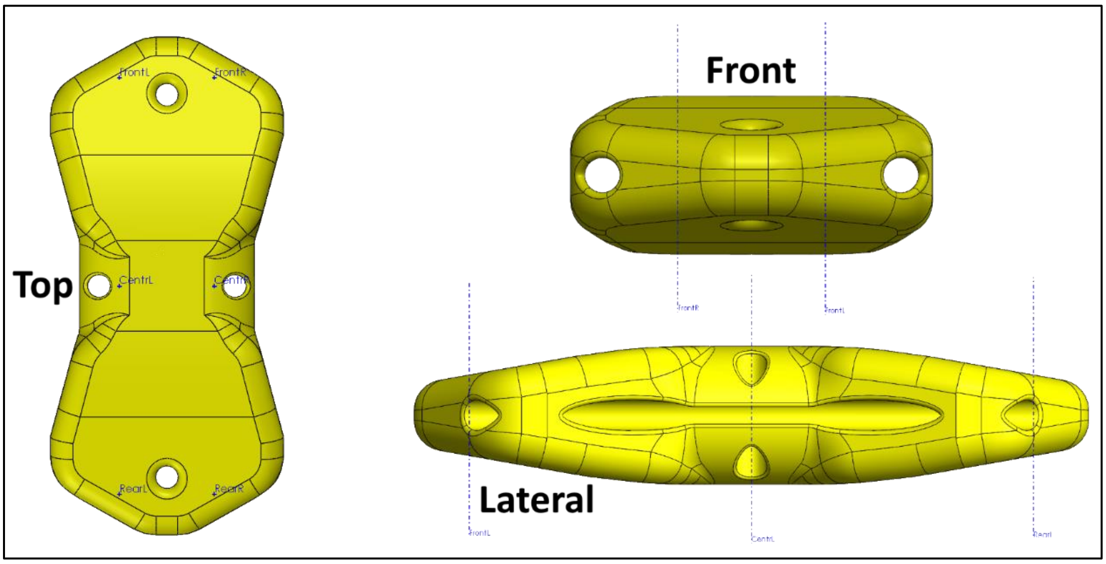

Figure 2.20: Top, front and lateral views of the hull mockup.

The hull design started from drawing a mockup of the whole vehicle. This mockup has guided the whole design process, because the most important requirement of the AUV shape is to maximize the fluid-dynamics efficiency of the vehicle especially in the closed configurations. For this reason, it has been chosen a flat shape able to hold all the vehicle thrusters and all the inner modules, as visible in Figure 2.20.

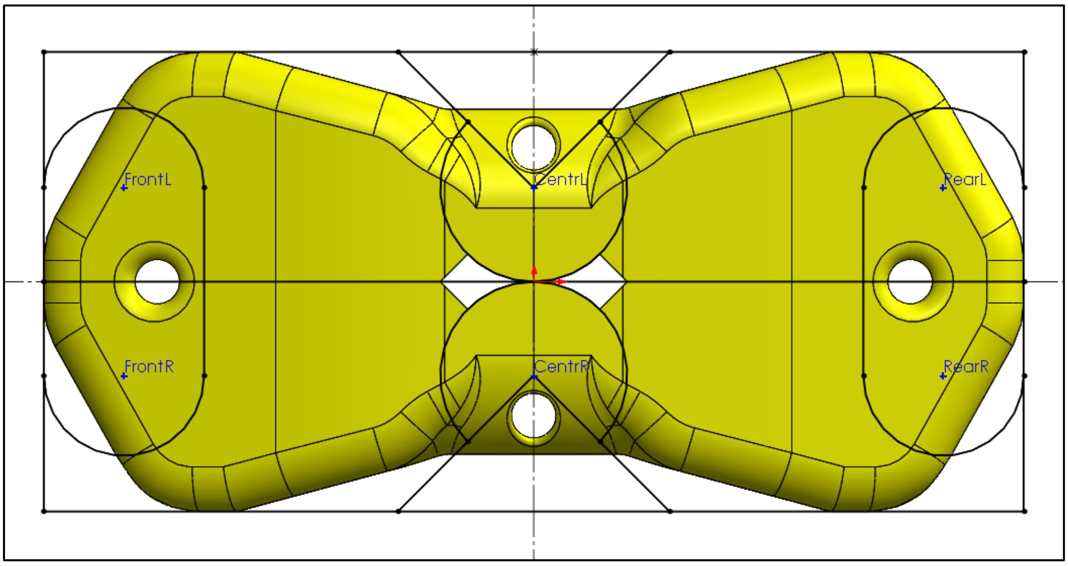

Figure 2.21: Hull cutting lines.

The definition of hull shape is not the only challenge of the hull design. Indeed, the hull shape has to be divided in different parts to allow the vehicle transformation. The hull partitioning is bounded by the necessity to maintain the highest efficiency possible, with respect to original shape; for this reason, each hull part has to fit perfectly with the nearest one, when the vehicle is closed. The best fitting could be obtained with circular cuts centered on joints axis, as visible in Figure 2.21. In this way, the hull parts cannot hit each other during the transformation.

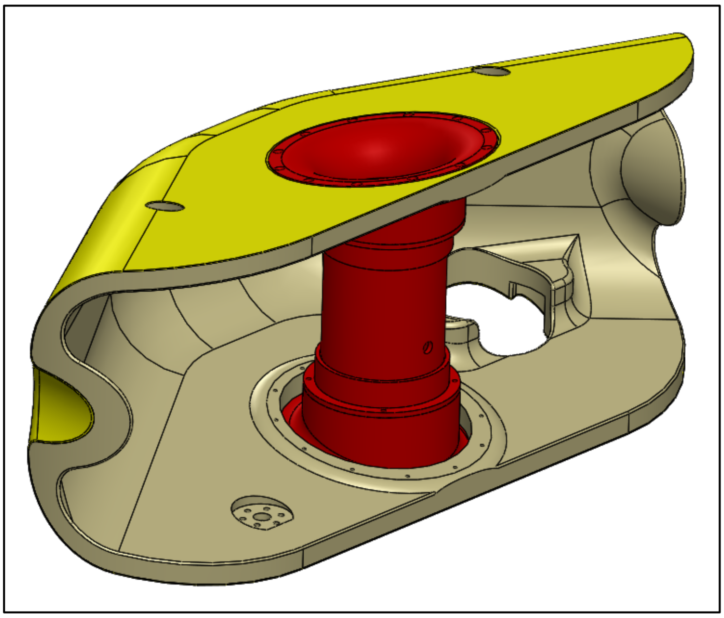

Figure 2.22: Rear hull part.

Regarding the constructive solution, hull parts are built with syntactic foam element covered by a carbon fiber shell. The thickness of foam elements has been chosen to provide the whole buoyancy to the vehicle. The purpose of the carbon fiber shell is to increase the components stiffness to protect the foam by impacts and to help the connection of pieces of foam, needed to shape the hull part. In addition, carbon fiber helps to create an external smooth surface. An example of hull part is shown in Figure 2.22.

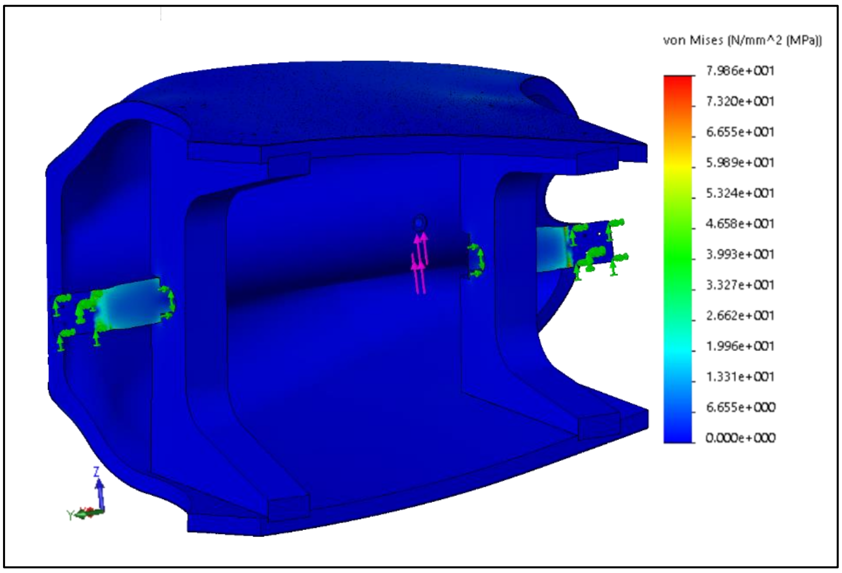

Figure 2.23: Stress on the lateral hull component during vehicle lifting.

Finally, FEM analysis for each hull part, to verify the values of stress and displacements of the hull elements subjected to own weight and loads due to thrusters and lifting action, has been made. In Figure 2.23 and Figure 2.24, for instance, stress and displacements of the lateral hull during a lifting action are reported. For this reason, the component is constrained to its support and is subjected to a loading force of a quarter of the vehicle total weight (625 N).

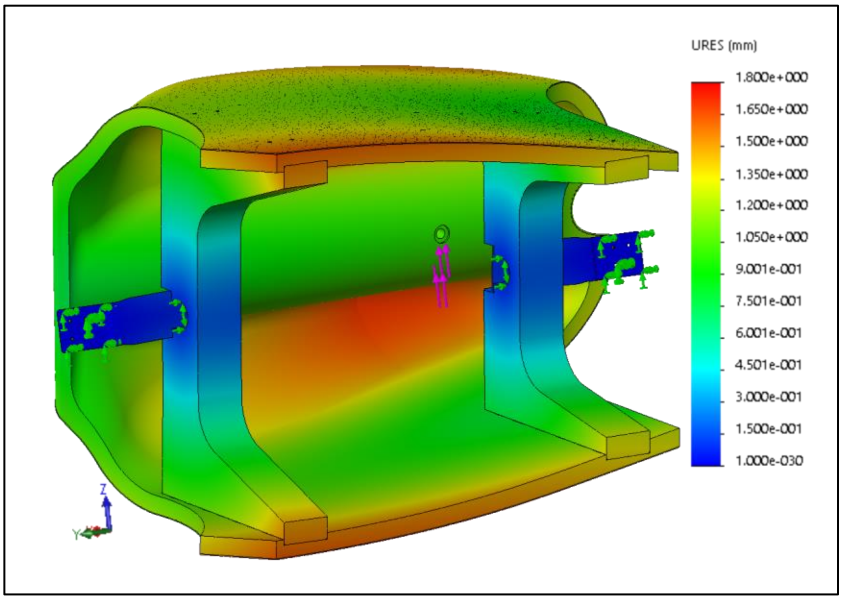

Figure 2.24: Displacements on the lateral hull component during vehicle lifting.

2.3.4 Electronics casing design.

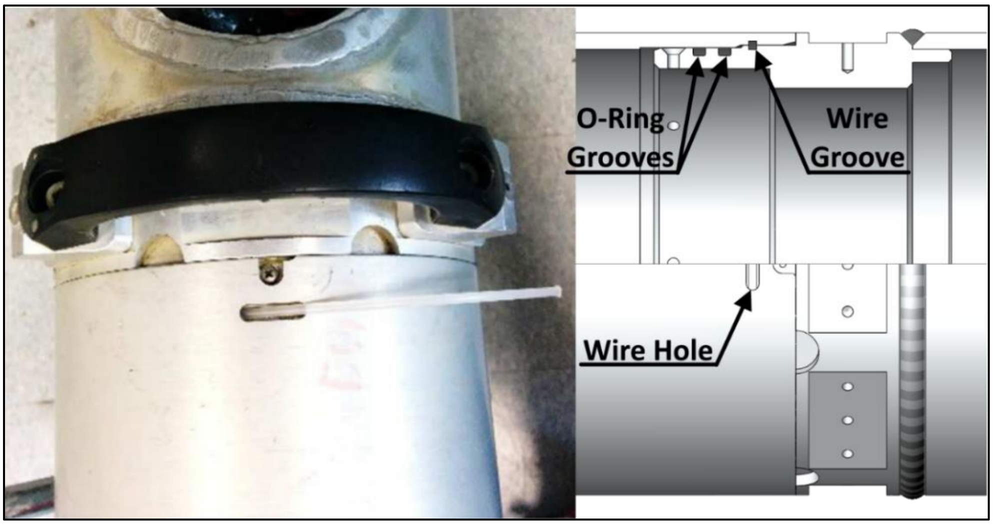

Figure 2.25: Wire locking system of MARTA AUV from UNIFI DIEF.

MARTA AUV modules [9] have inspired the design of the electronics casings. For this reason, each module has a cylindrical body, with two caps locked by wires, as visible in Figure 2.25. In addition, each module has a cap to put it under vacuum to verify and ensure its impermeability.

	Big Modules	Small Modules
Minimum Inner Diameter [mm]	130	100
Length [mm]	455	300

Table 2.4: Preliminary dimensions of tubes modules.

Each module has to contain electronics components, so their dimensions are related to the number and the dimensions of the electronics boards. Obviously, each group of electronic parts (Core Module, Power Module, etc.) occupies a different volume, but using tubes of different diameters for each module is not a smart solution, as it increases the vehicle cost and the number of components (decreasing thus the standardization). For this reason, only two different diameter values will be adopted to choose the thickness of the tubes for the casings: the "big one" for Core Module, Battery

Module and Antenna Module, the “small one” for Power Module, Driver Module and Connection Module. The choice of two diameters is due to the great difference of volume between these two groups of modules. Indeed, Power Module, Driver Module and Connection Module would have too low density using the same tube for all the modules and would be necessary using a great quantity of lead to balance them. In addition, from the volume occupied by electronics components the maximum lengths of each tubes are estimated. Table 2.4 summarizes the preliminary modules dimensions to define tubes thickness.

Material	Young Module [MPa]	Yield Strength [MPa]	Poisson Module [-]	Density [kg/m³]
Stainless Steel 316L	190000	480	0.265	7870
Carbon Fiber	120000	1650	0.28	1600
Aluminum 6082/T6	69000	240	0.33	2700

Table 2.5: Mechanical properties of the materials taken into account.

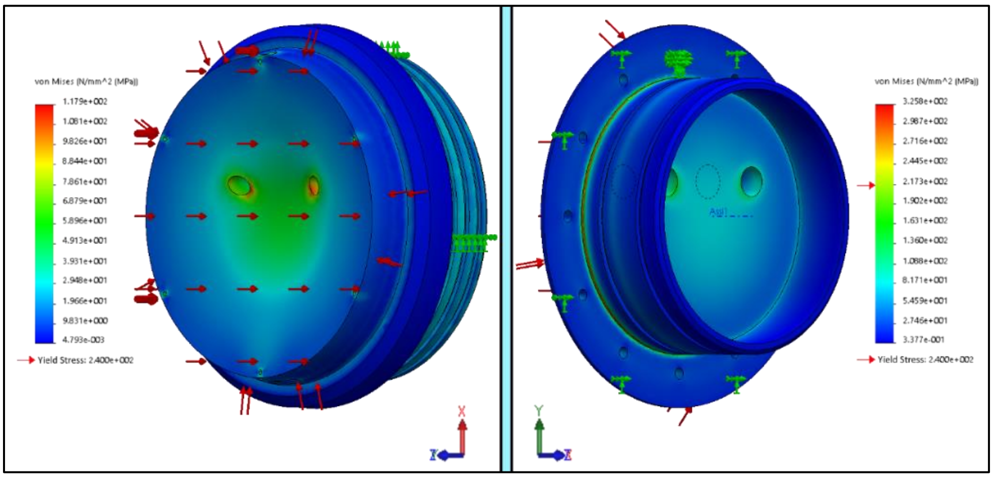

Figure 2.26: Stress comparison with and without taper joint.

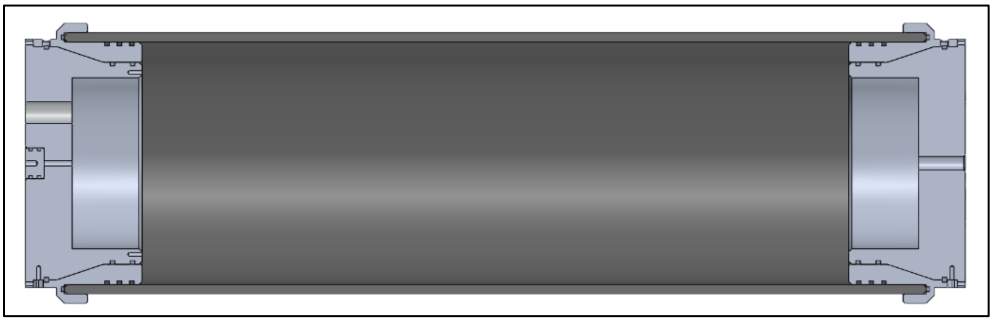

Figure 2.27: Example of electronics casing (Core Module).

The definition of preliminary tube dimensions is a focal point to calculate the thickness and to choose the material of casing tubes. Compared materials are shown with their mechanical properties in Table 2.5. As it possible to see, there is an unconventional material: carbon fiber. This material is taken into account, because the high pressure brings to high value of tubes thickness and for this reason high weight tube. The calculation of tubes thickness has been made with the methodology propose by C.T.F. Ross in 2009 [26] [27], based on R. Von Mises relation for thick-walled circular cylinders under-external hydrostatic pressure. Indeed, an empty container at depth of 1500 m collapse due to buckling instability. The thickness calculation has been made with a safety factor of 1,25 and a pressure design of 15 MPa.

Material	Big Modules		Small Modules	
	Thickness [mm]	Weight [kg]	Thickness [mm]	Weight [kg]
Stainless Steel 316L	5	7.6	3.5	2.7
Carbon Fiber	6	1.9	4	0.63
Aluminum 6063/T6	8.5	4.5	6.5	1.8

Table 2.6: Comparison bet ween weight and thickness of the tubes.

Table 2.6 shows the results and highlights the different weight between all materials; taken into account. From these resulting data, it is clear that the best material for electronics casing is carbon fiber, because the weight saving is conspicuous. Obviously, it is necessary to add flanges at the ends of the tube to support the caps and complete the casings. The presence of flanges requires the use of tubes with bigger diameters, because it is very important being able to insert the electronics boards into the casings. For this reason, a new structural verification has been made and the final dimensions are those shown in Table 2.7.

	Big Modules	Small Modules
Inner Diameter [mm]	156	120
Thickness [mm]	6	5

Table 2.7: Dimensions of modules sections.

Another big challenge of the electronics casing design has been the definition of a suitable caps shape. Indeed, it has been necessary to adopt a taper joint between the caps and the flanges to avoid stress concentration and mechanical collapse of the cap, as clearly visible in Figure 2.26. Moreover, in Figure 2.27 an example of electronics casing (Core Module) is visible. In addition, buckling stability at 1500 m depth (15 MPa of pressure) of each type of tubes is checked through with FEM analysis. An example of this is visible in Figure 2.28.

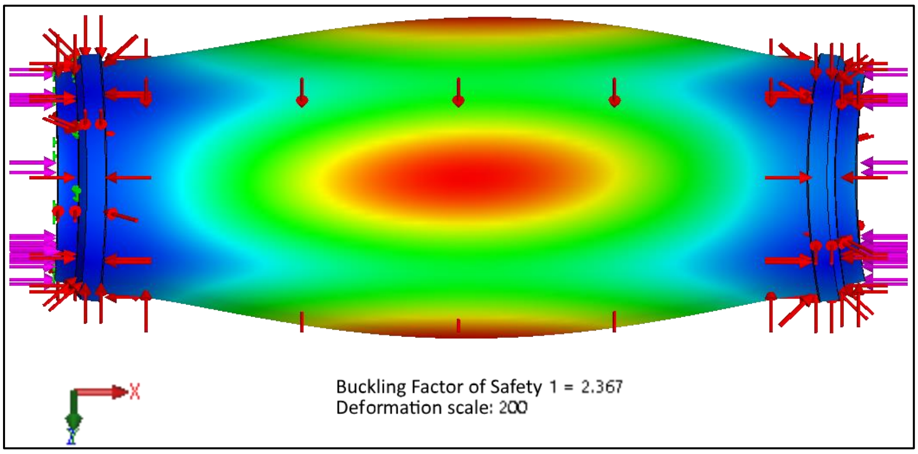

Figure 2.28: Buckling analysis of Core Module.

The connection between the tubes and the flanges is another crucial point for casings design. Indeed, this connection has to ensure the insulation of electronics boards and water. The simplest solutions is gluing carbon tubes to flanges. Obviously, future mechanical test will be necessary to verify the reliability of this solution, because the glue has to resist to deformations due to pressure and deferential expansions caused by temperatures. In any case, it is possible to change this approach, i.e. using a solution that employs a proper combination of glue and O-rings or the conceptual idea used for hull element could be extended. More in details, casing made by syntactic foam covered by carbon fiber could be designed. This solution could be very interesting especially for high-weight module, such as Battery Module, because it makes easier modules balancing.

In conclusion, the adopted solution allows obtaining modules with a good balance between robustness and lightness, as visible in Table 2.8.

	Density [kg/m³]	Volume [dm³]	Weight [kg]
Core Module	812	13.46	10.94
Antenna Module	976	9.15	8.94
Battery Module	1149	10.04	11.54
Power Module	973	4.78	4.64
Driver Module	1023	6.77	4.88
Connection Module	1181	3.90	4.61

Table 2.8: Bouyancy data of modules.

2.3.5 Casing balancing and supports.

The connection between the modules and the hull components or the frame is ensured by four types of support. The main differences between these supports are related to the modules density and dimensions. Indeed, two of them are suitable for big modules and the others for small modules, but each support has the same main features. More in details, each support is based on a clamp system to lock a module and has special groves to hold aluminum guides needed to place balancing weights or foams.

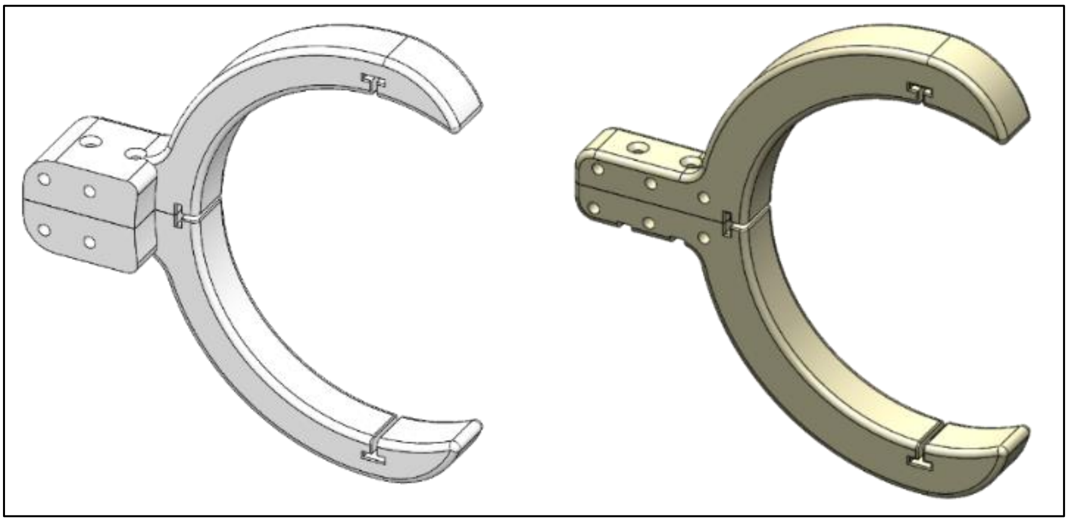

Figure 2.29: Supports for big modules: ABS support on the left and syntatic foam support on the right.

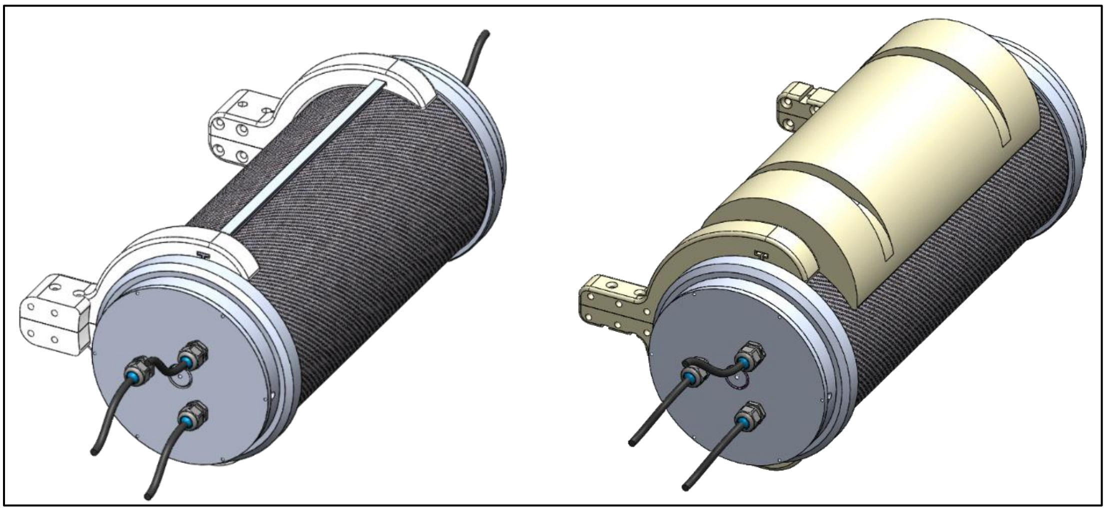

Figure 2.30: Examples of supports mounted on modules: Antenna Module with alluminium guide on the left and Battery Module on the right.

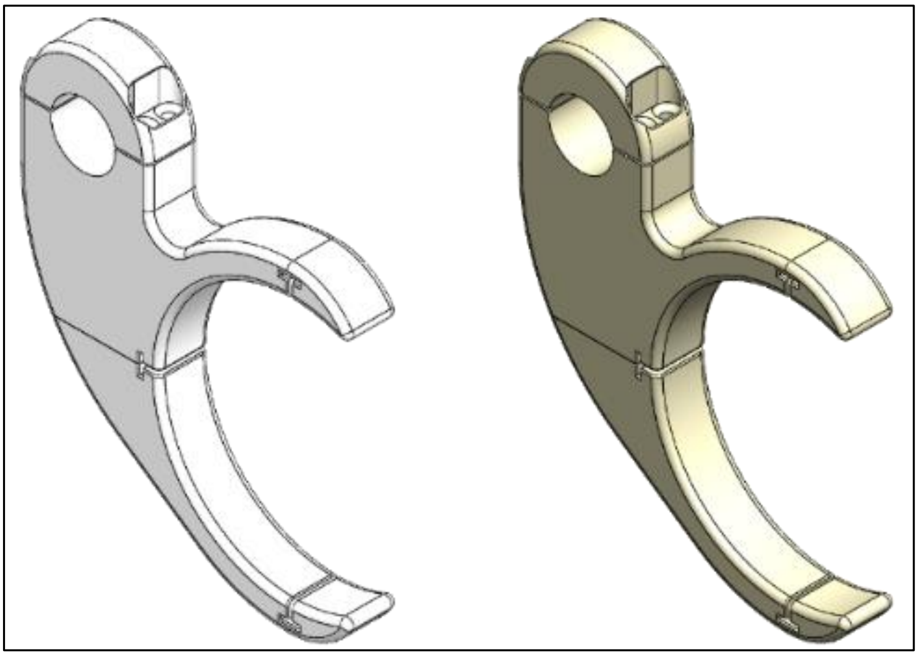

Figure 2.31: Supports for small modules: ABS support on left and syntatic foam support on right.

Big modules could be connected directly to the hull parts with two kinds of support (Figure 2.29): one made in ABS (Acrylonitrile Butadiene Styrene), the other in the same syntactic foam of the hull parts. The shape of these kinds of support is substantially the same. More in details, each support is made of two different elements connected each other by two screws. In addition, these supports are designed to connect the modules directly to the hull. Obviously, ABS supports are thought for modules with density similar to water or even lower. On the other hand, the supports made in syntactic foam are thought for modules with higher density and they allow helping the balancing of this kind of modules. Figure 2.30 shows examples of modules with their support and aluminum guides for balancing elements.

The supports for the small modules are designed to connect them directly to the vehicle frame, so, in addition to the clamp to lock the modules, they have another clamp to lock themselves to the rod of the vehicle frame. For this reason, they are composed of three different pieces (Figure 2.31). Also, the supports for small modules could be made in ABS or syntactic foam, according to the modules density.

As mentioned above, a perfect balancing of the modules is a critical requirement for the vehicle stability both in navigation and during its transformation. Obviously, the presence of modules with different density requires two different approaches. The balancing of high-density modules is obtained with supports in syntactic foam and additional shaped pieces of foam locked to the module through stainless steel cable ties. On the contrary, the balancing of low-density modules is made with balancing weights and balancing foam locked on aluminum (6082/T6) guides on the modules, as visible in Figure 2.30. The balancing weights are designed in two ABS components with a cavity able to house a calibrated quantity of lead. The two parts could be linked each other and locked on the aluminum guide with a screw (Figure 2.32). The balancing foams are simply shaped syntactic foam pieces and can be locked on the aluminum guide in the same way of the balancing weights (Figure 2.32). The dimensions of the balancing foam depend on the modules balancing. The aluminum guide allows an optimal positioning of the balancing weights and foams on the module. Finally, Table 2.9 summarizes the balancing weights and balancing foams required to balance each module with its supports. These data are based on the estimated weights of the modules.

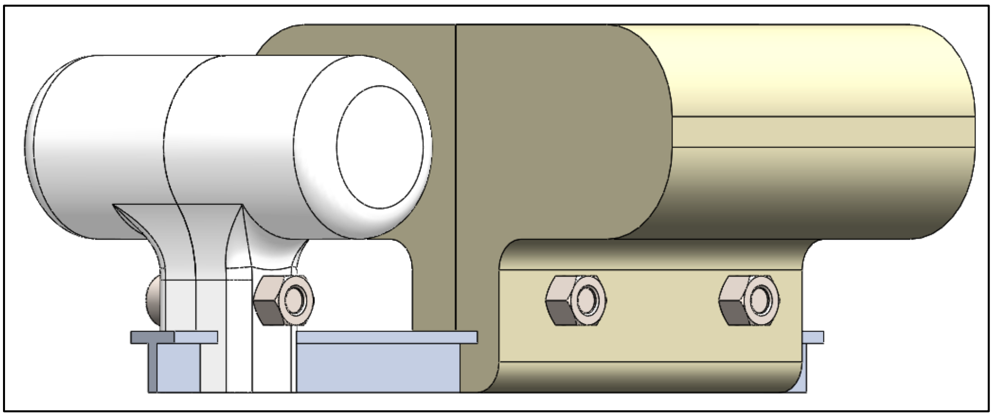

Figure 2.32: Examples of a balancing weight (in white) and a balancing foam (in sandy) on the aluminum guide.

	Density [kg/m³]	Fresh Water (1000 kg/m³)		Salt Water (1030 kg/m³)	
		Foam [l]	Lead [kg]	Foam[l]	Lead[kg]
Core Module	823	-	2.49	-	2.91
Antenna Module	981	-	0.18	-	0.48
Battery Module	1.111	1.95	-	1.86	-
Power Module	981	-	0.10	-	0.26
Driver Module	1029	0.18	-	-	0.03
Connection Module	1086	0.64	-	0.39	-

Table 2.9: Bouyancy corrections and balance corrections of the modules with supports.

Finally, Figure 2.33 shows the disposition of the modules in the vehicle under the hull parts.

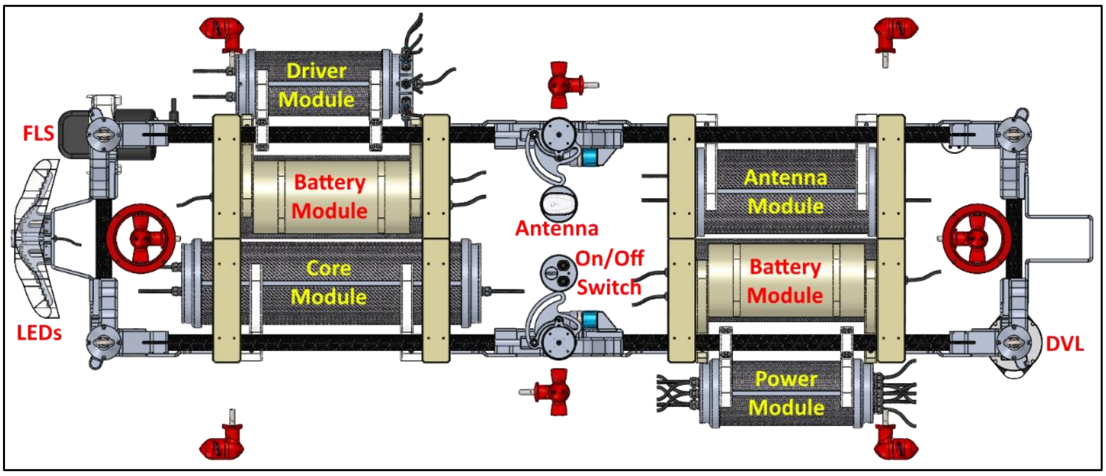

Figure 2.33: Disposition of the modules in the vehicle.

Chapter 3

Evolution of thrusters

3.1 BlueRobotics thrusters.

BlueRobotics [28] thrusters are the most innovative motors for marine applications in recent years. The basic idea behind their design is the realization of a low cost and extremely reliable thruster for small and medium UUVs. The project was presented in August 2014 on the crowdfunding platform named Kickstarter, raising $102,000 over a 30-day period and selling more than 1200 thrusters, serving a broad range of customers, from middle school MATE teams to researchers at Woods Hole Oceanographic Institution, in 25 counties. This shows the great interest aroused of this new kind of thrusters for marine application. The central idea of the project was reducing the complexity of a typical underwater motors to improve the reliability and reduce both production and maintaining costs. The technology is based around a three-phase brushless motor like the one you would find on a model aircraft or drone, tailored to work directly submerged in water. The main structural difference is the presence of a closed rotor to reduce the energy losses during the rotation in the water. Indeed, a common brushless motor for drone has big windows on the rotor to cool the stator winding. This solution in water entails remarkable fluid dynamics losses and for this reason the BlueRobotics engineers designed a fully closed rotor. This modification with respect to standard brushless motor does not compromise the motor cooling, because the high specific heat capacity of the water, and allows the motor to cool effectively. In addition, the windings and magnets are protected from corrosion with a multi-layer protective coating and the typical steel bearings were replaced with high-performance plastic bushings designed for underwater use. This solution removes the lubrication needs and leaves a single moving part in the thruster. The final result of this work are two motors models (Figure 3.1): M100 and M200.

Figure 3.1: BlueRobotics motors; M100 on the left and M200 on the right.

These two models differ from each other for their performances. The M100 is the smallest one and is suitable for small ROVs and AUVs. Otherwise, the M200 is the most powerful and is suitable for medium-size underwater vehicles.

Table 3.1, given here below, reports their specifications:

	M100	M200
Operating Voltage [V]	6 - 16	6 - 20
Max Current [A]	12.5	22
Max Power [W]	135	350
RMP/V	540	490
Torque [Nm]	0.28	0.5
Length [mm]	54	62
Diameter [mm]	32	36
Shaft Diameter [mm]	4	5
Mounting Hole Spacing [mm]	19 & 16	24 & 19
Mounting Holes	M3 x 0.5	M3 x 0.5
Weight in Air [g]	90	100
Weight in Water [g]	71	82

Table 3.1: M100 and M200 specifications, from the datasheet [29].

The BlueRobotics team not only has developed underwater motors, but it also has designed around them complete thrusters with propellers and nozzles. The structure of the motor is entirely built of injection molded plastic UV resistant. The motor is completely immersed in water, so there are no enclosed air or oil cavities and for this reason the traditional pressure limitations are eliminated. These thrusters have been tested to a maximum depth of 3000 m with no damage, but the expectation is to operate at even greater depths. In addition, the typical steel bearings were replaced with high-performance plastic bushings designed for the underwater use. In this way, the team eliminated the required lubrication and left a single moving part in the thruster, improving the reliability with respect to classic thrusters. The results of this work are two different thrusters models (Figure 3.2): T100 and T200. Table 3.2 reports their specifications, while Table 3.3 reports the propeller specifications.

Figure 3.2: BlueRobotics motors: T100 on the left and T200 on the right.

These thrusters are very interesting due to both cost and, less than 200 $, and performance. In addition, their power-weight ratio gives great advantages in the development of UUVs propulsion system, reducing the maintenance of the vehicle and gives assuring reliability. For all these reasons, the use of these motors, especially the T200, became a standard in many projects of the UNIFI DIEF MDM Lab: according to this, not only the new vehicles were developed mounting these thrusters, but also the oldest vehicles were upgraded exploiting these thrusters.

	T100	T200
Maximum Forward Thrust @12V [N]	23.6	35.5
Maximum Forward Thrust @16V [N]	-	51
Maximum Reverse Thrust @12V [N]	18.2	30
Maximum Reverse Thrust @16V [N]	-	41
Minimum Thrust [N]	0.1	0.1
Rotational Speed [RPM]	300 - 4200	300 – 3800
Operating Voltage [V]	6 – 16	6 - 20
Max Current [A]	12.5	22
Max Power [W]	135	350
Length [mm]	102	113
Diameter [mm]	100	100
Propeller Diameter [mm]	76	76
Mounting Hole Spacing [mm]	19	19
Mounting Holes	M3 x 0.5	M3 x 0.5
Weight in Air [g]	295	352
Weight in Water [g]	120	157

Table 3.2: T100 and T200 specifications, from the datasheet [30].

	T100	T200
Propeller Diameter [mm]	76.2	76.2
Hub Diameter [mm]	40	40
Pitch [mm/rev]	48	94
Number of Blades [-]	2	3

Table 3.3: T100 and T200 propellers specifications, from datasheet [30].

3.2 MARTA upgrades.

3.2.1 Previous thrusters vs BlueRobotics thrusters.

Figure 3.3: Marta AUV thrusters position: tunnelled thrusters (4) in circle red and stern thrusters (2) in circle purple.

MARTA AUV was developed, built and tested during the European ARROWS project (2012-2015). The project of MARTA AUV required a thrusters layout based on 6 motors, as visible in Figure 3.3, to provide to the vehicle the widest range of motion. MARTA has a torpedo shape and for this reason, the control of the roll is not necessary; indeed, it has been chosen to give to the vehicle a buoyancy stability, setting its center of mass under its center of buoyancy. The lateral motion and the yaw rotation are provided by two lateral tunneled thrusters, placed one on the bow and the other on the stern with their rotational axis lying on horizontal plane of the vehicle. In the same way, the vertical motion and the pitch rotation are provided by other two tunneled thrusters, placed in the same module of the previous two, with their rotational axis lying on the vertical plane. The other two thrusters are placed on the stern and provide the required longitudinal thrust to the AUV.

In the light of the above, it is clear that MARTA AUV is equipped with two kinds of thruster: 4 tunneled thruster and 2 common thrusters. The old thrusters, i.e. the first ones designed and used on board, had some differences especially because the tunneled thrusters could not have a conventional nozzle due to space limitations as visible in Figure 3.4. For this reason, the main difference between them was the terminal part (the part with the propeller) and the blocking system, while the watertight motor module was the same.

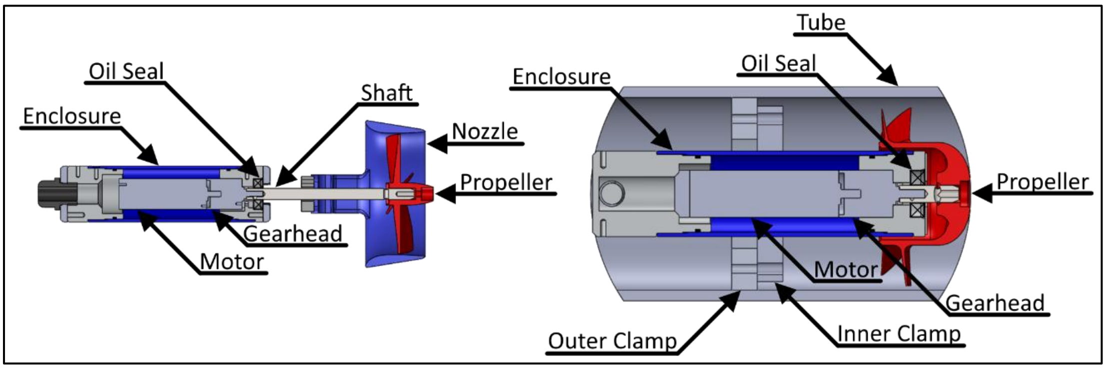

Figure 3.4: MARTA AUV old thrusters: the stern thruster on the left and the tunnelled thruster on the right.

The stern thrusters had a long shaft with a propeller type Ka 4-70 [31] (a very common one), that for this application is very efficient, screwed at the end. This propeller was coupled to a nozzle No. 19a [31] that maximizes the forward thrust. On the other hand, tunneled thrusters had short shaft with propeller screwed at the end. This solution was needed due to limited dimensions of the tube placed in the AUV hull. In addition, the lack of an efficient nozzle entails the necessity to use a different kind of propeller, with respect to the stern thrusters. For this reason, a customized propeller has been designed. To determine the optimal propeller geometry, various shapes have been tested, varying the number of blades and the p/d ratio. With regard to the blocking systems, the stern thrusters were locked to the hull with Al Anticorodal (Al 6082/T6) and ABS custom supports and some screw. The tunneled thrusters instead were locked to their tubes with two Al Anticorodal custom clamps. A screw pushed on the tube the outer clamp, while another screw tightened the second clamp around the motor module. Finally, other two screws connect together the inner and the outer clamps. However, both of the thrusters type were built around a unique custom motor module. The module was made of a watertight casing containing an electric motor with its gearhead submersed in oil. More in details, three main elements of Al Anticorodal compose the casing: a tube and two end caps. Two O-rings between the tube and each end cup assure the impermeability of the motor casing. In addition, an oil seal assures the separation between oil and external water due to the presence of a shaft for the propeller.

	1 Rotor	1 Stator	2 Plastic Bushings	2 Ball Bearings	1 Tube	2 End Cups	2 O-rings	1 Gearhead	1 Oil
BlueRobotics Motor	+	+	+	−	−	−	−	−	−
Old Custom Motor	+	+	−	+	+	+	+	+	+

Table 3.4: Comparison between MARTA old motor and BlueRobotics motor components.

As mentioned above in the first paragraph of this chapter, the first thing that stands out by comparison between the BlueRobotics motors and the old MARTA motors is the highest degree of simplicity of the first ones, as visible in Table 3.4. This condition is the first great advantage of the new commercial motor, because a lower number of components ensures a higher reliability. In addition, the new motor solves three non-negligible problems:

1. Sealing;
2. Oil;
3. Gearhead.

The sealing of MARTA motors was obtained with O-rings and a seal lip on the propeller shaft. Unfortunately, the seal lip allows a good separation between motor and water, but it increases the power losses. Indeed, the seal lip applies a resistant torque on the propeller shaft, reducing the available power. In addition, this resistant torque increases with the depth, because external pressure pushes the lip of the seal on the shaft. For this reason, the power consumption of the motor increases with the depth, reducing the operative mission time of the vehicle.

The presence of oil was very important for the old MARTA motors, because it allowed not only to cool and lubricate the motor, but also to endure the high external water pressure. But on another hand, the presence of oil was a big problem for two main reason. First, the oil seal on the shaft did not ensure the perfect insulation from the water. Indeed, the oil seal had some leakages that increased with its wear. This condition can bring to a loss of oil, which as its effect had a leakage of water and air in the casing. The water, especially, salt water, cause the deterioration of all the motor components, because it oxidizes the mechanical and magnetic parts and generates short-circuits in the electrical components. The presence of air is very dangerous even if its quantity is low. Indeed, the absorption of air through the oil seal can occur only when the vehicle sails on the surface, but the presence of air in the motor casing can cause the deformation of the casing itself under the water pressure. This condition entails the failure of the O-rings and compromises the tightness of the motor module. For this reason, it is extremely important to check very frequently the oil and the oil seal status, refilling or changing the oil, if contaminated by water, and changing the oil seal regularly.

Figure 3.5: Comparison between the old and the new version of MARTA stern.

The gearhead was a fundamental component for the old motor module, because during the MARTA AUV development cheap direct drive motors, with the dimensions and the performance desired, were not available. Indeed, for marine propulsion applications a motor can ensure a good level of torque at low revolutions. The motor chosen for MARTA thruster was a Maxon® EC 22 100 W power (no longer available), with a nominal speed of 28300 RPM and a nominal torque of 49 mNm. This speed was too high for this application, and for this reason a planetary gearhead with a ratio of 1:3.8 (GP 22 A) was added to the motor. Even if its presence was very important for the thruster performance, it entailed two problem. First, the planetary gearhead adds to the motor some power losses, increased by the presence of oil around gears. In addition, the typical use of the thruster entails a remarkable wear of the gears. Indeed, to control the position of the vehicle in the water the propellers need to change rapidly their rotation direction. This condition cause shocks between the gears that degrade the gearhead over the time. For this reason, it was very important often to check the gearhead clearances changing it if necessary.

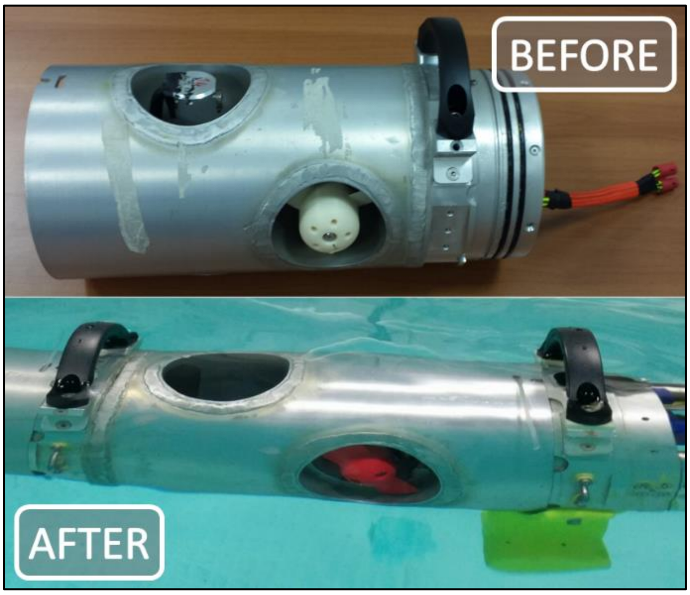

Figure 3.6: Comparison between the old and the new version of MARTA tunneled thrusters.

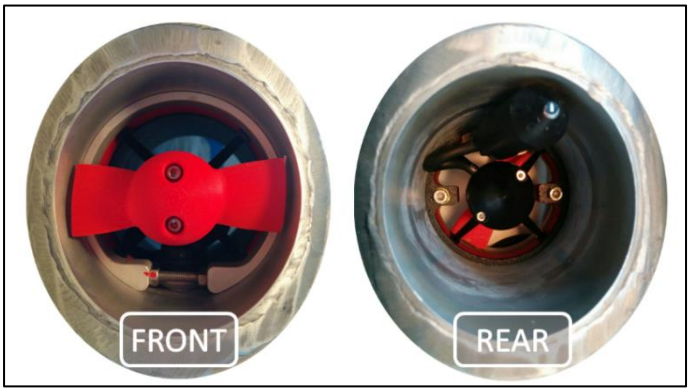

Figure 3.7: Detailed views of thenew tunneled thruster.

In summary, the presence of the sealing system, the oil and the gearhead heavily affected thruster performances, because they reduced the efficiency and required many attentions to work properly. These conditions heavily reduced the usability of the vehicle, because more power consumption caused a reduction of the operative mission time and the high number of critical components caused frequent and expensive maintenance and repairing works. For all these reasons, MARTA had to be upgraded.

Actually, the upgrades of MARTA were quite easy. Indeed, for the stern thrusters directly two BlueRobotics thrusters were employed, just printing new stern supports was needed (with the

Stratasys Dimension Elite of UNIFI DIEF MDM Lab), as visible in Figure 3.5. On the contrary, the tunneled thrusters required more modifications, but, however, the solution adopted was very simple also in this case. The BlueRobotics thruster was disassembled and only the motor and the internal support were used. Then a new propeller and a circular support were printed in order to connect the motor support to the inner clamp in the thruster tube. Finally, all the components had been assembled (Figure 3.6). In addition, it worth noticing that small dimensions of the BlueRobotics leave free a larger section of the tunneled thruster, ensuring a higher and "better" water flow and thus a higher thrust (Figure 3.7).

Finally, an evolution of the actual tunneled thruster was been tested and this was embedded in the innovative reconfigurable vehicle described in previous chapter. This new solution is visible in the figure here below (Figure 3.8).

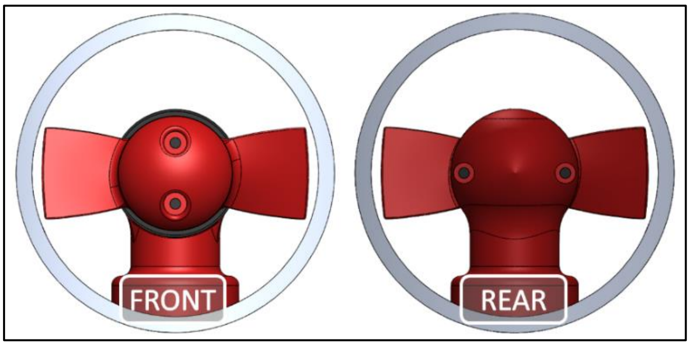

Figure 3.8: Detailed views of the new modified tunneled thruster.

3.2.2 Experimental thruster test rig.

For the estimation of the bollard thrust of a certain actuator, it is possible to perform dedicated bollard thrust tests in a pool. This is one of the most common way to identify the response of the coupling between motor and propeller and evaluate their performance. To execute a preliminary comparison between old MARTA thrusters and the BlueRobotics thrusters, it has been necessary to use a measurement test bench/test rig. The test rig used for these preliminary tests is an old version/architecture of the measurement test bench developed during the European ARROWS [12] projects to carry out an experimental measurements campaign, needed to identify the best propeller profiles for MARTA thrusters and to verify the performances of these designed thrusters. This test rig was cheap and quite simple (it is visible in Figure 3.9). The tested thruster is directly connected to a support structure by means of a linear guide. This linear guide suppressed 4 DOFs allowing to the thruster only the longitudinal motion and the rotation around longitudinal direction. Others 2 DOFs were suppressed by two load cells that allow measuring the thrust and the reaction couple of the thruster. Neglecting the friction on all the other joints, the longitudinal thrust was measured directly by the thrust load cell, located behind the motor. I.e. neglecting the friction on all the other joints, the torque was calculated measuring the reaction provided by the torque load cell that blocked the rotation around the longitudinal direction. Both the load cells were low cost anodized aluminum load cells and they were made suitable to immersion using a plastic spray film. In addition, in order to improve the measurement quality, signal-conditioning units (cell amplifiers) had to be placed near to the cells and were protected with watertight protection gel. By means of this simple test rig it could be possible to measure all the required data to estimate the thrusters performances. More in details, the cells voltages were measured with a voltage meter and allowed to calculate the forces acting on the cells. Since rotor speed sensors are not always present, in the proposed testing layout the rotational speed was estimated through electric measurements directly performed on motor phases. In particular, the fundamental harmonic drive component is extracted from the driving voltage waveform through a spectrum analyzer. Additional measurements were performed with a digital power analyzer that provided measurements of current, voltage and power consumption of the electric motor.

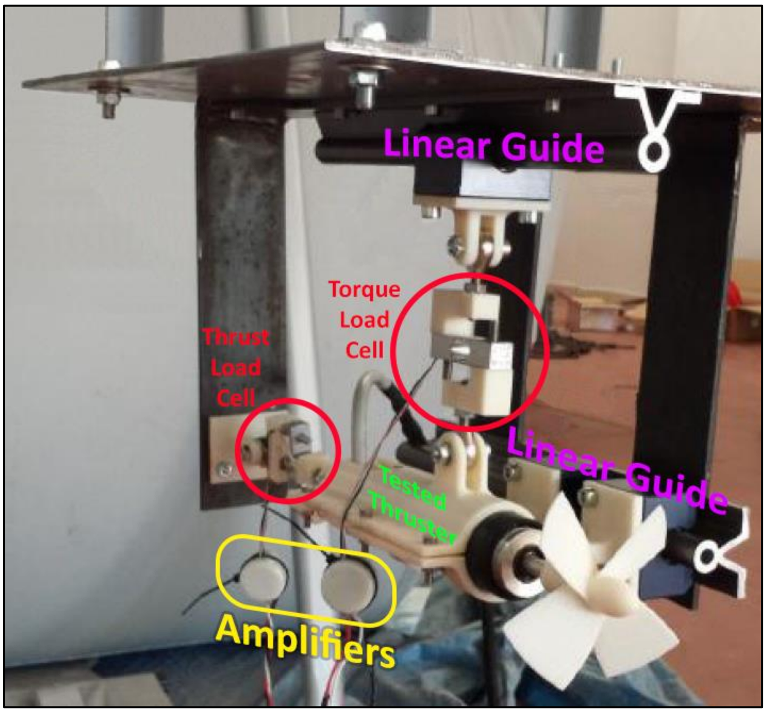

Figure 3.9: Old thruster test rig.

3.2.3 Performance comparison.

Preliminary tests had two main aims:

1. Verifying if BlueRobotics could work safely with 6s Li-Po (Lithium Polymer) batteries.
2. Verifying if BlueRobotics could represent an improvement for MARTA AUV propulsion system.

Regarding the old data of MARTA thrusters, it is very important to underline that Maxon® motors worked out of specifications. Indeed, as mentioned above, this motor was a 100 W power motor with nominal voltage of 18 V and maximum continuous current of 9.11 A, but on MARTA it worked with a power supply of 6s Li-Po battery (nominal voltage 22.2 V – maximum voltage 25.2 V). For this reason, the tests of these motors were performed reaching about 170 W. This kind of application was possible for this kind of motors, because these motors worked in an Aluminum case filled in oil and submerged in water. This condition allows a better cooling with respect to the use of the same motor in air. The technical specifications (on the datasheet) were referred to the use of the motor in air, so using these motors with higher tension inside the water was not a problem, as their reliability over the years confirmed. The only restriction applied to this kind of thruster was the limitation of the current supplied to the motor. The current limit was about 7 A, 2 A under the current motor limit. In addition, all the tests, were carried out with a power supply of 24 V.

Figure 3.10 and Figure 3.11 show the comparison between an old MARTA thruster (placed on MARTA stern) and a commercial BlueRobotics thruster. The comparison has been made taking the power as a reference, because ranges of rotational speed are completely different: a peculiar behavior of thrust coefficient for BlueRobotics has been detected, i.e. the thrust coefficient of these thrusters seem to link to their rotational speed (this particular behavior will be widely discussed in §3.4.3).

Figure 3.10 and Figure 3.11 also highlight that BlueRobotics thrusters are a great improvement for MARTA AUV. Indeed, not only BlueRobotics thrusters can be used to reaching a higher power than the old MARTA thrusters, but also provide more thrust at the same power. More in details, it is possible to see that the thrust in the forward direction at about 160 W can even increase by a 42%. The advantage brought by the new propulsion solution is lower in the backward direction, however it is still significant. Indeed, at low power the thrust provided by the old MARTA thruster is slightly higher than the BlueRobotics one (about +21%). This behavior is probably related to the coupling between the propeller and its nozzle. However, at about 160 W the BlueRobotics solution provides 21% of thrust more than the old one, with a peak of 39% at about 100 W.

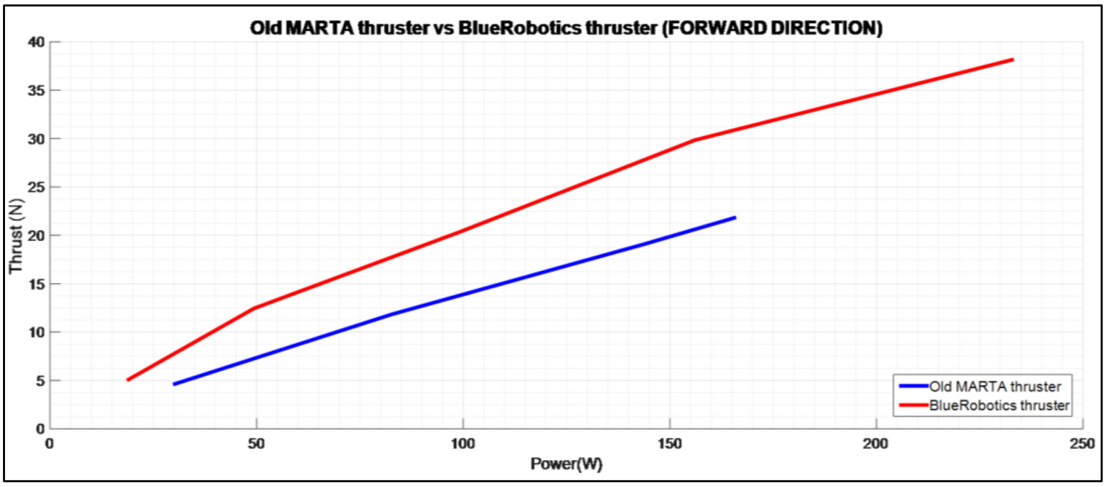

Figure 3.10: Comparison between old MARTA thruster and BlueRobotics thruster in the forward direction.

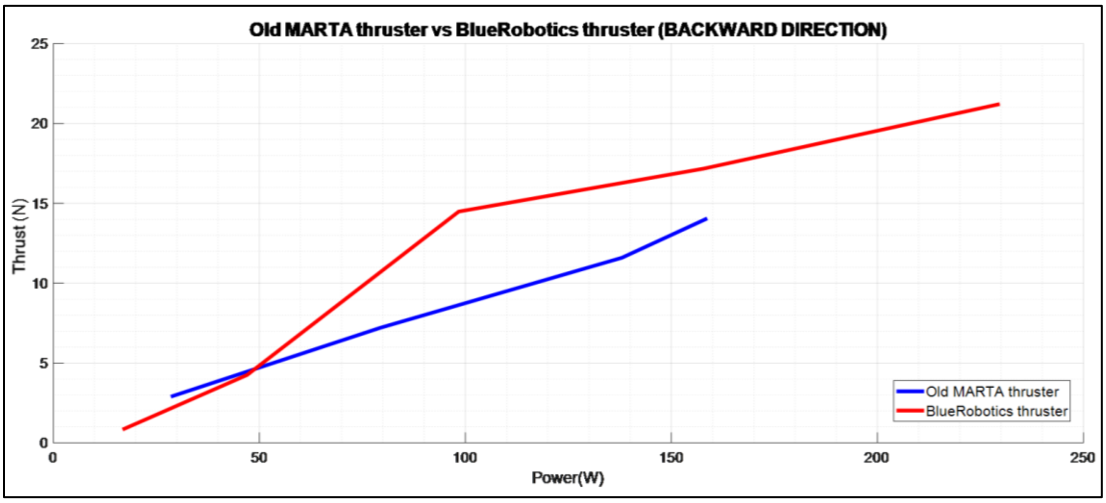

Figure 3.11: Comparison between old MARTA thruster and BlueRobotics thruster in the backward direction.

Figure 3.12 and Figure 3.13 show the comparison between old MARTA tunneled thruster and custom tunneled thruster made with a BlueRobotics locked in the tube with a clamp system, similar to one reported in Figure 3.7. As did before, also this one has been made taking the power as a reference. For this kind of thrusters, the improvement is even greater than the previous one. Indeed, the new tunneled thruster provides a higher value of thrust than the old one for each value of power. More in details, the new one provides an improvement of forward thrust of 32% and of backward thrust 36% at the maximum power of the old thrusters. In addition, the new thruster has a more symmetrical behavior. Indeed, the difference between the forward and the backward thrust decreased from about

26% to about 20%. This improvement is mainly related to the increase of free section into the thruster tube, due to the smaller dimensions of the BlueRobotics motor (Figure 3.7).

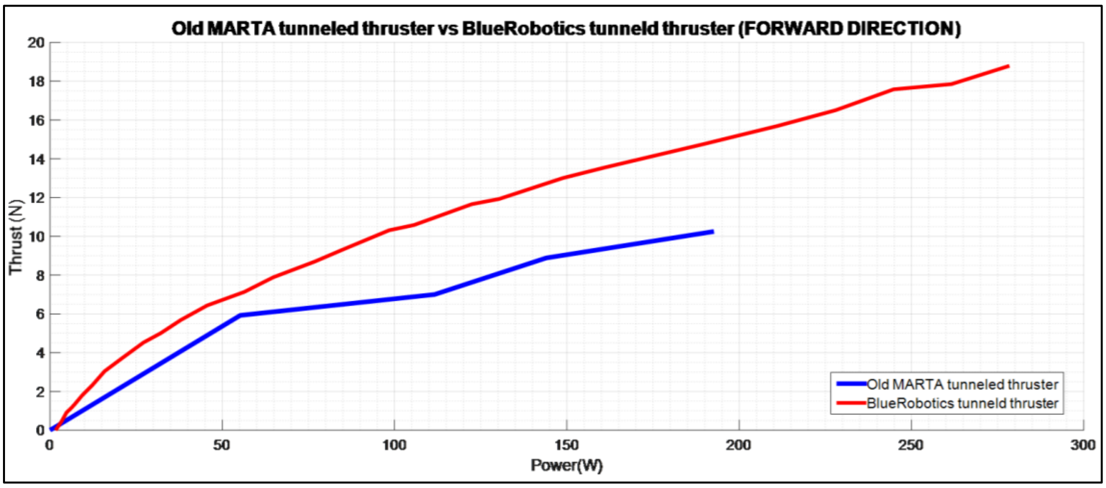

Figure 3.12: Comparison between old MARTA tunneled thruster and BlueRobotics tunneled thruster in the forward direction.

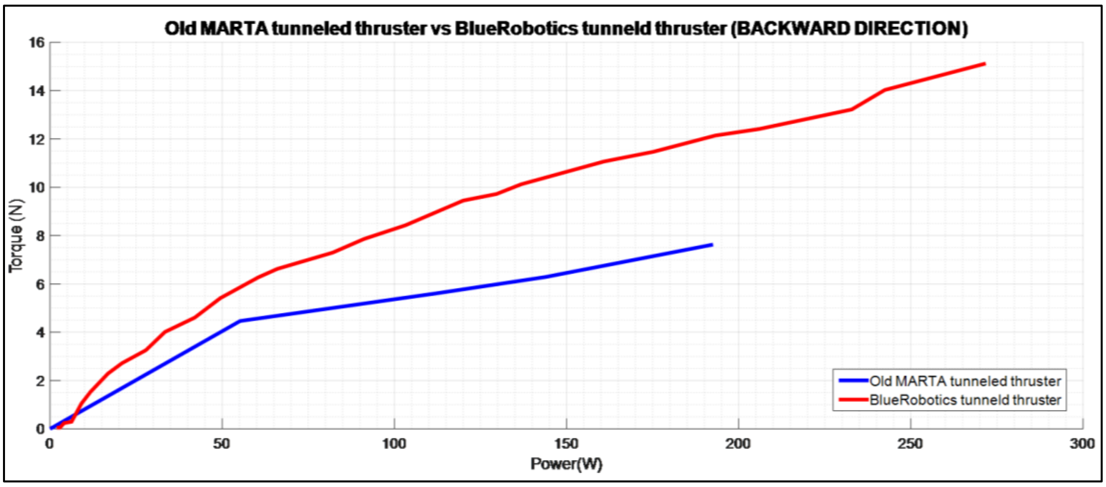

Figure 3.13: Comparison between old MARTA tunneled thruster and BlueRobotics tunneled thruster in the backward direction.

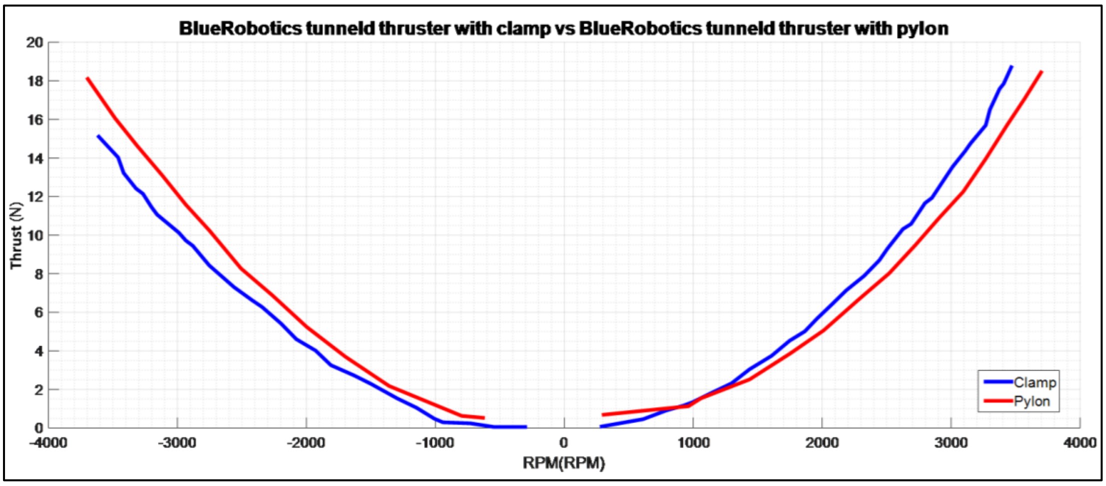

Figure 3.14: Comparison between BlueRobotics tunneled thruster with clamp and BlueRobotics tunneled thruster with pylon.

As mentioned in §3.2.1, for the new tunneled thruster an improved version has been tested to eliminate this residual 20% of asymmetry. The modified solution uses a shaped pylon to support the BlueRobotics (Figure 3.8) motor instead the clamp system to minimize the fluid dynamic into the tube of the thruster. As visible in Figure 3.14, this solution succeeds in eliminating the tunneled thruster asymmetrical behavior. More in details, only about 2% of difference between the forward and the backward direction persists.

3.3 ZENO design.

3.3.1 Main vehicle features.

ZENO AUV design, developed during the European ARCHEOSUb project, is rugged and with hydrodynamic characteristics to allow a good navigation performance even in presence of substantial marine currents. Two modules constitute the main structure the central housing and the supply system (visible with other components before the assembling Figure 3.15). These are in Anticorodal type 6082 T6 (main housing) and 6061 T6 (battery module), the modules have been theoretically studied for a design depth of 150 m (even if the operative depth of the vehicle is 100 m), investigating both yielding and buckling collapse [32] and, then, have been validated through FEM (Finite Element Method) Analysis. In addition, they have been finally tested in the pressure chamber of the MDM Lab of the University of Florence at 15 MPa. The vacuum cap, the switching on cap, antenna support and custom eyebolts, the other metallic elements, are in steel AISI 316L.

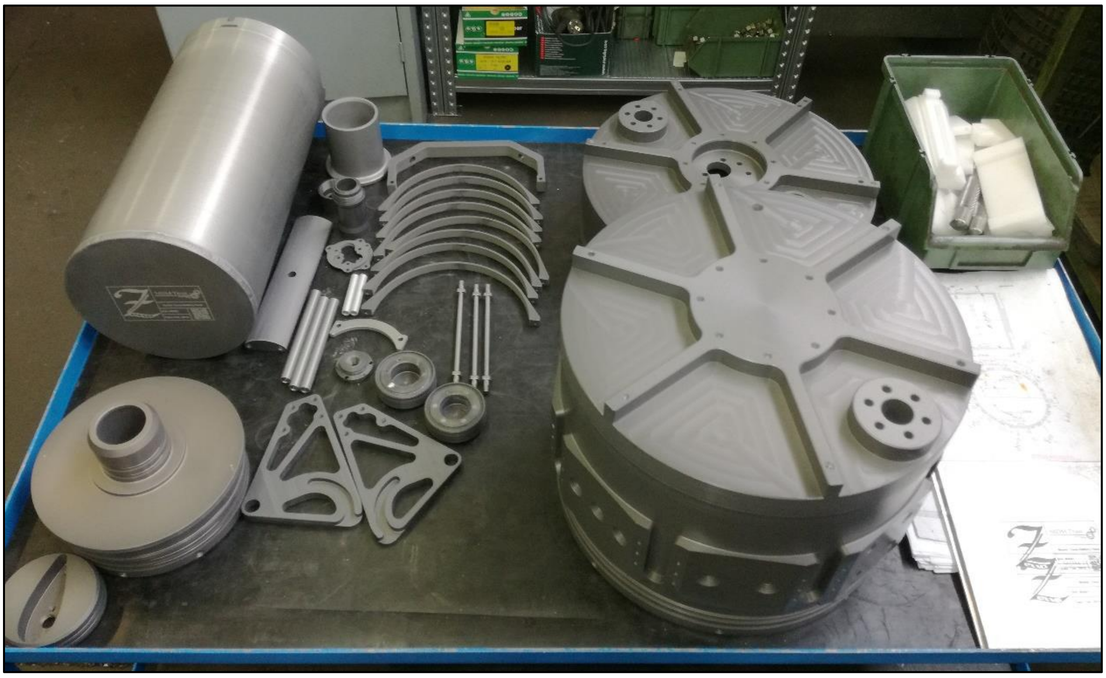

Figure 3.15: Some aluminium components ready to be assembled.

The main frame is in carbon fiber matching external twill fiber pattern with 10 inner unidirectional motif dipped in epoxy resin, connected by junctions in PolyOxyMethylene (POM) and surrounded by foam board in closed-cell PVC (PolyVinyl Chloride) usable up to 300 meters underwater. The main elements are highlighted in Figure 3.16. The carter, composed of two mirrored fiberglass shells, provides protection and attachments, not visible in Figure 3.16.

Finally, ZENO performances can be summarized as follow:

- Operating depth: 100 m.
- Cruising speed: 2 kn (up to 3 kn).
- Weight: about 45 kg.
- Dimensions: 1060x840x269+225 of antenna mm.
- Autonomy: 3 h of operations with each battery module.
- Navigation accuracy: 2%.
- Power supply voltage: 14,8 V.
- Customization: different sensors and payloads available.
- Hovering capability: thanks to 8 thrusters the vehicle has 6 DOFs fully controllable.

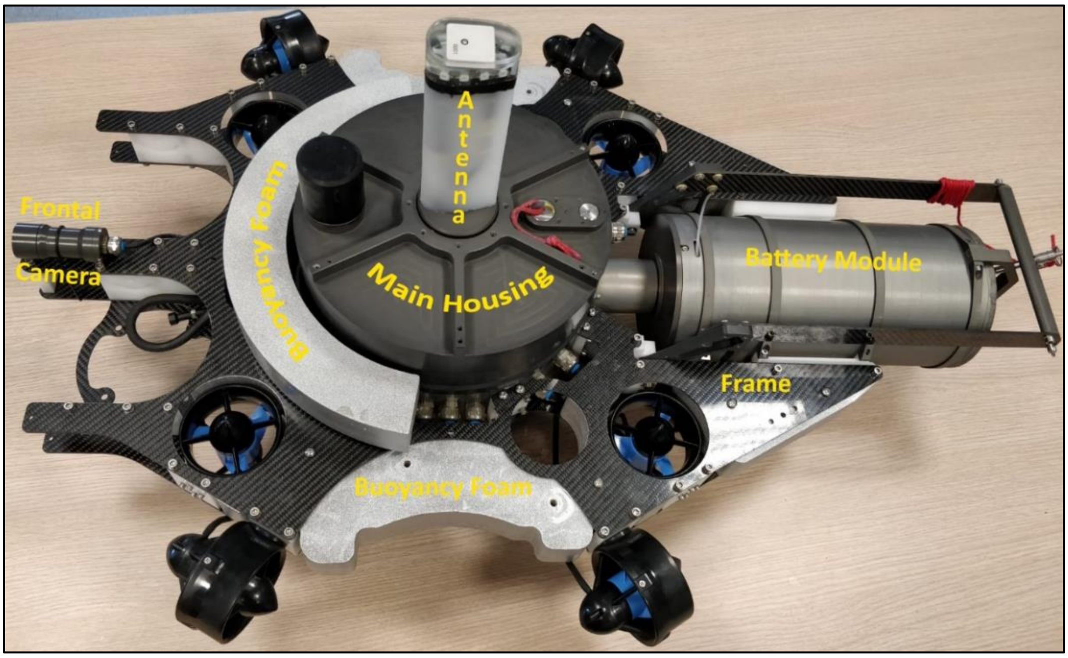

Figure 3.16: Outline of the main elements.

Regarding the payload, the vehicle can be equipped with different sensors and payloads; the balancing in the different configurations is guaranteed by the predisposition of appropriate weights. Its design allows the housing of different payloads according to the archaeological mission to be performed:

- Navigation and communication: IMU with magnetometer, Depth Sensor, Echo Sounder, GPS, Radio Modem, Wi-Fi, Single-axis FOG DSP-1760 of KVH (optional), Doppler Velocity Log DVL 1000 of Nortek (optional), Acoustic modem S2CR 18/34 of Evologics (optional).
- Optical and acoustic payload: Frontal and Vertical Cameras, Illuminators LEDs, Side Scan Sonar (SSS) OSM2 of DeepVision, 2D FLS BlueView M900 of Teledyne®.

3.3.2 Motors layout.

The main aims of ZENO AUV design have been realizing a compact, multipurpose, cheap, powerful and agile vehicle. For this reason, ZENO has been designed starting from the thrusters disposition, giving to this AUV the ability to control all its 6 DOFs. This condition, as noticed in §1.4, can be obtained only with at least seven thrusters. The first proposed solution has been a vectored layout with three vertical thrusters and four vectored thrusters on the horizontal plane. The choice of a vectored layout is related to the necessity of giving to the vehicle a remarkable hovering capability. This layout, as observed above, allows moving the vehicle with great precision, smoothness and sensitivity on the horizontal plane. In this way, the AUV can easily maneuver even near underwater object, without damaging them. Unfortunately, this first proposed layout had a drawback, due to the presence of the three vertical thrusters. Indeed, these thrusters have to be placed in a symmetrical way on the vehicle to avoid undesirable rotation during vertical motion. For this reason, one of them had to be placed exactly on the longitudinal axis of the vehicle, but in this way this thruster occupies an area of the vehicle usually suitable to place payloads or other devices. This condition would bring to the necessity to lengthen the vehicle in order to place components ahead of the thruster. In addition, this solution can disturb the acoustic payloads, due to the air bubbles generated by the thruster (when the AUV is near to the surface). For all these reasons, this first solution has been abandoned in favor of an eight thrusters solution, as reported in Figure 3.17. In this way, it has been possible to reduce the dimensions of the vehicle, optimizing the spaces around the main housing. In addition, it has been decided to maximize ZENO forward thrust and thus an asymmetrical vectored layout on the horizontal plane has been chosen. Indeed, all the vectored thrusters provide their maximum thrusts when the vehicle navigates in the forward direction (as visible in Figure 3.17, all their nozzles have been oriented in the same way/direction).

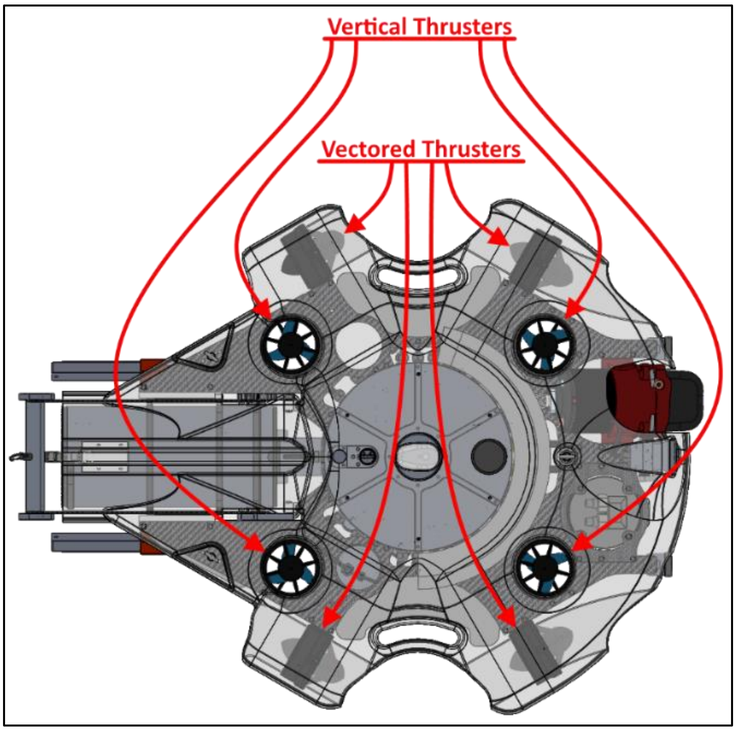

Figure 3.17: ZENO thrusters layout.

Similarity to MARTA and FeelHippo AUV, the thruster chosen for ZENO AUV has been BlueRobotics T200 motor (cheap, reliable and compact). Finally, to connect all the thrusters to the main housing a sandwich structure has been designed, made of two carbon fiber sheets, with buoyancy foam and POM elements/supports to be used as attachment points.

3.3.3 ZENO battery module prototype.

The battery module houses the AUV Li-Po batteries needed to provide power to the vehicle and to feed the thrusters. The choice of Al 6082 T6 has been dictated by different needs: it is light but mechanically strong. Obviously, because of a possible use in salt water, all the external mechanical components have been anodized. In addition, there are sacrificial anodes in zinc or magnesium to protect the overall structure. The two caps, one of the battery module one of the main housing, are connected through Nylon wires (Nyofil), resistant but quick and easy to use. The NBR (Nitrile Butadiene Rubber) O-rings are type 70 shore A and guarantee the water insulation.

In Figure 3.18 the content of the battery module is shown: 2 Li-Po Batteries (by Tattu) of 22000 mAh, 325.6 Wh, 4 cells 14.8 V 25 C; the relay, the DC/DC and electronics necessary to manage ignition, recharging, balancing and power supply. The support plates for the batteries and the electronics are in PMMA (PolyMethyl MethAcylate - Plexiglas®), while the ring supports and the other white ones are in ABS and they were printed with the 3D Stratasys Dimension Elite printer of the UNIFI DIEF MDM Lab. The custom battery module connector is observable instead in Figure 3.19. In particular, there are three pins with 80 A each and three pins with 22 A each; the support is in PEEK (PolyEther Ether Ketone). The bigger pins provide the power to the vehicle, while the smaller ones provide the connection for switching on the system and for the water leakage sensor.

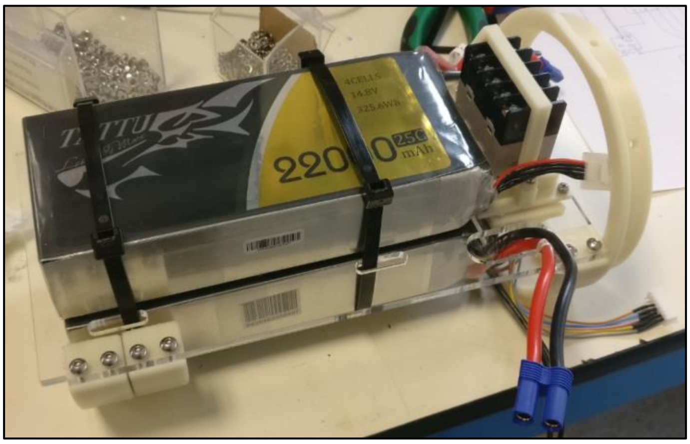

Figure 3.18: Inside of ZENO battery module.

The switching on and off is controlled by a magnetic switch while the cap is in aluminum with cavity containing a NdFeB (Neodimio-Ferro-Boro) magnet coated by nickel.

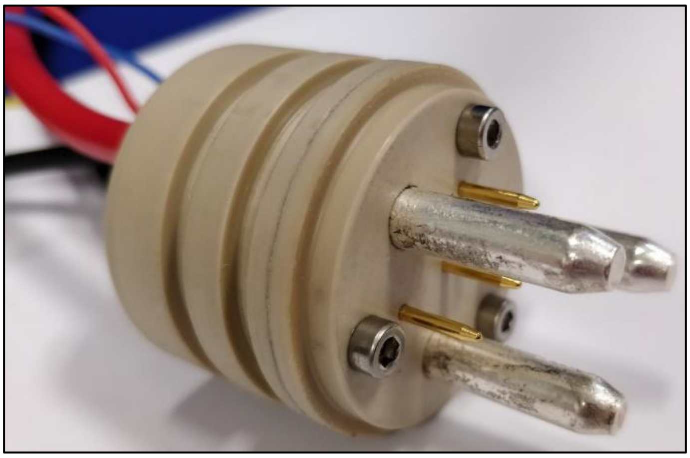

Figure 3.19: Detail of the battery module custom connector.

ZENO AUV battery module can be easily and quickly replaced thanks to a leverage system; without considering the recovery and deployment of the vehicle, it takes about 20 s to replace the battery module. Therefore, with two battery modules, based on an average cruising speed of 2 knots, the overall mission autonomy is about 6 hours. In addition, just charging the spare module "continuous field operations" are possible (with very short time between two successive missions). The leverage system has been designed for a thrust necessary to insert the battery module equal to about 300 N, which corresponds to a push of the hand of 60 N.

The buoyancy and the balancing are guaranteed by shaped foam and lead sheets according to the interchangeability of the payloads; an overall buoyancy of 250 g is expected in both salt and fresh water.

After the mechanical assembly, the seals and the main housings have been tested in the pressure chamber of the UNIFI DIEF MDM Lab. Even if the vehicle is designed for a depth of 150 m, the test pressure, monitored by the manometer, has been performed at 12.5 bar (125 m). Neither losses, leakages or structural mechanical problems have been observed.

3.3.4 ZENO first testing.

The preliminary tests have been performed in this sequence: first of all, the assembled components have been evaluated in the laboratory pool, to obtain the propellers force/speed (§3.4.3) curve and to obtain a satisfying tuning of the PID gains to control vehicle navigation. Secondly, the AUV has been tested in fresh water at Roffia Lake (San Miniato, Pisa, Italy) and successfully performed some simple missions on surface and underwater, both in ROV and AUV modalities.

ZENO AUV has been prepared for the official tests in salt water too; the first sea trials were done at the CSSN base of the Italian Navy (La Spezia, Italy) and allowed the verification and the tuning of the developed software and hardware. Then an official demonstration Tuscany at the end of July 2018, at the Melania shipwreck (close to Cecina Livorno, Italy). An integrated system made up of the underwater sensor nodes and divers in addition to the ZENO AUV (Figure 3.20). The Melania shipwreck monitoring thanks to both cameras and the onboard Side Scan Sonar by Deep Vision.

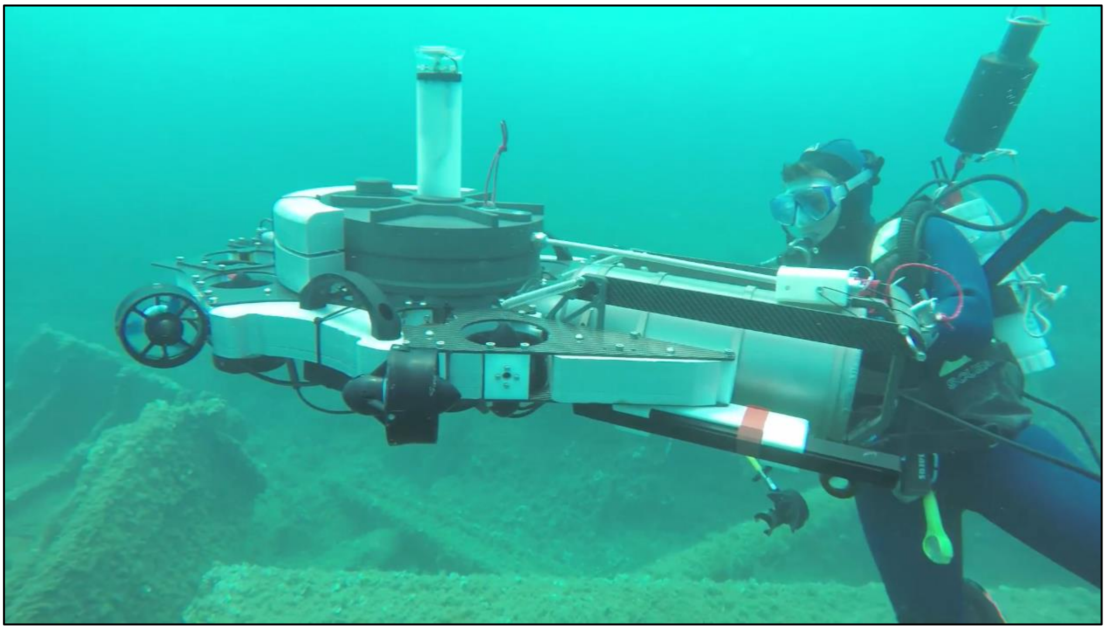

Figure 3.20: ZENO AUV, with a diver during an official test at sea (Cecina, Italy).

3.4 Thrusters awareness.

3.4.1 The importance of knowing thruster performance.

Autonomous underwater vehicles usually have complex control systems to dive and navigate autonomously. These control systems need to measure the state of the vehicle under control. The measurement or the estimation of all the parameters that represent the state of the vehicle is a critical point, because the data quality is extremely important for the stability of the control system and thus for the navigation accuracy. The knowledge of the thrusts, provided by the thrusters, is very important, because these are the actions that allow the vehicle movement. For this reason, the quality of thrusts estimation can influence the quality of the control system actions (e.g. in particular if the control architecture exploits the AUV dynamic model [33]). More in details, the knowledge of thrust is related to the ability of estimating or measuring the rotational speed of the motors, because the propeller and nozzle ensure a specific relationship between the thrust and the motor speed. For this reason, a deep knowledge of the relationship between the driver input and the motor thrust could make the difference, especially when the thruster does not have a speed sensor. More in details, to improve the estimation of the BlueRobotics T200 a dedicated study of the behavior of the thruster and its motor driver has been made. In this particular case, the study was not so easy because of the lack of specifications of the very low cost selected components, compared to professional products. This is a normal situation for the examined components since there are mainly designed for hobbyists. A remarkable example of this fact is the examined ESC (AFRO ESC 20A with a custom firmware by BlueRobotics), visible in Figure 3.21. Indeed, only few specifications (Table 3.5) and a very short user manual [34] are available.

Figure 3.21: AFRO ESC 20°.

AFRO ESC 20A specifications

Current Draw [A]	20
Voltage Range [-] ([V])	3s-8s (11.1-29.6)
Input Frequency [kHz]	1
Default Firmware	Afro_HV.hex
Battery Wire Dimension [AWG]	16
Battery Male Plug [mm]	3.5
Motor Wire Dimension [AWG]	17
Motor Male Plug [mm]	3.5
Weight [g]	28
Size (with capacitor) [mm]	65x27x11

Table 3.5: Available AFRO ESC 20A specifications.

For this reason, electro-fluid-dynamic relations, such as the ones discussed in [35] [36] [37] [38], have not been considered; on the contrary extremely simplified relations have been studied: the proposed relations are thus specific for the actuation chain under study. In addition, this choice not only has been guided by the lack of component information (probably the ESC sets the voltage of the motor changing the servo command value), but also by the idea of minimizing the computational load of the estimations, looking for the best trade-off between computational effort and performances, in order to integrate them in the control system of the UNIFI underwater vehicles [33]. Moreover, a particular behavior of the examined thruster has been detected. This behavior not immediately related to the technical literature [31] [35] [36] [37] [38] and will be shown and discussed in §3.4.3.

3.4.2 New experimental rig.

Although the old setup of test rig, presented in §3.2.2, has been widely used for the preliminary characterization of MARTA AUV propulsion system, the measurements showed a not sufficient repeatability and accuracy. The cause of thrust measurements inaccuracy was due to the presence of a load cell that give to the measurement chain too flexibility causing load cell misalignment. In addition, the low measurement repeatability was given by the high friction of on the linear guide and on UniBall joints that connect the thruster to the support. Furthermore, using that measurement configuration, the thruster had to operate at low depth and this condition was not optimal (e.g. cavitation issues) and added measurements uncertainty. The adopted load cells were unidirectional, so each time the propeller rotation changed the direction of the load cell had to be changed.

In order to increase measurements accuracy, a new test rig has been designed changing the whole old structure. The new design is based on a leverage system to place the thruster far from the water surface and to give to the measurement system the capability of mechanical amplifying the thruster thrust. More in detail, the thrust measurement is obtained as the result of the ratio between the thruster arm and the cell arm of the force exerted on the central joint. The new scheme is visible Figure 3.22.

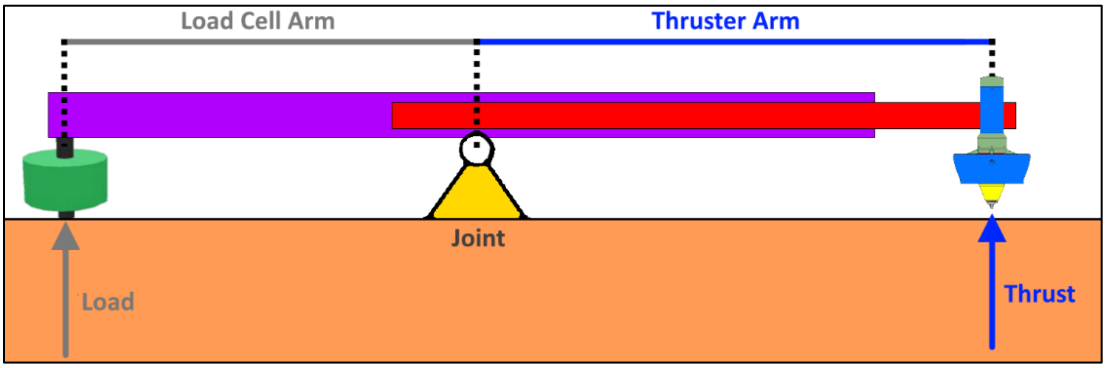

Figure 3.22: New test rig scheme.

The implementation has been made using standard aluminum profiles and components purchased from ITEM. This solution gives a high stiffness to the measurement chain reducing measurement uncertainly and inaccuracy. The length of both arms indeed can be easily regulated through a screw, in order to set different force ratios. As regards the load cell, a factory calibrated one has been selected, able to perform load measurements both in compression and in traction. The chosen load cell is TAS510 with its SIC-A2, a factory calibrated cell amplifier (produced by HT SENSOR TECHNOLOGY). This choice allowed to improve the measurement accuracy with respect to the extremely low cost old ones. Its characteristics are shown in Table 3.6, while the new test rig is visible in Figure 3.23.

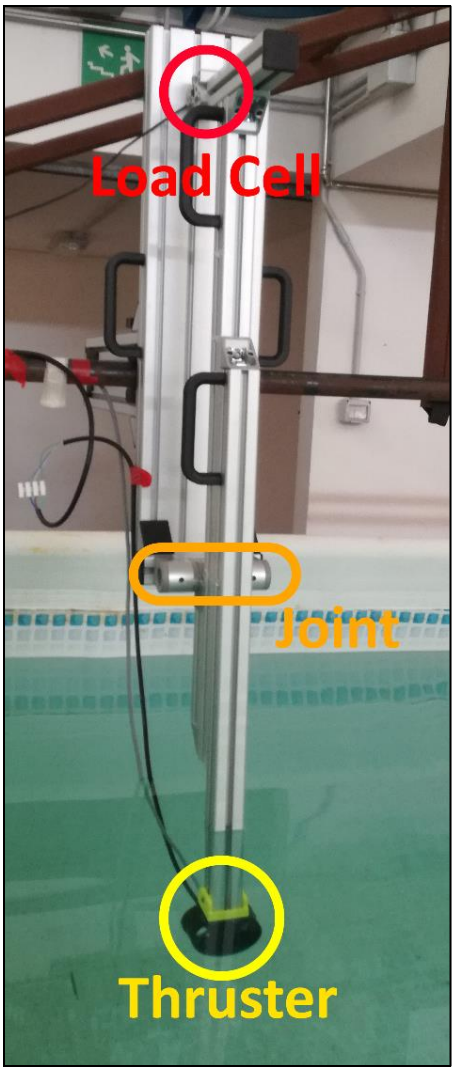

Figure 3.23: New test rig.

Load cell characteristics	
Capacity [kg]	30
Rated Output [VDC]	0±10
Combined Error [%FS]	±0.1
Non Linearity [%FS]	±0.1
Hysteresis [%FS]	±0.1
Repeatability %FS]	±0.1
Creep (30 min) [%FS]	±0.1
Zero Balance [%FS]	±0.1
Temperature Effect on SPAN [%FS/10 °C]	±0.1
Temperature Effect on ZERO [%FS/10 °C]	±0.1
Input Resistance [Ω]	725±25
Output Resistance [Ω]	700±1
Recommended Excitation [VDC]	24
Insulation Resistance [MΩ]	≥5000
Compensated Temperature Range [°C]	-10 to 40
Operating Temperature Range [°C]	-20 to 55
Safe Overload [%FS]	120
Ultimate Overload [%FS]	150

Table 3.6: TAS510 load cell characteristics.

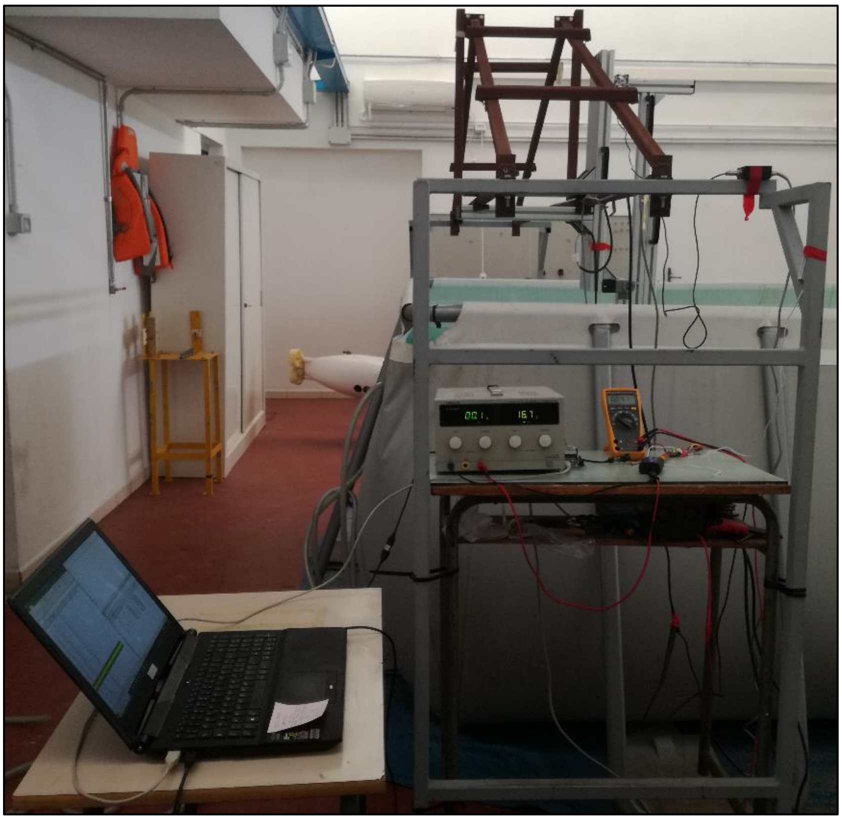

Figure 3.24: The whole new thruster measurement chain, during the last thruster test.

As regards the remaining measurement chain elements, it has been chosen not to make changes. The thruster rotational speed is thus measured acquiring the fundamental harmonic drive component from the driving voltage waveform through a spectrum analyzer. The load cell is acquired measuring directly the output voltage with a multimeter. The whole measuring system used during last test described in Chapter 4 is visible in Figure 3.24.

3.4.3 Data analysis.

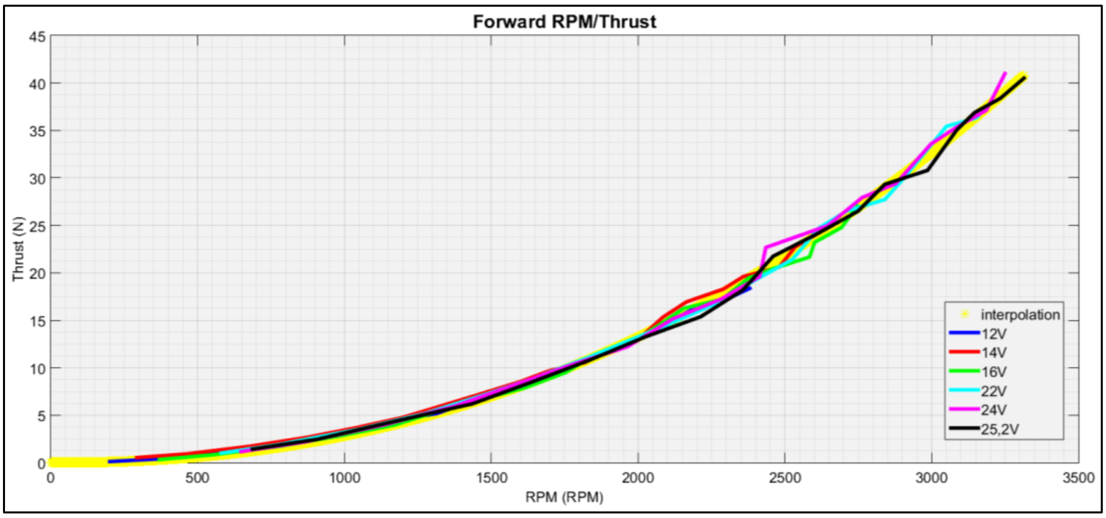

Figure 3.25: Relations between speed and thrust in the forward direction.

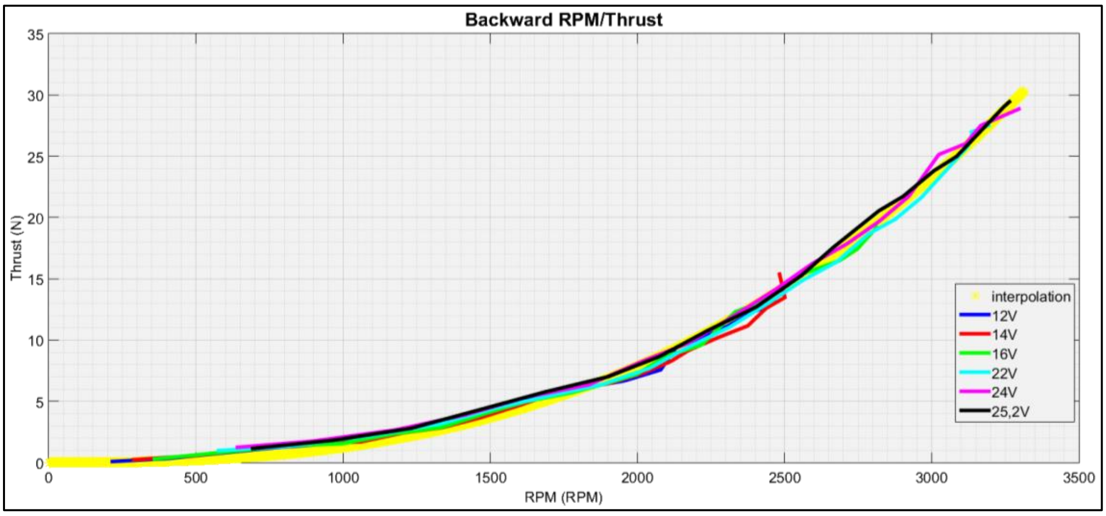

Figure 3.26: Relations between speed and thrust in the backward direction.

As mentioned above, the first aim of this test has been identifying the relations that link the main parameters of the thruster and the ESC controller, to improve the estimation of the thruster status during vehicle navigation. For this reason, tests have been performed with different voltage alimentations: 12 V, 14 V, 16 V, 22 V and 25.2 V. These values have been chosen taking into account the voltage supply of MARTA, FeelHippo and ZENO. Indeed, MARTA and FeelHippo are powered by 22.2 V Li-Po batteries (6s) that provide a voltage between 25.2 V and 21 V during discharging (on the vehicle the voltage emergency threshold is fixed at 22 V). On the other hand, ZENO is powered by 14.8 Li-Po batteries (4s) that provide a voltage between 16.8 V and 13.6 V during discharging (on the vehicle the voltage emergency threshold is fixed at 13.8 V). For this reason, with the chosen voltage values it is possible to cover the most interesting ranges.

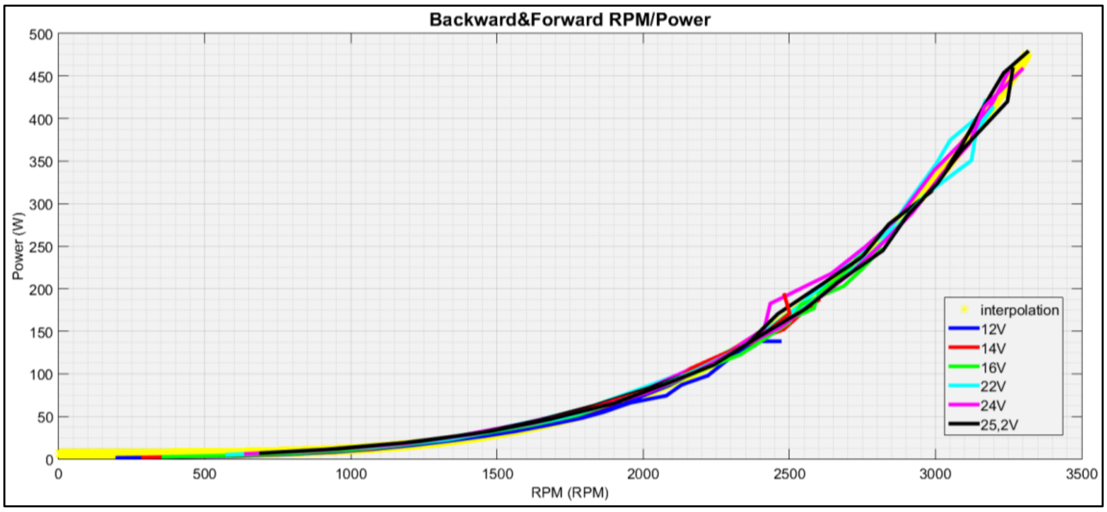

Figure 3.27: Relations between speed and power.

In Figure 3.25 and Figure 3.26, all the data about bollard thrust and rotational speed are reported. The data are divided between forward and backward direction because the nozzle of the BlueRobotics thruster is asymmetrical, so the relations between thrust and speed in these directions are different. However, the most interesting thing observable from these figures is that the curves acquired at different voltage are very closed each other. This condition assures that the acquired data are of good quality. Indeed, the relation between thrust and speed of a coupling nozzle and propeller is univocal and has to be the same at every voltage. For this reason, the data of all voltage values have been used to define the interpolant curves. In each direction, the interpolant curve used is the power law:

$$\boldsymbol{Thrust = a_T * RPM^{b_T}} \tag{3.1}$$

In the forward direction constant values are:

$$\begin{aligned} \boldsymbol{a_T} &= \boldsymbol{5.805 * 10^{-7}} \\ \boldsymbol{b_T} &= \boldsymbol{2.229} \end{aligned} \tag{3.2}$$

While, in the backward direction constant values are:

$$\begin{aligned} \boldsymbol{a_T} &= \boldsymbol{1.22 * 10^{-8}} \\ \boldsymbol{b_T} &= \boldsymbol{2.66} \end{aligned} \tag{3.3}$$

The choice to use a generic power law instead of a quadratic one (see also §Appendix A) [31] [39] [40] (as the definition of the thrust coefficient would require) is related to the observation that a generic power law has a better R-square in each direction. Indeed, in the forward direction the R-square value is 0.9918 for quadratic relation while 0.9971 for a generic power law. In the same way, in the backward direction the R-square value is 0.9616 for quadratic relation while 0.9949 for generic power law. The choice to define a coefficient non- standard thrust coefficient is related to the fact that a more conventional non-dimensional procedure does not take into account the registered phenomena (better described below, at the end of this Chapter).

Even for the power data; it is possible to observe that all the obtained curves are very close to each other (Figure 3.27). The only difference with respect to the previous data is that here there is no difference between the forward and backward directions, because the power is related to the electro-mechanic behavior of the motor. Also in this case, the selected curve to interpolate the data is a power law. The only difference is the presence of an additive constant, that represents the standby power of the system:

$$\boldsymbol{Power = a_P * RPM^{b_P} + c_P} \tag{3.4}$$

The values of the constants are:

$$\begin{aligned} \boldsymbol{a_P} &= \boldsymbol{2.276 * 10^{-11}} \\ \boldsymbol{b_P} &= \boldsymbol{3.782} \\ \boldsymbol{c_P} &= \boldsymbol{6.34} \end{aligned} \tag{3.5}$$

with a value of R-square of 0.9969.

Differently from previous relation, the study of the relation between the servo command and the thruster rotational speed has been more complex. Indeed, referring to Figure 3.28 and Figure 3.29 data acquired at different voltage levels seem quite different to each other. Fortunately, showing the data for the forward and backward directions in a single chart (Figure 3.30) it has been possible to make interesting observation.

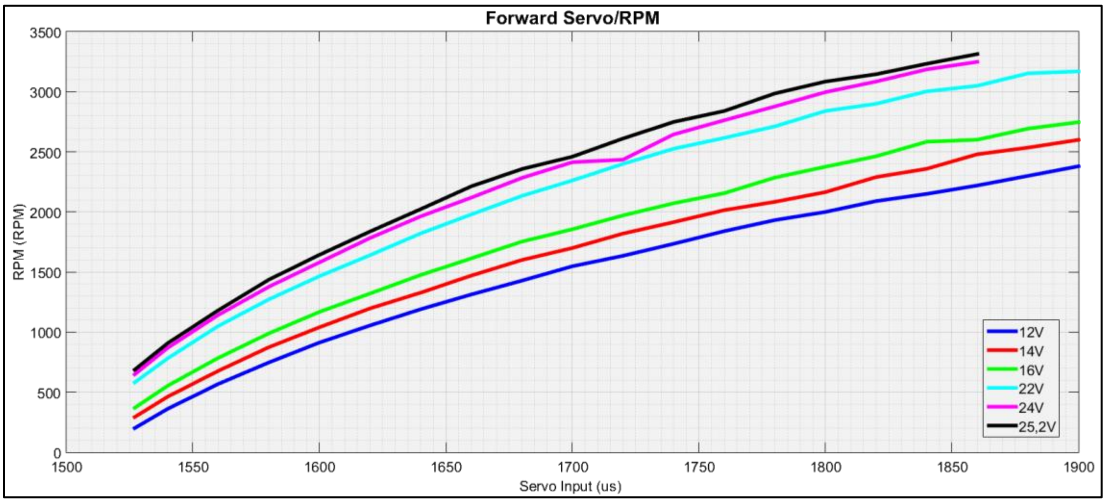

Figure 3.28: Relations between servo command and speed in the forward direction.

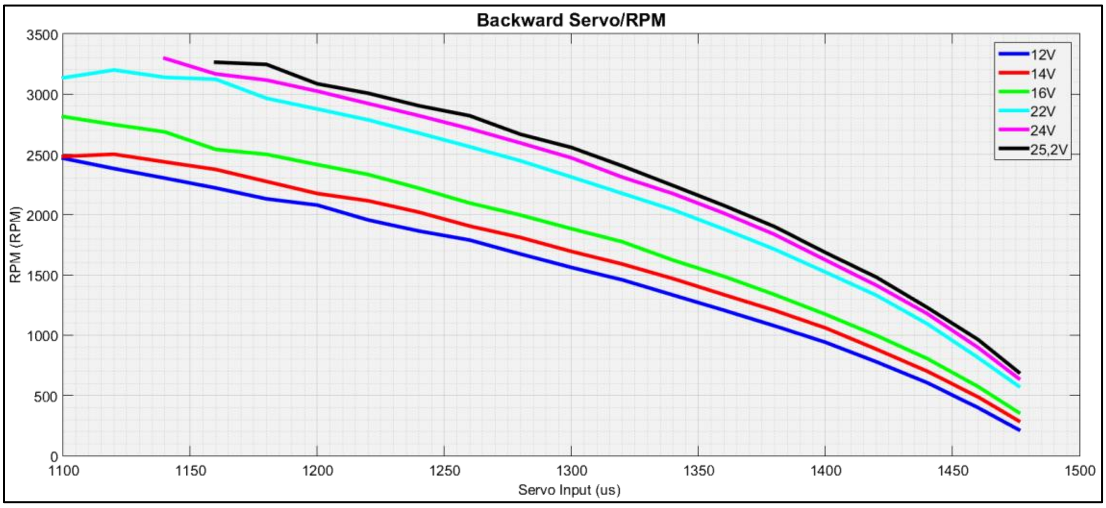

Figure 3.29: Relations between servo command and speed in the backward direction.

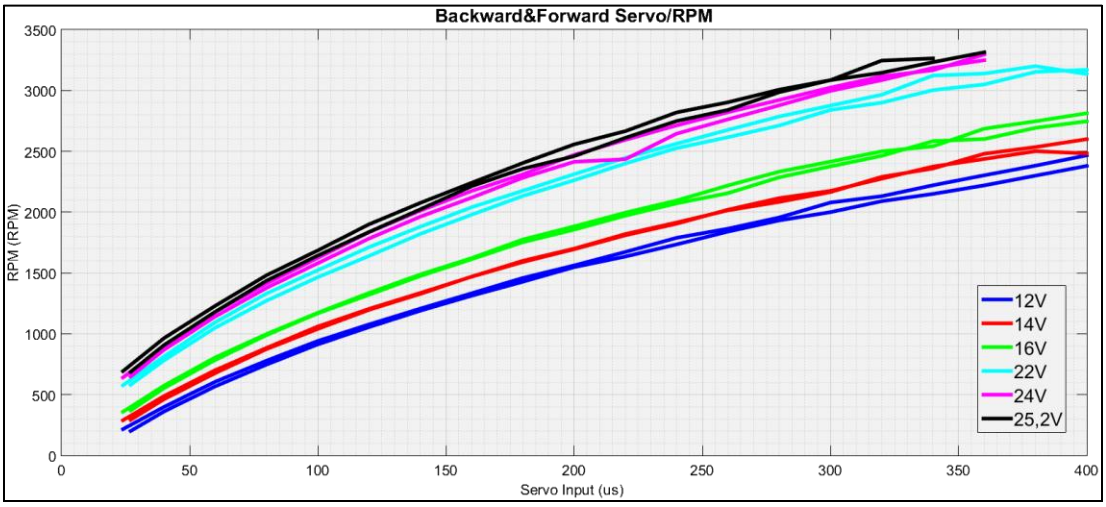

Figure 3.30: Relations between servo command and speed in both forward and backward direction.

Firstly, showing the servo command, with central value of 1500 μs it is possible to observe that the relation between the servo command and the rotor speed is the same both for forward and backward direction and for each voltage value, i.e. the data are very close to each other. Secondly, it is possible to observe that the distribution of the data at different voltages seems to have a similar shape. More in details, the hypothetical curves that represent the relation between the servo command and the speed seem to derive from a same curve by means of a scaling process. As each couple of datasets is acquired at different power voltage, it has been supposed that this scaling effect is connected to the voltage supply. The solution of this problem has been found multiplying the servo command with the corresponding voltage. In this way, all the dataset overlaps to each other quite well, as visible in Figure 3.31. In this case, the best fitting curve is a quadratic equation:

$$\boldsymbol{Servo\ command * Voltage = a_{SV} * RPM^2 + b_{SV} * RPM + c_{SV}} \quad (3.6)$$

Where the values of the constants are:

$$\begin{aligned} \boldsymbol{a_{SV}} &= \boldsymbol{6.5825 * 10^{-4}} \\ \boldsymbol{b_{SV}} &= \boldsymbol{0.30075} \\ \boldsymbol{c_{SV}} &= \boldsymbol{270} \end{aligned} \quad (3.7)$$

with a value of R-square of 0.9964.

As visible in Figure 3.32, the results of the estimation by means of the interpolating curves are very satisfactory. Indeed, the estimated values, represented in the figure with points, are very close to the corresponding experimental dataset. More in details, the estimated values of the servo commands do not diverge from the corresponding dataset by more than 23%. In particular, the maximum error values are connected to low value of rotor speed. This condition, probably, is related to bigger uncertainties on thrust measurements due to very low voltage output for low value of thrust. However, the mean errors between the estimated servo command and the dataset do not overcome the 6%.

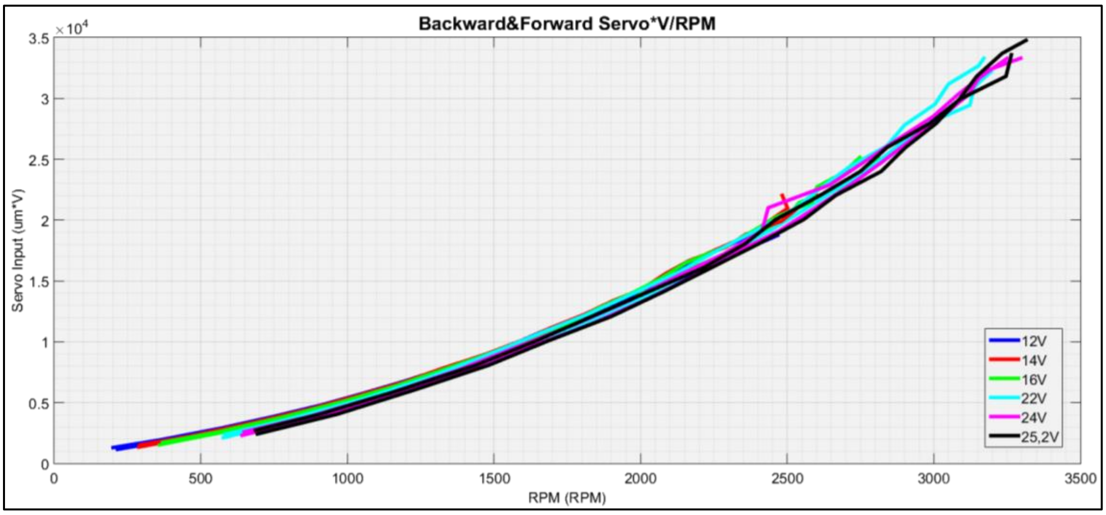

Figure 3.31: Relations between speed and servo command.

To verify the quality of the estimation provided by the proposed relations some dedicated experimental test have been performed. The relation between the speed and servo command (3.6) has been used to estimate the command required to run the thruster to the required speed.

Subsequently, the provided thrust has been measured and compared with the thrust estimated by means of relations (3.1). As visible in Table 3.7 and Table 3.8, both in the forward and in the backward directions, the estimated values of the rotor speeds are very close to the measured ones, while instead the results of thrust comparison are quite different. Regarding the forward direction the estimated thrusts are extremely close to the measured ones. Differently, in the backward direction the thrust estimation results are poorer especially at low speeds. This condition is, likely, related to some residual problems in the measurement chain of the new test rig. Indeed, in the backward direction the thrust values are lower than in the forward direction and noise has thus much more influence. In addition, in the backward direction, the load cell is compressed and the connection clearance between the load cell and the test rig bar adversely affects the measurements.

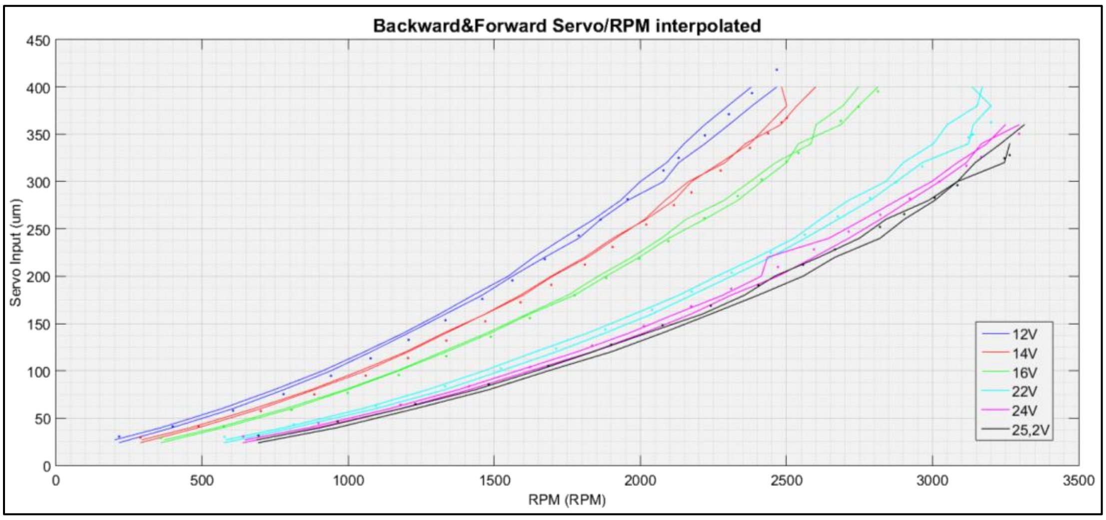

Figure 3.32: Comparison between the acquired data (line) and the estimated values (point).

Forward Direction						
Voltage [V]	Desired Speed [RPM]	Estimated		Measured		Error [%]
		Servo [µs]	Thrust [N]	Speed [RPM]	Thrust [N]	
11,98	1000	1603	2,82	930	2,58	-9,36
11,93	2000	1794	13,24	1970	12,94	-2,30
11,93	600	1558	0,90	554	0,86	-5,07
17,92	1500	1623	6,97	1460	6,82	-2,13
17,92	2200	1730	16,37	2185	16,26	-0,66
20,46	800	1546	1,72	812	2,05	16,15
20,44	1950	1664	12,51	1943	12,49	-0,13
14,66	1350	1628	5,51	1299	5,34	-3,19

Table 3.7: Comparison between the estimated parameters and the measured one in the forward direction.

Backward Direction						
Voltage [V]	Desired Speed [RPM]	Estimated		Measured		Error [%]
		Servo [µs]	Thrust [N]	Speed [RPM]	Thrust [N]	
11,93	1000	1397	1,24	950	1,75	29,19
11,82	2000	1204	7,89	2020	8,34	5,45
11,93	600	1442	0,32	590	0,68	53,54
18,03	1500	1378	3,66	1504	4,63	20,97
17,8	2200	1269	10,17	2250	10,92	6,89
20,44	800	1454	0,68	854	1,54	55,71
20,43	1950	1336	7,37	1980	8,61	14,37
14,69	1350	1372	2,76	1331	3,62	23,72

Table 3.8: Comparison between the estimated parameters and the measured ones in the backward direction.

The experimental evidences show that the difference between the conventional model and the here proposed relation between rotational speed and thrust of these particular thrusters is due to some physical phenomena. A known phenomenon able to affect the thrust coefficient is the presence of a transitional flow around the propeller but, in this case the flow around the propeller in completely turbulent: indeed, the minimum rotor speed provided by the ESC is about 200 RPM (at 12 V of power supply). For this reason, the uncommon behavior of the thruster has to be related to another physical phenomenon. This behavior may be related to a main feature of the Bluerobotics thrusters. Indeed, unlike common professional thrusters the Bluerobotics thrusters are equipped with bushings instead of ball bearings. This is an important feature of this kind of thrusters and has allowed to reduce the weight, the dimensions, the price, to enhance the reliability of these thrusters and, especially, to maximize the ratio between performance and price. The choice of bushings needs the presence of proper clearances between the shaft, the locked system of the shaft and the bushings to work properly. In this way, the rotor can be moved by the turbulent flow of the water in the neighborhood of the equilibrium position due to the interaction between rotor magnets and stator windings.

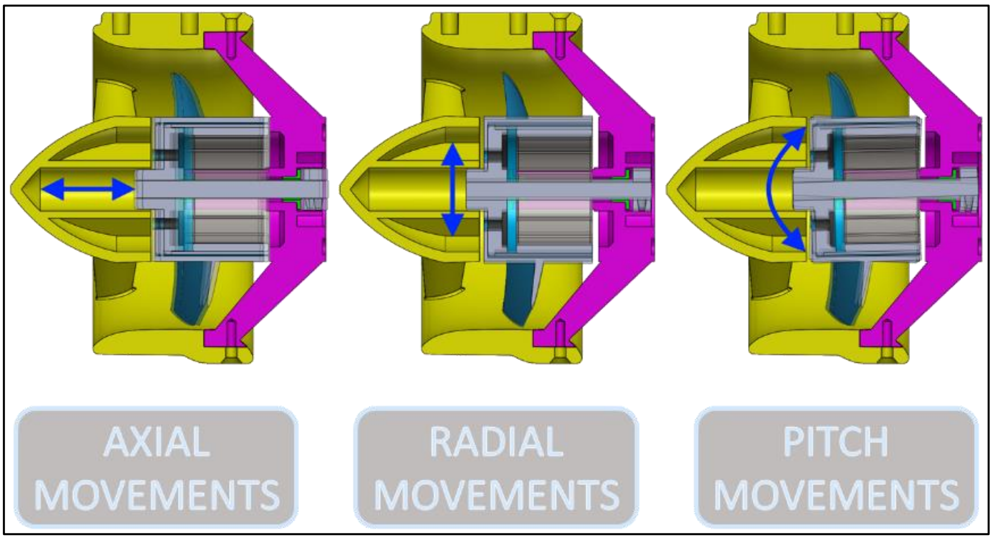

Figure 3.33: Motions of the rotor of a BlueRobotics thruster due to bushings clearences.

As visible in Figure 3.33 the rotor can move in the neighborhood of its equilibrium position in three different ways:

1. Axial movements;
2. Radial movements;
3. Pitch movements.

For this reason, the rotor does not turn coaxially with respect to the nozzle, but it orbits around the nozzle axis with a non-null pitch angle. Obviously, this motion between the propeller and the nozzle affects the provided thrust and this effect seems to be related to the rotor speed (as the experimental data shown), because the actual relative position between the rotor and the nozzle is due to the actual water flow. This behavior is also clearly visible in the steady condition in Figure 4.7 and Figure 4.9 (in §4.3). Indeed, at different rotational speed the frequency and the amplitude of rotor oscillations change, and in some conditions, it seems to appear a self-excited behavior as visible around 1500 RPM in Figure 4.7, where the amplitude of the oscillations increases remarkably.

In the near future, a BlueRobotics thruster will be modified replacing its bushings with ball bearings in order to remove the clearances between the shaft and its supports. In this way, will be possible to check if the lack of clearances brings the thruster to a more common behavior.

Some mechanical improvements scheduled in the near future will improve the quality of the measurements and thus the quality of the estimation curves.

Finally, to verify the effectiveness of the obtained relations some pull tests with ZENO AUV has been performed. More in details, ZENO has been connected to the bar of the bench test with a rope to use the load cell to measure the global thrust of ZENO in bollard condition. These tests have been performed requiring to ZENO control to push the vehicle with some desired thrusts. The results, visible in Table 3.9, shown that the control is able to provide the required global thrust to the vehicle with good precision, estimating the drivers inputs by means of the relations proposed in this chapter.

ZENO Thrust		
Desired Thrust [N]	**Measured Thrust [N]**	**Error [%]**
10	9,61	-3,90
15	13,89	-7,39
20	18,17	-9,14
30	31,01	3,38
40	39,58	-1,06

Table 3.9: Results of thrust tests on ZENO.

Chapter 4

BlueRobotics customization

4.1 The need to know the RPM.

As mentioned in §3.4.1, estimating the propeller thrust is a good improvement for the control systems performances, but knowing the motor speed is extremely important to obtain the best control performances. Indeed, knowing the propeller speed allows knowing the thruster thrust, as for each couple of propellers and duct an unambiguous relation between the rotational speed and the thrust exists. Obviously, the quality of the speed measurement influences the control performances, so it is very important to use a measurement system with high reliability and high precision.

I.e., the measurement of the motor speed simplifies the study of the dynamical model of an underwater vehicle and its control scheme, because the important parameters remain the thrust coefficients, but these are given in the technical literature for a wide number of pairs of propeller and nozzle.

4.2 Upgrade design.

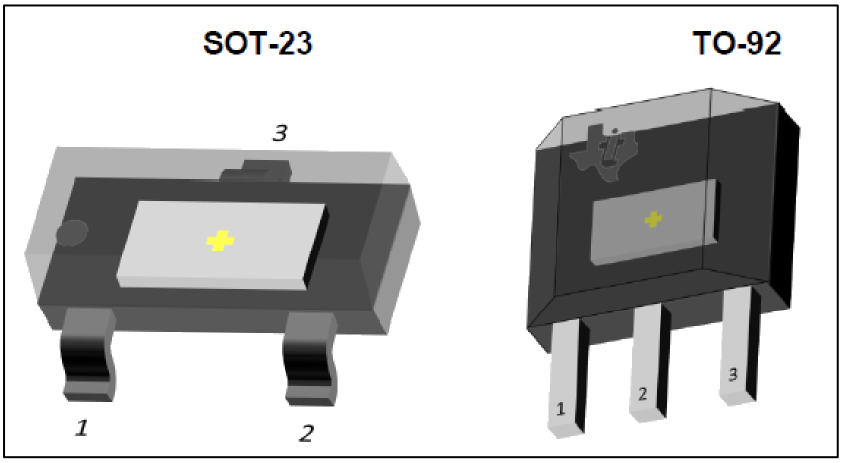

Figure 4.1: Two packages of Texas Instrument® DRV5013 [41].

Using sensored thrusters on AUV usually entails a relevant increase of the vehicle cost. Indeed, both thruster and motor drivers are very expensive. In addition, sensored thrusters are bulkier and heavier with respect to BlueRobotics thrusters. For these reasons, an upgrade for this kind of thruster has been studied, implemented and tested. The upgrade is based on the integration of a Hall effect sensor. This choice has been made to obtain a compact and reliable measurement system, because a Hall effect sensor is a very small sensor, and measuring electromagnetic fields result extremely reliable in harsh environment. Another possible solution is represented by optical sensors. With optical sensors it is possible to realize encoders with small size, but this kind of sensors does not work properly in presence of dust. For this reason, a speed sensor based on optics could stop working inside water with suspended particles. A Hall effect sensor can instead measure magnetic field changes even in presence of suspended particles without damages. More in details, for the BlueRobotics upgrade

Texas Instrument® DRV5013 (Figure 4.1) has been chosen. This choice has been made for its particular features:

- Digital sensor;
- Supports a wide voltage range: 2.5 to 38 V;
- No external regulator required;
- Reverse Supply Protection (up to 22 V);
- Output Short-Circuit Protection;
- Output Current Limitation;
- Small Package and Footprint: Through-Hole 3-Pin TO-92 (LPG) (4.00 mm × 3.15 mm).

The magnetic field is indicated via a digital bipolar latch output by the sensor. The output state is dependent on the magnetic field perpendicular to the package: a south pole near the marked side of the package causes the output to pull low, and a north pole near the marked side of the package causes the output to release. In this way, the state of the sensor can be represented only with a bit and this condition greatly reduces the noise. In addition, the lack of an external regulator and a power supply up to 38V ensure that the sensor can work without pick up noise, even if close to the motor and with a long cable. All the additional electrical protections ensure high reliability. Finally, the small package allows inserting the sensor directly into the motor.

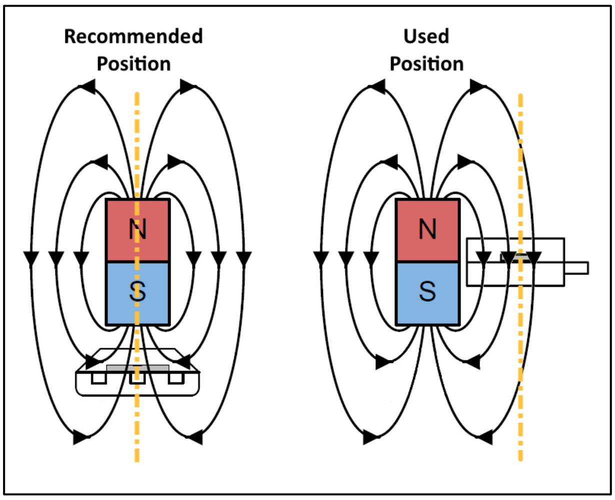

Figure 4.2: Hall effect sensor position with respect to the magnetic field.

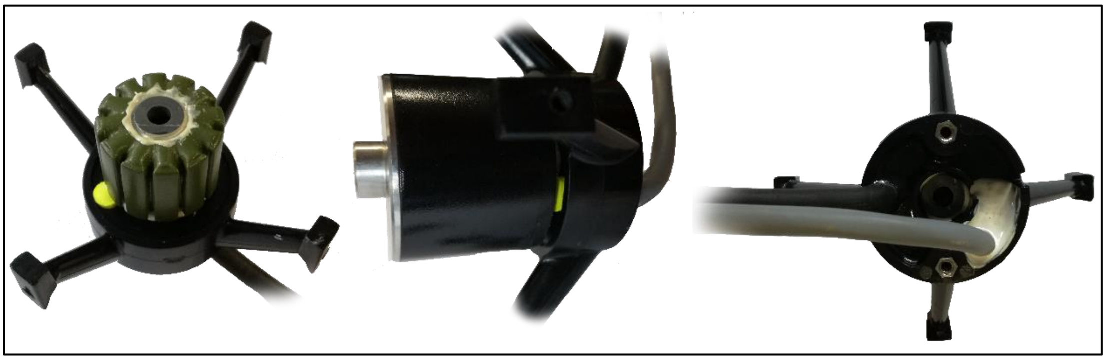
Figure 4.3: Mounting of the Hall effect sensor on the motor.

Usually a speed sensor based on the Hall effect uses a permanent magnet to provide the referring electromagnetic fields. In this case, to reduce the speed sensor dimensions it has been chosen to use directly the permanent magnets of the motor, because they are already on the rotor and they are easily accessible. The biggest problem of using these magnets is finding the best position for the sensor. Theoretically, the best solution is to align the sensor to the magnetic field direction of the rotor magnets, but in this case placing the sensor in this position is impossible. Indeed, magnetic field direction is aligned to the rotor radial direction, so the sensor should be placed exactly in the same place of the propeller. To solve this problem, several tests have been made with the aim of verifying the possibility to use the sensor in a different position with respect to the recommended one (Figure 4.2) and to find the optimal distance from the rotor. The performed tests demonstrated that the sensor works properly even in this new position and in Figure 4.3 it is possible to see how the sensor has been integrated in the testing BlueRobotics thruster. Figure 4.4 shows the sensor integrated in the thruster.

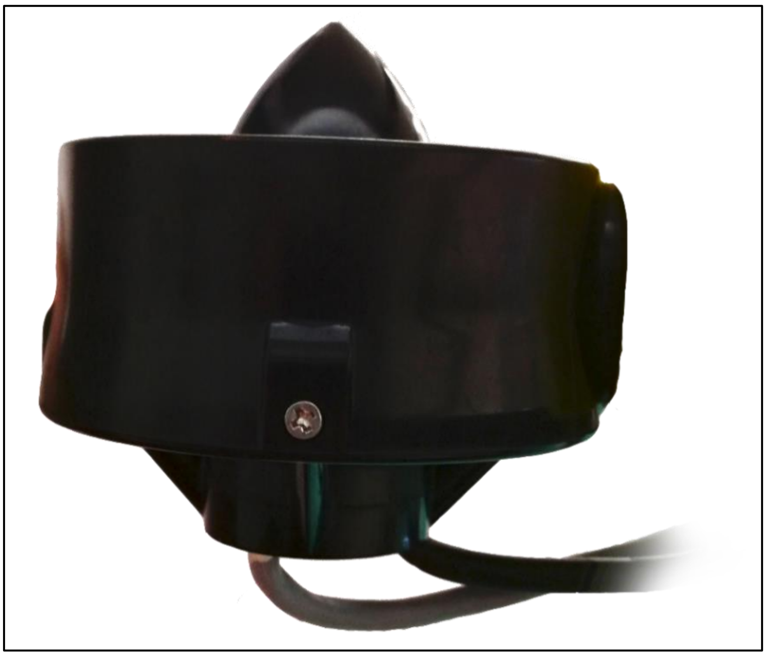

Figure 4.4: Modified BlueRobotics thruster.

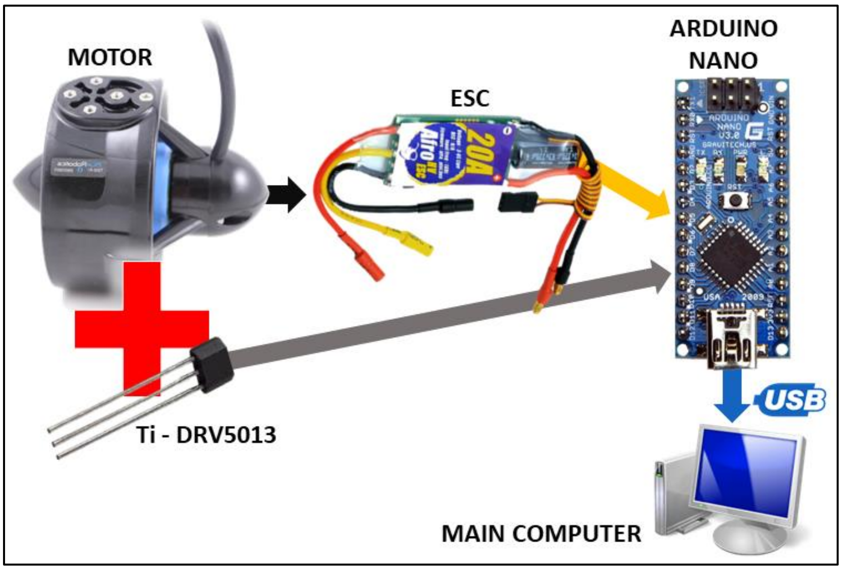

Figure 4.5: Thruster control system scheme.

Obviously, with the addition of the Hall effect sensor it is necessary to upgrade even the motor driver. As mentioned above, a motor driver for sensored motor is very expensive, so the solution has been to add a cheap microcontroller to the low cost driver of the BlueRobotics thruster. More in details, an Arduino Nano has been inserted between the main pc and the motor driver, as visible in Figure 4.5. This element performs four important functions:

1. Measures the duration of high state of the sensor;
2. Provides servo command to the driver;
3. Controls the motor speed;
4. Provides the communication between driver and the main pc.

The measurement of high state of sensor allows calculating the rotational speed of the motor (in RPM) with the relation (4.1), where the high state time is measured in seconds and the number of rotor poles is 14.

$$\boldsymbol{RPM} = \frac{\left(\mathbf{60} * {}^{\mathbf{1}}/_{\boldsymbol{high\ state\ time}}\right)}{\boldsymbol{number\ of\ rotor\ poles}\ /\mathbf{2}} \tag{4.1}$$

This information allows generating the correct servo command for the motor driver with a simple PID controller. The main pc provides to the microcontroller the referring value of the motor speed through of an USB communication.

4.3 Testing the thruster evolution.

Several tests have been made mounting the sensored BlueRobotics thruster on a long stick, to be able to manually provide some external disturbance. These external actions have been provided as motion under the water surface or using thruster both straddling the water surface and out of the water surface. In this way, it has been possible to change the resistant torque on the propeller in order to verify the functionality of the driver controller. Obviously, tests have been performed both with and without the control active. In addition, to verify the improvements of the controlled solution, tests have been performed at the same target speed in both cases and for both the forward and backward directions. More in details, for the tests with the control on the desired speed has been provided as a speed value directly to the microcontroller via USB communication, instead the for tests without the active control the desired speed has been provided as a proper servo command to the microcontroller via USB communication calculated with relation presented in §3.4.3.

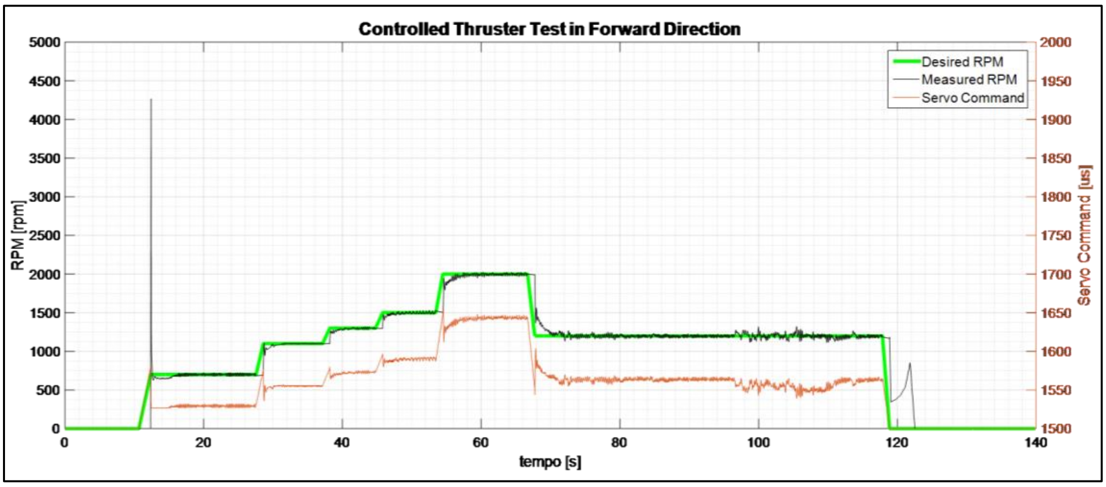

Figure 4.6: Controlled thruster test in the forward direction.

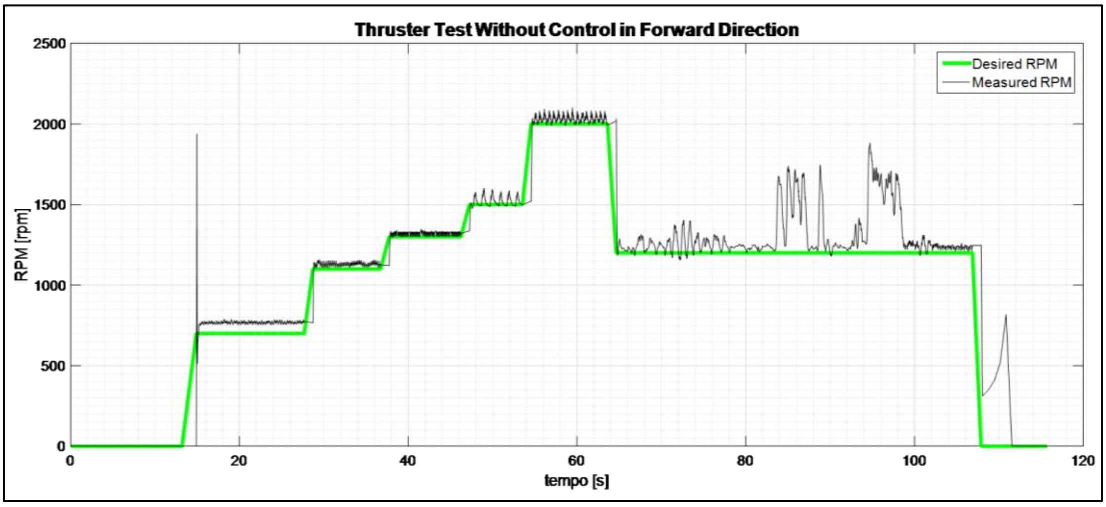

Figure 4.7: Thruster test without control in the forward direction.

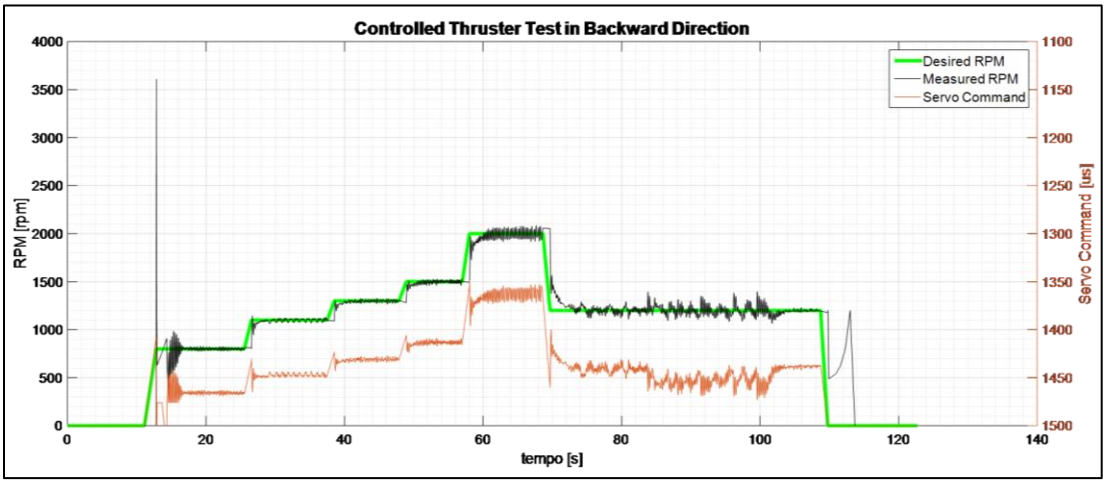

Figure 4.8: Controlled thruster test in the backward direction.

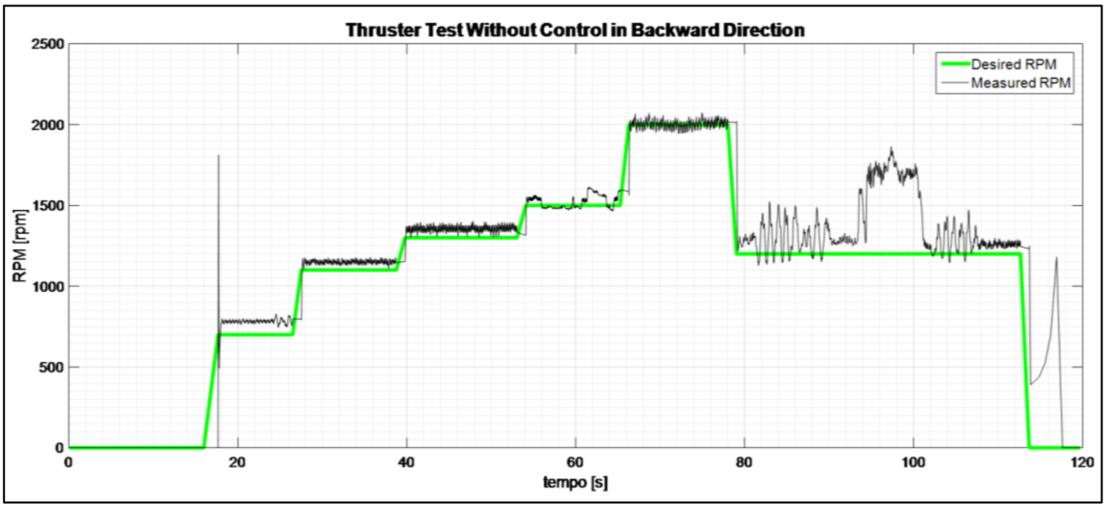

Figure 4.9: Thruster test without control in the backward direction

The resulting data are very interesting because they demonstrated the effectiveness of the proposed and adopted solution. Indeed, considering Figure 4.6 and Figure 4.7 it is possible to observe that the measured RPM in the forward direction are more closed to the desired ones with control activated, especially between 80 s and 100 s with the thruster straddling the water surface and out of the water surface. The same behavior is observable in the backward direction as visible in Figure 4.8 and Figure 4.9. More in details, in the forward tests the error decreases from 683 RPM to 122 RPM (-82%) at 1200 RPM, while in the backward tests it decreases from 664 RPM to 196 RPM (-70%) at 1200 RPM. Regarding the initial peak present in each graph, it is a peak due to the startup of the electric motor. On the other hand, the high frequency oscillations at steady state may be related to the clearance between the shaft of the rotor and the bushings, as already discussed in §3.4.3.

Conclusion and future developments

Conclusions and future developments

The main aims of the presented work have been the design of an innovative reconfigurable AUV and a deep study of new thrusters to improve the performances of the UNIFI DIEF vehicles and to optimize the performances of the new designed vehicle.

Regarding the development of an innovative AUV, not only it has been defined a conceptual design of the vehicle, but also it has been made a preliminary design that allowed verifying the feasibility of the project and an affordable budget. In addition, the concept of the new AUV has been submitted for a patent application in July 2018. The next step of this work will be the study and the testing of the electronic casings and the actuated joint, to check if these elements could have some problems.

Future developments for the new vehicle will be the study and the design of an underwater recharging system and custom robotic arms. Indeed, thanks to a recharging system the vehicle will be able to monitor wide areas of seabed, being close to resident AUV. A possible application for this vehicle will be the monitoring and the surveying of different points of interest placed at a certain distance from each other. Moreover, innovative custom arms, perfectly balanced inside water, will have to be developed to provide proper manipulation capabilities to the vehicle.

As concerns, instead the study of the BlueRobotics thruster and motor applications, a good improvement of the UNIFI DIEF vehicles performances has been reached. Dedicated experimental tests, have allowed to estimate with a good precision all the thrusters parameters; it is thus now possible to know with good precision the motor rotation speed and thrust in order to enhance, e.g. the navigation capabilities of the vehicle. In addition, a cheap sensored motor driver and an improved BlueRobotics thruster have been developed and tested. The reported results of these tests have demonstrated the effectiveness of the proposed solution. Obviously, the obtained results can be further improved with extended tests to define the multi-quadrant behavior of the thruster and fluid dynamic analysis [42]. In the near future, a new motor test rig will be built by UNIFI DIEF for this purpose. The preliminary design of this test rig is very similar to a wind tunnel. The main element of the test bench will be a long tube needed to define a controlled space and useful to contain a stable and controlled water flow. In this way, it will be possible to simulate the relative motion between a thruster and the water. A support system will be placed in the tube to lock a thruster inside. This support system will be able to measure the propeller thrust and will allows to lock the thruster with a known angle with respect to the internal water flow.

Appendix A

Brief summary of non-dimensional coefficients for marine propellers [31] [39] [40]

A.1 Bollard conditions analysis.

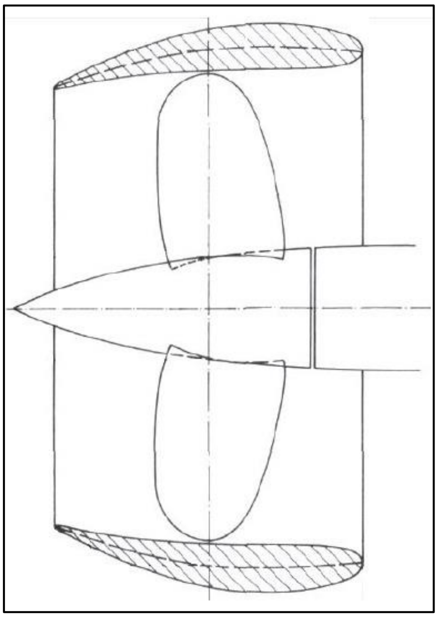

Figure A.1: Example of ducted propeller.

By means of Buckingham π theorem it is possible to define non-dimensional parameters to study and catalog propellers. These non-dimensional parameters are very important, because they allow comparing propeller with different blade profile, shape and dimension. The main non-dimensional parameters are the thrust coefficient (K_T) and the torque coefficient (K_Q). They are defined as follow in bollard conditions (zero speed of advance):

$$\boldsymbol{K_T = \frac{T}{\rho n^2 D^4}} \tag{A.1}$$

$$\boldsymbol{K_Q = \frac{Q}{\rho n^2 D^5}} \tag{A.2}$$

Where

- T is the thrust produced by propeller rotation;
- Q is the torque on the propeller;
- D is the diameter of the propeller;
- n is the rotational speed of the propeller;
- ρ is the density of water;

Propellers can be then placed into nozzles to modify their behavior (Figure A.1). Indeed, the presence of a nozzle around a propeller changes the water flow around the propeller increasing or decreasing the provided thrust both in the forward and backward direction. In addition, nozzles with different profile produces different effect on the same propeller. For this reason, each couple of nozzle and propeller has different values of the thrust coefficient (K_T). It is very interesting to observe that in technical literature there a many of data available for a lot of standard propellers and nozzles.

A.2 Multi-quadrant analysis.

In the previous paragraph, the proposed coefficients describe the couple of nozzle and propeller only when the thruster is not moving (bollard condition). When a thruster move itself the waterflow around it modifies the provided thrust. For this reason, it is necessary to define the advance angle β as the arctangent of the ratio between the speed of advance (V_a) and the local velocity of the blade, calculated at 70% of the diameter:

$$\boldsymbol{\beta} = \mathbf{atan}\frac{\boldsymbol{V_a}}{\mathbf{0.7}\boldsymbol{\pi n D}} \tag{A.3}$$

By means of β parameter it is possible to define the four quadrants as follow:

- I quadrant: $0° \leq \beta \leq 90°$◦, with $V_a > 0$ and $n > 0$;
- II quadrant: $90° \leq \beta \leq 180°$◦, with $V_a > 0$ and $n < 0$;
- III quadrant: $180° \leq \beta \leq 270°$◦, $V_a < 0$ and $n < 0$;
- IV quadrant: $270° \leq \beta \leq 360°$◦, with $V_a < 0$ and $n > 0$;

The definition of the advance angle β allows to describe the behavior of a couple of nozzle and propeller with modified thrust and torque coefficients:

$$\boldsymbol{C_T} = \frac{\boldsymbol{T}}{(\boldsymbol{\pi}/\mathbf{8})\boldsymbol{\rho}\left[\boldsymbol{V_a}^2 + (\mathbf{0.7}\boldsymbol{\pi n D})^2\right]\boldsymbol{D}^2} \tag{A.5}$$

$$\boldsymbol{C_Q} = \frac{\boldsymbol{Q}}{(\boldsymbol{\pi}/\mathbf{8})\boldsymbol{\rho}\left[\boldsymbol{V_a}^2 + (\mathbf{0.7}\boldsymbol{\pi n D})^2\right]\boldsymbol{D}^3} \tag{A.6}$$

Also in this case, the relations to calculate this to coefficients are available in literature. These coefficients are usually defined through Fourier series representations as follows:

$$\boldsymbol{C_T} = \sum_{\boldsymbol{k}=\mathbf{0}}^{\mathbf{20}} \boldsymbol{A_k}\,\mathbf{cos}(\boldsymbol{k\beta}) + \boldsymbol{B_k}\,\mathbf{sin}(\boldsymbol{k\beta}) \tag{A.7}$$

$$\boldsymbol{C_Q} = \sum_{\boldsymbol{k}=\mathbf{0}}^{\mathbf{20}} \boldsymbol{C_k}\,\mathbf{cos}(\boldsymbol{k\beta}) + \boldsymbol{D_k}\,\mathbf{sin}(\boldsymbol{k\beta}) \tag{A.8}$$

Appendix B

Published articles during the PhD period

[2016] B. Allotta, M. Pagliai, L. Pugi, "Reconfigurable Propulsion Systems for the inspection of off-shore power generation plants.", 16 IEEE International Conference on Environment and Electrical Engineering, June 2016.

[2016] B. Allotta, M. Pagliai, A. Nocentini , L. Pugi, G. Lutzemberger, A. Pretto, "Integrated Design of an Hydraulic Servo-System Fed by Vehicle Regenerative Braking.", 2016 AEIT International Annual Conference (AEIT), October 2016.

[2016] B. Allotta, M. Pagliai, L. Pugi, "Design and Modelling of Innovative Propulsion Layouts with Pivoted Thrusters For Underwater Vehicles.", IFAC-PapersOnLine, Volume 49, Issue 21, 2016, Pages 454-459.

[2016] B. Allotta, M. Pagliai, A. Nocentini , L. Pugi, G. Lutzemberger, A. Pretto, "Design of a hydraulic servo-actuation fed by a regenerative braking system.", Applied Energy, Volume 187, 1 February 2017, Pages 96-115.

[2017] B. Allotta, A. Ridolfi, M. Bianchi, F. Fanelli, J. Gelli, N. Monni, D. Nocciolini, M. Pagliai, L. Paulucci, T. Pecorella, "Employment of an Autonomous Underwater Vehicle as mobile bridge among heterogeneous acoustic nodes", IFAC-PapersOnLine, Volume 50, Issue 1, July 2017, Pages 12380-12385.

[2017] B. Allotta, M. Pagliai, A. Nocentini , L. Pugi, G. Lutzemberger, A. Pretto, "Sistema elettro-idraulico per il retrofit di impianti oleodinamici convenzionali." OLEODINAMICA PNEUMATICA, October 2017, Pages 68-78.

[2017] B. Allotta, A. Ridolfi, M. Bianchi, F. Fanelli, J. Gelli, N. Monni, D. Nocciolini, M. Pagliai, N. Palma, "An IMU and USBL-aided buoy for underwater localization", Proceedings of VII International Conference on Computational Methods in Marine Engineering (MARINE 2017), May 2017.

[2017] B. Allotta, L. Pugi, M. Pagliai, L. Paolucci, "Marine Engineering: Emerging Developments and Global Challenges/Chapter 2. Innovative Redundant and Reconfigurable Propulsion Systems: Fast Prototyping Through Simplified Simulation and Design Procedures", 2017, ISBN 978-1-53612-499-6, Pages 1-27.

[2017] B. Allotta, M. Pagliai, L. Pugi, "A robust propulsion layout for underwater vehicles with enhanced manoeuvrability and reliability features", Proceedings of the Institution of Mechanical Engineers, Part M: Journal of Engineering for the Maritime Environment, March 2017.

[2018]	B. Allotta, M. Pagliai, L. Pugi, "Redundant and reconfigurable propulsion systems to improve motion capability of underwater vehicles", Ocean Engineering, Volume 148, January 2018, Pages 376-385.
[2018]	J. Gelli, A. Meschini, N. Monni, M. Pagliai, A. Ridolfi, L. Marini and B. Allotta, "Development and design of a compact Autonomous Underwater Vehicle: ZENO AUV.", 11th IFAC Conference on Control Applications in Marine Systems, Robotics, and Vehicles. Opatija, Croazia, 10-12 September 2018.
[2018]	J. Gelli, A. Meschini, N. Monni, M. Pagliai, A. Ridolfi, L. Marini, B. Allotta, "Design and Testing of a Compact Autonomous Underwater Vehicle for Archaelogical Surveying and Monitoring.", Conference IEEE AUV 2018, Porto, 6-9 November 2018.
[2018]	J. Gelli, A. Meschini, M. Pagliai, A. Ridolfi, B. Allotta, "Design of a Reconfigurable Autonomous Underwater Vehicle for Offshore Platform Monitoring and Intervention.", Conference IEEE AUV 2018, Porto, 6-9 November 2018.
[2018]	R. Limosani, A. Manzi, A. Faggiani, M. Bianchi, M. Pagliai, A. Ridolfi, B. Allotta, P. Dario, F. Cavallo, "Low-cost solution in international robotic challenge: Lessons learned by Tuscany Robotics Team at ERL Emergency Robots 2017", Journal of Fields Robotics, Wiley, December 2018.

References

[1] R. D. Chris e R. L. Wernli, The ROV Manual. 1st Edition. A User Guide for Observation Class Remotely Operated Vehicles, Elsevier, 2014.

[2] G. Icolari, The ROV HandBook: A User Guide for ROV Pilot Technician, Atlantis Deep Sea ltd.

[3] H. R. Widditsch, SPURV - The First Decade, 1973.

[4] L. Freitag, M. Grund, C. von Alt, R. Stokey and T. Austin, “A shallow water acoustic network for mine countermeasures operations with autonomous underwater vehicles,” Ubderwater Defense Technology (UDT), 2005.

[5] «GAVIA AUV,» [Online]. Available: http://www.teledynemarine.com/gavia-auv.

[6] B. Allotta, F. Bartolini, A. Caiti, R. Costanzi, F. D. Corato, D. Fenucci, J. GellI, P. Guerrini, N. Monni, A. Munafò, M. Natalini, L. Pugi, A. Ridolfi and J. R. Potter, "Typhoon at CommsNet 2013: experimental experience on AUV navigation and localization," in *19th IFAC World Congress*, August 24-29, 2014.

[7] B. Allotta, L. Pugi, F. Bartolini e A. Ridolfi, «Preliminary design and fast prototyping of an Autonomous Underwater Vehicle propulsion system,» *Proceedings of the Institution of Mechanical Engineers, Part M: Journal of Engineering for the Maritime Environment,* p. 248–272, 2015.

[8] B. Allotta, R. Costanzi, L. Pugi e A. Ridolfi, «Identification of the main hydrodynamic parameters of Typhoon AUV from a reduced experimental dataset,» *Ocean Engineering,* vol. 147, pp. 77-88, 1 January 2018.

[9] B. Allotta, S. Baines, F. Bartolini, F. Bellavia, C. Colombo, R. Conti, R. Costanzi, C. Dede, M. Fanfani, J. Gelli, H. T. Gündogdu, N. Monni, D. Moroni, M. Natalini, M. A. Pascali, F. Pazzaglia, L. Pugi, A. Ridolfi, M. Reggiannini, D. Roig, O. Salvetti and E, "Design of a modular Autonomous Underwater Vehicle for archaeological investigations," in *OCEANS 2015*, Genova, May, 2015.

[10] A. Ridolfi, R. Costanzi, F. Fanelli, N. Monni, B. Allotta, S. Bianchi, R. Conti, J. Gelli, L. Gori, L. Pugi and A. Rindi, "FeelHippo: a low-cost autonomous underwater vehicle for subsea monitoring and inspection," in *2016 IEEE 16th International Conference on Environment and Electrical Engineering (EEEIC)*, June, 2016.

[11] J. Gelli, A. Meschini, N. Monni, M. Pagliai, A. Ridolfi, L. Marini e B. Allotta, «Development and design of a compact Autonomous Underwater Vehicle: Zeno AUV,» in *11th IFAC Conference on Control Applications in Marine Systems, Robotics, and Vehicles*, Opatija, Croazia, 2018.

[12] "ARROWS project," [Online]. Available: http://www.arrowsproject.eu/.

[13] Centre for Maritime Research and Experimentation (CMRE), «Student Autonomous Underwater Challenge - Europe (SAUC-E),» [Online]. Available: http://sauc-europe.org/.

[14] «Eurathlon 2015,» [Online]. Available: https://www.eurathlon.eu/.

[15] «ERL (European Robotics League) Emergency Robots,» [Online]. Available: https://eu-robotics.net/robotics_league/.

[16] "ARCHEOSUb project," [Online]. Available: http://www.archeosub.eu/index.php/en/.

[17] B. Meyer, K. Ehlers, C. Osterloh and E. Maehle, "Smart-E - An Autonomous Omnidirectional Underwater Robot," *PALADYN Journal of Behavioral Robotics,* pp. 204 - 210, 2013.

[18] S. K. Choi, G. Takashige and J. Yuh, "Experimental study on an underwater robotic vehicle: ODIN," *Proceedings of IEEE Symposium on Autonomous Underwater Vehicle Technology (AUV'94),* 1995.

[19] "SEASTICK - Autonomous and Remotely Operated Underwater Vehicle," [Online]. Available: https://www.seastick.net/.

[20] J. C. Kinsey, D. R. Yoerger, M. V. Jakuba, R. Camilli, C. R. Fisher and C. R. German, "Assessing the Deepwater Horizon Oil Spill with the Sentry Autonomous Underwater Vehicle," in *2011 IEEE/RSJ International Conference on Intelligent Robots and Systems*, San Francisco, CA, USA, September 25-30, 2011.

[21] D. R. Yoerger, M. Jakuba, A. M. Bradley and B. Bingham, "Techniques for Deep Sea Near Bottom Survey Using an Autonomous Underwater Vehicle," *The International Journal of Robotics Research,* 1 January 2007.

[22] K. Y. Pettersen, P. Liljebäck, A. J. Sørensen, Ø. Stavdahl, F. Lund, A. A. Transeth and J. T. Gravdahl, "Underwater manipulator arm robot". Patent US20180021945A1, 29 01 2015.

[23] J. E. Manley, S. Halpin, N. Radford e M. Ondler, «Aquanaut: A New Tool for Subsea Inspection and Intervention,» in *OCEANS 2018 MTS/IEEE Charleston*, Charleston, SC, USA, USA.

[24] M. Carreras, C. Candela, D. Ribas, A. Mallios, L. Magí, E. Vidal, N. Palomeras e P. Ridao, «SPARUS II, design of a lightweight hovering AUV,» in *5TH MARTECH International Workshop On Marine Technology*, 2013.

[25] M. Carreras, J. D. Hernández, E. Vidal, N. Palomeras, D. Ribas e P. Ridao, «Sparus II AUV - A Hovering Vehicle for Seabed Inspection,» *IEEE Journal of Oceanic Engineering,* n. 43 , Issue: 2, pp. 344 - 355, April 2018.

[26] C. Ross, A. Little, G. Brown and A. Saphiu, "Buckling of near-perfect thick-walled circular cylinders under-external Hydrostatic pressure," *Journal of Ocean Technology,* pp. 84-103, 2009.

[27] C. T. F. Ross, Pressure vessels external pressure tecnology, Woodhead publishing in materials, 2011.

[28] «Bluerobotics website,» [Online]. Available: https://www.bluerobotics.com/.

[29] «Bluerobotics motor website,» [Online]. Available: https://www.bluerobotics.com/product-category/thrusters/motors/.

[30] "BlueRobotics thruster website," [Online]. Available: vailable: https://www.bluerobotics.com/product-category/thrusters/.

[31] J. Carlton, Marine Propeller and Propulsion, Butterworth - Heinemann.

[32] D. N. Veritas, *Buckling Strength of Shells. Recommended Practice DNV-RP-C202,* Høvik, Norway.

[33] B. Allotta, A. Caiti, L. Chisci, R. Costanzi, F. Di Corato, C. Fantacci, D. Fenucci, E. Meli e R. A., «An unscented Kalman filter based navigation algorithm for autonomous underwater vehicles,» *Mechatronics,* vol. Volume 39, pp. Pages 185-195, November 2016.

[34] «AFRO ESC 20A user manual,» [Online]. Available: https://www.flyingtech.co.uk/sites/default/files/product_files/AfroESC%2020A%20USER%20MANUAL_0.pdf.

[35] W. Louis L. e D. R. Yoerger, «Comparative experiments in the dynamics and model-based control of marine thrusters,» in *Challenges of Our Changing Global Environment'. Conference Proceedings. OCEANS '95 MTS/IEEE*, San Diego, California, USA, USA, 9-12 October 1995.

[36] W. Louis L. e D. R. Yoerger, «Preliminary experiments in model-based thruster control for underwater vehicle positioning,» *IEEE Journal of Oceanic Engineering,* pp. 495 - 506, October 1999.

[37] R. Bachmayer, L. L. Whitcomb e M. A. Grosenbaugh, «An accurate four-quadrant nonlinear dynamical model for marine thrusters: theory and experimental validation,» *IEEE Journal of Oceanic Engineering,* vol. 25, n. 1, pp. 146 - 159, January 2000.

[38] P. Luca, J. Tor Arne e S. Øyvind N., «A Four-Quadrant Thrust Estimation Scheme for Marine Propellers: Theory and Experiments,» *IEEE Transactions on Control Systems Technology,* vol. 17, n. 1, pp. 215-226, 13 June 2008.

[39] M. Oosterveld, «Wake adapted ducted propellers,» Netherlands Ship Model Basin, 1970.

[40] M. Oosterveld, «Ducted propeller characteristics,» RINA Symposium on Ducted Propellers, London, 1973.

[41] «DRV5013 datasheet,» [Online]. Available: http://www.ti.com/lit/ds/symlink/drv5013.pdf.

[42] S.-K. Lee, «CFD Simulation for Propeller Four-Quadrant Flows,» in *2006 SNAME Propeller/Shafting 2006 conference*, 2006.